Materials Science & Engineering R 140 (2020) 100544

Contents lists available at ScienceDirect

Materials Science & Engineering R

journal homepage: www.elsevier.com/locate/mser

Review

Advances in finite element modelling of graphene and associated nanostructures

Y. Chandra[a], S. Adhikari[a,*], E.I. Saavedra Flores[b], Ł. Figiel[c]

[a] Zienkiewicz Centre for Computational Engineering, Swansea University, Swansea SA1 8EN, UK
[b] Departamento de Ingeniería en Obras Civiles, Universidad de Santiago de Chile, Av. Ecuador 3659, Estación Central, Santiago, Chile
[c] International Institute for Nanocomposites Manufacturing (IINM), WMG & Warwick Centre for Predictive Modelling (WCPM), University of Warwick, Coventry CV4 7AL, UK

ARTICLE INFO

Keywords:
Graphene sheets
Carbon nanotube (CNT)
Hybrid nano-composites
Atomistic model
Mechanical properties of graphene and CNT based composites
FEM

ABSTRACT

Graphene and its associated nanostructures (GANS) have been widely investigated by means of experimental and numerical approaches over the last decade. GANS and GANS reinforced composite materials show exceptional promise towards superior mechanical and thermal properties along with limitless opportunity to tailor, control, design, modify and manipulate such properties. These attributes make graphene and its associated nanostructures as one of the most important future material technologies in aerospace, automotive, medical, civil and military sectors of the 21st century. Among the various numerical methods used to analyse GANS and GANS reinforced composite materials, the finite element method (FEM) plays a prominent role. The FEM has been the standard analysis and simulation method for conventional structural and mechanical problems over the past half a century. However, its growing role and impact in atomistic-scale numerical simulation in general, and GANS, in particular, is not well known within the wider scientific and engineering modelling and simulation research community. There is a compelling need to document the expansive use of the finite element method, its advantages, shortcomings, relevance and purpose in a way which is pertinent to both material science and numerical simulation researchers. This paper serves this need by discussing the current state of the art of finite element methodologies available to study GANS and GANS reinforced composites in the most comprehensive manner. A detailed description of the popular space frame based numerical simulation strategy widely used to represent GANS is given. An extensive survey is conducted on more than 600 research papers in order to examine the finite element predictions of the mechanical and thermal properties of graphene and its associated composite materials. These properties are selected in view of their direct relevance to crucial future technologies, such as high-performance automotive components, aerospace and bioengineering systems, energy technologies, and advanced therapeutic and surgical devices. Omissions of some fundamental mechanical and thermal modelling issues for GANS have been identified and insightful guidance towards future research directions to comprehensively address them is given. By reviewing a significant breadth of publications across several academic disciples, a large scatter in the numerical predictions of essential material constants arising from the differences in fundamental assumptions and approximations has been reported. The origin of such discrepancies has been identified, analysed and established. The paper further focuses on the idealization of nanostructures and nanocomposites by means of representative volume elements (RVEs). The need for this multiscale modelling strategy to mature in order to include the simultaneous description of different material length scales within multiphysics simulation problems has been discussed. This paper will serve as standalone reference material for future research works and will pave the way for novel investigations in the context of atomistic simulations and their potential applications to the development of next-generation engineering devices and cutting-edge technological applications.

1. Introduction

Since the Nobel prize-winning discovery of Graphene in 2004, various branches of pure science, applied science and engineering have exploited its outstanding properties in their respective disciplines. Consequently, a very large body of literature exists covering a wide

* Corresponding author.
E-mail address: S.Adhikari@swansea.ac.uk (S. Adhikari).

https://doi.org/10.1016/j.mser.2020.100544
Received 6 June 2019; Received in revised form 31 October 2019; Accepted 7 January 2020

research landscape. This paper is focused on graphene and its associated nanostructures (GANS), primarily from the standpoint of mechanical/aerospace engineering and material science. There are two key aspects which underpin research in this area. These are:

1. the methodologies proposed/used by investigators to develop understandings of GANS, and
2. results obtained by the application of the proposed novel methods.

With regards to the first point above, extensive experimental and numerical approaches have been employed to investigate GANS. In this paper, we are focusing primarily on numerical methods. Among the various numerical methods used to analyse GANS and GANS reinforced composite materials, we further limit our attention to the finite element method (FEM). The FEM has been established as the standard analysis and simulation method for conventional structural and mechanical problems since the mid-1960s. This paper, for the first time, comprehensively documents the widespread use and impact of the finite element method in the area of graphene and its associated nanostructures.

With regards to the second point above, the 'results' obtained by the researchers include, but not limited to, electrical, mechanical, thermal, electronic, magnetic properties as well as biological, chemical, environmental and medical aspects. This review paper limits the discussions on the results primarily on mechanical and thermal attributes in a comprehensive manner.

This paper reviews the current state of the art of finite element based computational modelling techniques used to investigate the mechanical and thermal properties of GANS and their composite materials. The review begins in Section 2, where a general background of FEM, GANS and their nanocomposites is presented. Section 3 introduces the main numerical methods available at present to study GANS. The most relevant works involving finite element modelling strategies and multiscale techniques are presented in Section 4. The representative element method (RVE) based micromechanical modelling of polymer nanocomposites is reviewed in Section 5. Several research works related to the prediction of the mechanical properties of GANS are selected and discussed in Section 6. Section 7 selects the most relevant works dealing with the modelling of the thermal properties of GANS and their nanocomposites. Recommendations towards future research directions of FEM in the context of GANS are given in Section 8. Finally, Section 9 summarises the main conclusions of the present review paper.

2. Background

2.1. Background on the finite element method

FEM has been evolving in the field of engineering sciences since its beginnings in 1943 [1]. The method involves the discretization of a large domain into a finite number of subdivisions known as elements and then, the computation of the physical behaviour of interest in each element. During the early days of FEM, the physical behaviours of main interest were related to structural applications, particularly the study of displacements and stresses. The points that connect a pair of elements are known as nodes. The basic ideas behind FEM date back to 1909 [Ritz method [2]] and 1915 [Galerkin method [3]]. The term "Finite Element" was first used by Clough [4] and pioneered by Zienkiewicz et al. [5] in the area of numerical methods and civil engineering. However, the advent of sophisticated computer technology has extended FEM into many other areas of engineering and sciences, ranging from aerospace engineering designs to electronic applications, for instance. Since the beginning of the current decade, FEM has been well established as a powerful tool to aid the decision-making process, industry-wide [6]. The current article sheds light on how FEM is playing a vital role in studying the mechanics of carbon-based nanostructures at atomic scales. These carbon-based nanostructures that are variants of graphene will be referred hereto as graphene associated nanostructures (GANS).

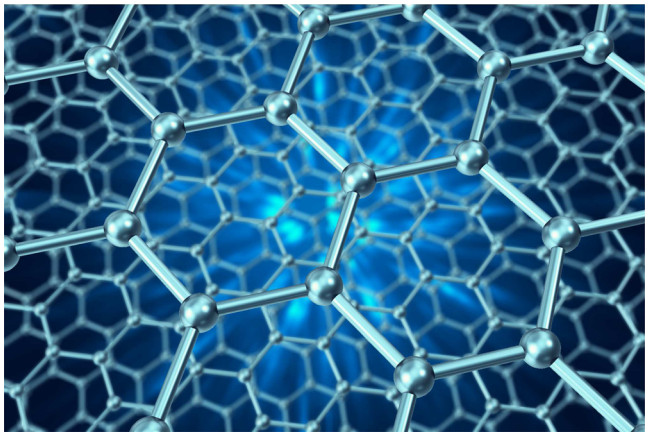

Fig. 1. Artistic impression of carbon atoms in graphene associated nanostructures (GANS).

2.2. Background on graphene associated nanostructures (GANS)

Graphene is a 2D array of carbon atoms, where atoms are connected to form hexagonal cells with the aid of sp^2 C—C covalent bonds. An artistic impression of these bonded carbon atoms can be seen in Fig. 1. The arrangement of carbon atoms can lead to single layer, bi-layer or multi-layer graphene sheets. Graphene is available in the market in several chemical forms such as graphene oxide (GO) [7,8], reduced graphene oxide (rGO) [9–11], graphene nano platelets (GNP) [12–15] and graphene flakes [16,17]. There are various forms of GANS such as CNT, buckyball, graphyne, graphene nanoribbons (GNR), carbon nano coil (CNC), carbon nanocone (CNCN) [18], carbon black [19], graphane, graphene nano fluoride [20], graphene nanoislands (GNI) [21] and the pristine graphene itself. CNT is a rolled-up cylindrical version of graphene that can be synthesised through chemical vapour deposition (CVD) and arc discharge processes. The CNT can the form of a single wall (SWCNT) [22] type or a multiwall (MWCNT) [23,24] type. Researchers are exploiting various structural and electrical benefits of CNT by constructing networks of long CNTs [25–28]. A buckyball is a spherical version of graphene that can be synthesised through the laser ablation process. GNR is a high aspect ratio flat version of graphene [29–32] that can be synthesised through exfoliation and CVD processes. CNCs are the helical form of CNT [33,34], and these can be synthesised through catalytic thermal decomposition [35]. Graphane is a hydrogen functionalized version of graphene [36,37]. Another important variant of GANS is the edge-carboxylated graphite, which can be created by ball mining of graphite [38]. Shi et al. [39] showed the possibility of various configurations of carbon nanorings by assembling several SWCNTs. Furthermore, Tserpes and Papanikos [40] envisaged a geometrically complex superstructure constructed by 2D and 3D arrays of CNTs. Wong et al. [41] conceptualised a graphene drum structure constructed with the aid of graphite flakes. Similar nano drums can also be found in [42]. In 2012, Sihn et al. [43] presented a concept known as pillared graphene structure (PGS) by combining a number of graphene sheets and CNTs to form a 3D nanostructure. Recently, these PGSs have been further studied by Song et al. [44]. Duan et al. [45] presented a mixing and dispersion technique to prepare a similar but geometrically irregular CNT-graphene network. Shi et al. [46] presented a composite network system that involved large CNT networks reinforced by graphene sheets. Graphyne is a complex array of carbon atoms connected by a mixture of sp and sp^2 covalent bonds and acetylene links [47,48]. There is no processing technology available for graphyne yet. Synthetic foams such as carbon graphitic foams [49] also fall under the category

of GANS. Yang et al. [50,51] proposed a woven fabric prepared by interlacing graphene ribbons and the resulting fabric was termed as graphene-based woven fabric. Zhang et al. [52] introduced arbitrary waviness to graphene sheets, and these sheets are known as graphene ruga. Nam et al. [53] experimentally combined graphene and CNT to produce a graphene-CNT layer. Cai et al. [54] presented a variant of graphene known as graphene kirigami which involved honeycomb re-entrant structure with negative Poisson's ratio. Currently, there are no synthesis technologies available for such kirigami nanostructures. Vertically aligned CNT arrays have also been a subject of interest [55–57]. Such nanoarrays can be synthesised through thermal or plasma-based CVD. In 2017, Ansari et al. [58] presented a hybrid structure that combined double-layer graphene sheets with double-wall CNTs. The authors indicated that such nanoscale concepts could be fabricated. Hetero-junction type CNTs have also been presented recently [59], that involve a combination of CNTs with small and large diameters through a taper. Yengejeh et al. [60] studied the buckling behaviour of these hetero-junction type CNTs. Furthermore, CNTs with two/three junctions and CNT/graphene junctions have also been envisaged [61,62].

2.3. Background on GANS nanocomposites

There are several types of GANS reinforced composite materials developed up to date. These composites mainly involve polymers as host materials. The most common polymer types reinforced by CNT/graphene are epoxy resin systems [63–85]. Rein et al. [86] showed that CNTs could act as strain sensors within the epoxy matrix. Gallo and Thostenson [87] investigated about CNTs performing the duty of microcrack sensors within the epoxy matrix. Furthermore, Lakshmi and Reddy [88] prepared specimens of carbon epoxy/carbon epoxy CNT composites and showed enhancement in interlaminar strength (ILS) due to the presence of CNT. Similar ILS benefit has been observed by Ning et al. [89] due to the presence of GO in carbon/epoxy composites and by Zhou et al. [90] due to the presence of CNT in epoxy/carbon matrix. Other types of host polymer materials being considered are polystyrene [91–94], polyethylene matrix [95–97], polymide LaRC-SI resin [98–100], polymide [101], polystyrene-co-butyl acrylate [102], polycarbonate [103–107], PMMA (polymethyl methacrylate) [15,108–110], polyvinyl alcohol (PVA) [111], polyvinylchloride (PVC) [112], alginate [113], rubber [114,115], polyethylene terephthalate (PET) [116,117], polypropylene [19,118–123], polyetherether-ketone (PEEK)[124], poly(m-phenylenevinylene)-co-[(2,5-dioctoxy-p-phenylene) vinylene] [125], poly-lactide [126], polyurethane [127,128], gelatin [129], high density polyethylene (HDPE) [130], poly(dimethylsiloxane) [45,131], polyvinylidene difluoride (PVDF) [132], bisphenol-A [13] and chitosan biological polymer [133,134]. Hou et al. [135] developed a multiple layers thin film composite with poly(aniline) emeraldine, CNT film, PVA and poly(sodium styrene-4-sulfonate). Faghihi et al. [136] reinforced poly(acrylic acid)/gelatin hydrogel with GO and reported mechanical benefits. Ray and Batra [137] proposed a nanotube-reinforced 13 piezoelectric composite by embedding SWCNT in a piezoceramic matrix (monolithic ceramic PZT). Electrical conductivity advantages have been gained by composition of A_nB_{20-n} block copolymer and CNT [138]. A composition of polycarbonate, polyamide 6 (PA6) and MWCNT also offers electrical conductivity benefits [139]. Randomly aligned fillers of CNT in an epoxy matrix offer damping benefits [140]. There is also the trend to use GANS as fillers in the resin of composite materials, such as using CNT within the resin of epoxy/glass fibre composite [141] and using rGO within the resin of polymide/glass fibre composite [142]. The CNT has also been used as a reinforcement of carbon fibre filaments in order to enhance transverse mechanical properties of carbon fibre/epoxy composites [143]. The authors [144] showed a process to cure carbon fibre-CNT buckypaper (0.2 mm thickness)-bismaleimide hybrid composite specimen out of autoclave. Li and Chou [145] used a network of CNT to monitor the damage behaviour within an epoxy/glass fibre system. Significant enhancement of thermal conductivity has been observed in epoxy-based adhesive due to the inclusion of CNT [146]. Authors [11] reinforced epoxy adhesive with rGO and reported an improvement in tensile strength and maximum strain. GANS are also being suggested as reinforcements for metallic materials. For example, Bakshi et al. [147] used CNT to reinforce AlSi matrix to concluded a decline in thermal conductivity, Morka and Jackowska [148] demonstrated an enhancement in ballistic resistance in aluminium plate due to CNT reinforcement, Wejrzanowski et al. [149] reinforced copper with multilayer graphene to show thermal conductivity benefits, Rouhi et al. [150] reported enhancement in thermal conductivity in aluminium due to CNT reinforcements and Nouri et al. [151] prepared specimens of CNT reinforced aluminium composite to report stiffness/hardness improvements. Soldering efficiency can be improved by supporting SnBi [152] and Sn58Bi0.7Zn [153] with graphene. GANS based fillers are also playing a role as reinforcements in ceramic materials such as amorphous silicon nitride [154], piezo-silica [155], SiC [156] and alumina matrix [157–159]. Civil engineers are considering CNT/graphene as reinforcements to enhance the tensile strength of cement [160], to enhance vibrational properties in concrete [161], to improve fracture toughness in concrete [162], to enhance impact resistance of concrete [163] and also to monitor structural health in cement [164]. Civil engineers have also attempted to improve the vibrational characteristics of masonry arches by using GNP reinforced carbon prepreg [165]. Graphene–graphane composite nanomaterials have also been suggested and these are mainly useful in nanoelectronic devices [36]. Other reported combinations are graphene/boron nitride heterostructures [166], rGO/$BiVO_4$ to develop semiconducting electrodes [167], graphene/Ag-nanowire for electrical tuning [168], rGO/polyelectro-lyte solution for cardiovascular therapy [169], polyethylene oxide matrix (PEO)/GO for biomedical battery applications [170], MWCNT/Au for electrical switching applications, GO/Au for photoacoustic imaging [10], graphene and hBN (hexagonal boron nitrade) for thermal conductivity benefits, Pt/rGO for gas sensor applications [171], graphene-reinforced TiAl matrix for lubrication applications [172], Si/graphene for polarizer applications [173], Au–graphene–Ag for surfaced enhanced Raman scattering [174,175], carbon/CNT for micro scale electronic applications, E-glass nonwoven fabric/CNT network for damage detection [176], graphene/ZnO for photo-sensing applications [177], copper–graphene for biosensor applications [178], graphene reinforced CNTs for strain sensing applications [46] and polyurethane/CNT-graphene (hybrid fillers) for dielectric applications.

3. An overview of numerical methods available to study GANS and relevant nanocomposites

Although many researchers are making use of real-time experimental setups to understand the behaviour of materials involving GANS [179–183], numerical and analytical methods are always the best alternatives, due to various reasons. The reasons include; no established supply chain for such materials, material preparation is labour-intensive, experimental set up is cost-intensive, handling of materials at the nanoscale is a complicated task, and many of the materials are still theoretical in nature. Analytical methods [183–188] are limited to simplified geometries and idealised physical behaviours. Apart from FEM, molecular mechanics/molecular dynamics (MM/MD) based tools are being widely used [183,186,189–198] to simulate materials relevant to GANS. In the MM algorithms, the equilibrium configurations of the molecular domain is obtained by minimising energy [196], whereas in the MD algorithms, the momentum equations involving interatomic forces are integrated over time [196]. Typical commercial tools available include LAMMPS, AMBER, GAUSSIAN, HyperChem, Materials Studio and TINKER. Other numerical methods include Ritz method [199], element-free kp-Ritz method [200,201], boundary element method [202,203], discontinuous Galerkin time-domain (DGTD)

[204,205], differential quadrature method (DQM) [206,207], distinct element method (DEM) [208], discrete singular convolution (DSC) method [209], finite difference method [210,211], finite strip method [212], incremental harmonic balanced method [213], Galerkin strip distributed transfer function method [214], shear-lag model method [215], nonlocal elasticity theory [216,217], density functional theory (DFT)[218], spectral element method [219], moving-least squares meshfree Galerkin method [188] and finite prism methods [220].

4. FEM as a material design tool to study GANS and relevant nanocomposites

The idea of implementing FEM to understand the physical behaviour at atomic and subatomic scales can be traced back to the year 1998, when Abraham et al. [221] used FEM to simulate the influence of macroscopic brittle fracture on the quantum mechanics of silicon. However, this methodology involved the coupling of FEM with atomistic MD and the quantum tight-binding (TB) method. After this, many other authors [82,222–226] coupled MD/MM with FEM to link nano-scale behaviour with macro scale behaviour. Furthermore, Pantano et al. [227] combined TB with FEM to identify the electromechanical characteristics of CNT. Xu and Liao [228] measured deformation of graphene sheets using both MD and FEM and concluded a mismatch in results as low as 5%. In addition, Arroyo and Belytschko [229] performed twisting studies on CNT using both FEM and MM tools and reported that both tools output identical twisting angles and strain energies. Furthermore, Chen and Cao [230] used both MD and FEM to simulate bending and twisting strain energies in SWCNT and concluded a correlation between these two methodologies. This indicates that the FEM acts as a reliable tool even at atomic scales. There is also an evident correlation between FEM and experimental results [231–234] and between FEM and analytical results [233–238]. FEM has also been used to post-process results from the experimental analysis, for example, Lee et al. [239] measured strain in SLGS and MLGS from Raman spectroscopy and then calculated the Young's modulus using FEM. An online survey about the number of publications that used FEM as a tool to simulate the behaviour of GANS and associated nanocomposites has been done here. In total, 835 articles have been identified. The compiled data encompasses from the year 2001 to 2018, and is shown in terms of a yearly histogram in Fig. 2. Majority of these publications considered CNT based GANS materials. As per the online survey conducted here, the year 2001 witnessed first five publications [228,240–243] that implemented FEM to understand the behaviour of GANS materials, 3 being on CNT and other two being on graphene sheets. One of these five publications, Choi et. [240] used FEM software, OPERA-3D to study the electric field distribution in CNT based triodes. Similarly, Ito et al. [241] also used FEM to calculate electric field distribution in CNT based triodes. Liu et al. [242] used the FE code ABAQUS to calculate rippling mode shapes in CNTs. Seol et al. [243]

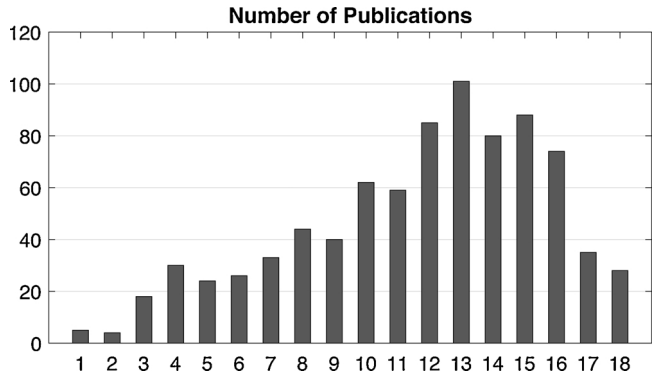

Fig. 2. Yearly growth of publications relevant to 'FEM in GANS research' from 2001 to 2018.

used the FE code ANSYS to calculate the thermal conductivity in graphene and displayed a correlation against analytical/experimental results. As previously mentioned, Xu and Liao [228] used MD, closed-form elasticity solution and the FEM to predict the deformation in a circular graphene sheet and reported acceptable levels of agreement among all three methods. In 2002, four publications [91,244–246] have been witnessed in the survey. All of these four publications cover the structure mechanical aspects of GANS based materials. As per Fig. 2, the number of publications has grown substantially since the year 2002. This indicates that the FEM is playing a vital role in the design of GANS based nanomaterials. Although the FEM has been used to simulate the electrical [22,26,30,87,135,247–252], electronic [240,241,253–263], gas transportation [264], mass transportation [265], microwave propagation [266,267], electrochemistry [167,268–270], electromechanical [271,272], semiconducting [273], solar energy [274], magnetic [275–278], electrostatic [279], piezoelectric [280,281], soldering [282], super-capacitance [53,283] and optical [284–291] characteristics of GANS based materials, the rest of the present article will predominantly focus on the literature that involves structure mechanics and thermal aspects of these nanomaterials. However, non-mechanical aspects of these nanomaterials will be briefly discussed in Section 6.

Modified variants of FEM are also being used as tools to design GANS materials, such as spring-based FEM (SpFEM) [292–296], nonlocal FEM [297–299], semi-continuum FEM [73], spectral FEM (SFEM) [300,301], extended FEM (XFEM) [162,302], global–local FEM [81], scaled boundary FEM (SBFEM) [303], atomic-scale FEM (AFEM) [304], object-oriented FEM (OOFEM) [147] and control volume FEM (CVFEM) [66]. Spring-based FEM involves spring elements to represent C—C covalent bonds. These elements are line elements offering all 6 degrees of freedom (DOF), and the element properties were derived from interatomic force constants of bending, stretching and torsion. This method of representing C—C bonds is similar to the ones used by the majority of other authors [233–236,305]. Nonlocal FEM [297] involves developing Mindlin plate equation of motion based on nonlocal elasticity and then solving this equation by FEM. The authors [73] performed structural analysis on a polymer/SWCNT nanocomposite and termed their method as a semi-continuum method since the SWCNT was represented by a lattice structure and the matrix was represented as continuum structure. The SFEM is suited for solving structural analysis problems in the high frequency domain and involves deriving the total energy-governing equation by minimising potential energy in a frequency domain. The authors [300,301] choose SFEM since the CNT based composite structures in their studies were subjected to high-frequency oscillations. The XFEM is able to extend the solutions obtained by FEM to discontinuous functions found in cracks. Due to this reason, the authors [162,302] used XFEM to study fracture behaviour in GANS materials. The authors [81,301] referred to their method as Global–Local, since initially, the entire nanostructure with a crack was analysed with a coarse mesh and displacement fields from this initial analysis was used to evaluate stress fields in a submodel involving finer mesh around the crack tip. SBFEM is a combination of BEM and FEM, that is useful in the analysis of probabilistic fracture in pre-cracked graphene sheets [303]. The AFEM offers the same level of accuracy as by MM method, yet less computationally expensive and is based on resolving stiffness matrix at each discrete atom [304,306]. OOFEM is a special purpose algorithm offered in the OOF2 software developed by the National Institute of Standards and Technology (NIST) [147]. This software is able to read the scanned images of microstructures and automatically generate FE meshes. Song and Youn [66] chose CVFEM in order to solve elliptical type partial differential equations that represented an RVE involving CNT, air and epoxy matrix. Similar to the Eulerian representation of the fluid flow and heat transfer in a controlled domain, CVFEM applied to a nano RVE [66] is dependent on the law of conservation.

The FEM has also been used as a tool to guide the processes of synthesising GANS materials. The FEM based codes can be used to

optimise and control the process parameters that govern the synthesising processes. For example, Alig et al. [118,139] used FEM to calculate the electric field required for optimum crystallisation of polymer/MWCNT composites. Kim et al. [32] used FEM to calculate the temperature in MWCNT during the process of extracting graphene nano-ribbons from MWCNT. Shenoy et al. [307] used FEM to simulate curling in graphene sheets in order to synthesise nanodevices. Lee et al. [20] used FEM code COMSOL to determine the electrostatic field required to reduce graphene fluoride to graphene. Luxmore et al. [308] implemented FEM to calculate charge density, electric field and temperature in graphene during the process of synthesising it from CVD and then fabricating it into field-effect transistors. With the aid of the FEM tool ABAQUS, Cao et al. [309] optimised the parameters that govern the fracture of bonding between graphene sheets and Cu/Si substrates during the CVD process. Han et al. [9] used FEM to calculate the thermal conductivity of graphene sheets in order to facilitate the process of reducing these sheets and then fabricate an rGO/epoxy composite. Nguyen [144] simulated heat transfer in pre-cured carbon fibre prepreg/CNT composite using FEM in order to facilitate an out of autoclave process to cure the composite system. Jang et al. [310] identified the failure modes in graphene sheets that might occur during the process the roll to roll transfers to CVD substrates, with the aid of FEM.

4.1. Finite element modelling strategies for carbon nano materials

The most widely used modelling strategy to represent graphene sheets and CNT has been the method of lattice space frame structure [95,233–236,245,305,311–319]. This methodology is based on the fact that the way the carbon atoms are arranged in hexagonal chicken wire fashion resembles a macroscopic space frame structure. Within the FEM, each carbon atom can be represented by a node and the covalent bond can be represented by a finite element. In the literature, there has been a general trend to represent carbon-carbon sp^2 as Timoshenko beams offering axial, out-of-plane and in-plane rotational degrees of freedom. The harmonic potential of these beam elements (C—C bonds) can be derived by [320–322]:

$$U_r = \frac{1}{2}k_r(\delta r)^2 \quad U_\theta = \frac{1}{2}k_\theta(\delta\theta)^2 \quad U_\tau = \frac{1}{2}k_\tau(\delta\varphi)^2 \tag{1}$$

Then the mechanical properties of the C—C bond such as E (Young's modulus) and G (shear modulus) can be determined with the aid of a beam mapping technique, enforcing the equivalence between the harmonic potential and the mechanical strain energies of a hypothetical structural beam of length L [323]:

$$\frac{k_r}{2}(\delta r)^2 = \frac{\mathrm{EA}}{2L}(\delta r)^2 \tag{2}$$

$$\frac{k_\tau}{2}(\delta\varphi)^2 = \frac{\mathrm{GJ}}{2L}(\delta\varphi)^2 \tag{3}$$

$$\frac{k_\theta}{2}(\delta\theta)^2 = \frac{\mathrm{EI}}{2L}\frac{4+\Phi}{1+\Phi}(\delta\theta)^2 \tag{4}$$

The stretching and axial deformation mechanism are governed by Eq. (2), while the torsional deformation of the Timoshenko beams (C—C bond) is governed by Eq. (3). Eq. (3) helps in calculating the pure shear deflection of the structural beam leading to an equivalent shear modulus G. Eq. (4) accounts for the shear deformation in the cross-section. For circular cross-sections, the shear deformation constant can be expressed as [323]:

$$\Phi = \frac{12\mathrm{EI}}{\mathrm{GA}_s L^2} \tag{5}$$

In Eq. (5), $A_s = A/F_s$is the reduced cross section of the beam by the shear correction term F_s [324]:

$$F_s = \frac{6+12\nu+6\nu^2}{7+12\nu+4\nu^2} \tag{6}$$

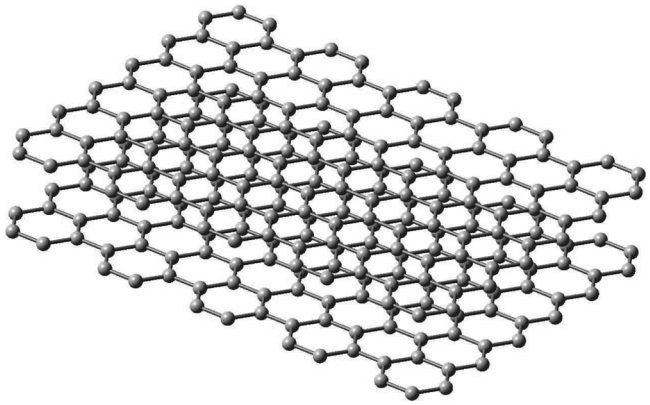

Fig. 3. Finite element based representation of bi-layer graphene. Carbon atoms and covalent bonds are represented by FE nodes and FE beams, respectively. The image is from Ref. [236].

The insertion of Eqs. (5) and (6) in Eq. (4) leads to a nonlinear relation between the thickness d and the Poisson's ratio ν of the equivalent beam [323]:

$$k_\theta = \frac{k_r d^2}{16}\frac{4A+B}{A+B} \tag{7}$$

where

$$A = 112L^2k_\tau + 192L^2k_\tau\nu + 64L^2k_\tau\nu^2 \tag{8}$$

$$B = 9k_r d^2 + 18k_r d^4\nu + 9k_r d^4\nu^2 \tag{9}$$

The values of the Morse force constants are $k_r = 8.74\times10^{-7}\,\mathrm{N\,mm^{-1}}$, $k_\theta = 9.00\times10^{-10}\,\mathrm{N\,nm\,rad^{-2}}$ and $k_\tau = 2.78\times10^{-10}\,\mathrm{N\,nm^{-1}\,rad^{-2}}$. The equivalent mechanical properties of the C—C bond can be calculated by performing a nonlinear optimisation of Eqs. (2)–(4) using a Marquardt algorithm [325][326]. The C-C bond can then be modelled as a two-noded FEM beam with a stiffness matrix described in [3], where the nodes represent the atoms. Such a finite element based beam representation of bi-layer graphene system can be seen in Fig. 3. Apart from the most common method described here; some authors used axisymmetric shell elements [228], membrane type shell elements [244], 3D brick elements [91,92,98,157,158,237,327–329], hexagon element with six nodes [330], quadratic (8-node) axisymmetric ring elements [331], 4-noded axisymmetric elements [332], 4-node plane-quad elements [69,93,147,231,242,333], shell finite elements [334–339], tria elements [340] and a single line of 3D line-beam elements [68,100,341] to represent GANS nanostructures. Furthermore, Nasdala and Ernst [342] formulated a novel 4-noded element to represent hexagonal atomic structures of CNT/graphene and implemented in commercial FEM codes FEMAP and ABAQUS. Similar to the numerical method discussed above, the derivation of this 4-noded novel element type is also based on bond stretching and bending force fields. However these element types involved translational DOF only and were able to represent interatomic energies with higher levels of accuracy. To model C—C bonds, Nasdala et al. [343] recommended to using beam elements with no rotational DOF and to use novel 2-, 3- and 4-noded elements in case of large deformations. Typical codes being used are ABAQUS [93,237,328,329,336–338], COMSOL, ADAGIO [67], ANSYS [71,98,316,320], MSC Marc [344], FEniCS [52], ALGOR [49] and also non-commercial FEM codes [133,229,317].

4.2. Element types for modelling nanostructures

Apart from using beam elements to model C—C bonds (described previously in Section 4.1), researchers have used various other element types to model C—C bonds and carbon nanostructures. This section will review various element types adopted by the researchers to represent

carbon nanostructures such as graphene, carbon nanotubes and graphyne. As per the literature reviewed here, the element types adopted by the researchers can be classified into 8 categories as listed below:

1. CC-Beams: Under this category, researchers have used beam elements to represent covalent bonds (C—C) in the carbon nanostructures.
2. CC-Springs: Under this category, researchers have used spring elements to represent covalent bonds (C—C) in the carbon nanostructures.
3. CC-TRF: Under this category, researchers have adopted truss or rod or frame elements to represent covalent bonds (C—C) in the carbon nanostructures.
4. Equiv-BTS: Under this category, researchers have used an equivalent beam or truss or frame elements to represent an entire carbon nanostructure.
5. 2D-Elem: Under this category, researchers have adopted two-dimensional planar elements to represent an entire carbon nanostructure.
6. Shell-Elem: Under this category, the researchers have used shell elements to represent an entire carbon nanostructure.
7. 3D-Elem: Under this category, researchers have used three dimensional solid elements to represent an entire carbon nanostructure.
8. Axisym-Elem: Under this category, researchers have used axisymmetric elements to represent an entire carbon nanostructure.
9. Spec-Elem: Under this category, researchers have adopted special-purpose customized elements to represent carbon nanostructures.

The statistical analysis in terms of a histogram representing the number of research articles implementing each of the above eight categories is shown in Fig. 4. As per the number of articles surveyed in the current article, the majority of the research articles implemented a space frame type finite element model to represent carbon nanostructures, wherein the C—C bonds were represented by beam elements. The number of articles that used such discretization method is 158(marked as CC-Beams in Fig. 4). For this purpose, both Euler Bernoulli and Timoshenko beam element types have been found in the literature. The ability to model tension, bending and torsion of C—C bonds is the main advantage of these beam elements [311]. Other benefits include simplicity and computational efficiency. It is a straight forward approach to link computational chemistry with computational structural mechanics. However, there are disadvantages associated with this modelling approach. The occurrence of beam element bending under CNT/graphene linear deformation is a disadvantage. Another disadvantage is the irrelevance of the beam element geometrical properties to the nature of chemical C—C bonds [345]. In the current survey on publications, 36 research articles that make use of spring based finite elements to represent C—C covalent bonds, have been identified(marked as CC-Springs in Fig. 4). The spring element-based approach can overcome the above-mentioned disadvantages of the beam element approach. The spring-based approach [292] involves using 12 spring elements to represent one hexagonal lattice of graphene, wherein 6 spring elements are used to model translations and the other 6 spring elements are used to model angular variations. The spring constants of these spring elements can be derived using k_θ and k_θ (Section 4.1). The spring-based approach is more appropriate to model non-linear behaviour of carbon nanostructures, as compared to beam-based approach [345]. The researchers have also used truss, rod and frame elements to represent C—C bonds. The current literature survey has identified 13 publications that used these elements (marked as CC-TRF in Fig. 4). For instance Scarpa et al. [323] used braced truss elements to model C—C bonds. Similar to spring-based model, this braced truss model also featured 12 elements to represent one hexagonal cell of graphene. Wherein, 6 truss elements simulated stretching and the remaining 6 truss elements simulated in-plane bending. The beam, spring and braced truss based models of a hexagonal cell of graphene are shown in Fig. 5. Another popular concept is to use a series of beam or truss or spring elements to represent carbon nanostructures. The current survey has identified 27 publications that made use of such concepts (marked as Equiv-BTS in Fig. 4). In the literature, finite element models have also made use of 2D elements such as plate, plane stress, and plane strain types. The current survey has identified 66 publications that made use of such a modelling approach (marked as 2D-Elem in Fig. 4). Other element types found in the literature are 3D solid elements such as hexahedral and tetrahedral (103 publications), axisymmetric elements (10 publications) and special-purpose elements (34 publications).

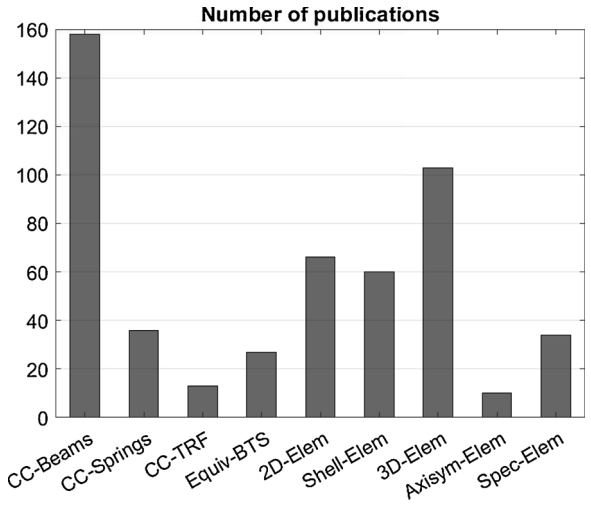

Fig. 4. Statistics on publications until 2018: various element types used to represent carbon nanostructures.

4.3. Thickness of graphene

In the case of developing atomistic finite element models, it is a common practice to calculate the thickness of beam elements using the expressions shown in Section 4.1. The element thickness in the form its diameter d can be calculated, while the constants k_r, k_θ and k_τ are known. The values of these constants in AMBER or MORSE format are available in the literature [346]. This requires the cross-section of the element representing C—C bond to be assumed as circular. It is important to note that the computational models of nanostructures with such element thickness d have been validated against experimental and analytical studies [233–236,318,319]. Therefore it can be concluded that it is appropriate to calculate d the thickness from MORSE or AMBER force fields and implement in atomistic models. However, if the carbon nanostructure is being represented by continuum elements such as shell or plate, it is conventional to assume the thickness to be 0.34 nm [347,348]. This thickness of 0.34 nm is derived, based on the interatomic/interplanar distance between carbon atoms in a multi-layer graphene system. However, there seems to be a scatter among theoretically and numerically determined thickness values of graphene sheets. This challenge of standardizing a physical sheet thickness along with its mechanical properties has been referred to as Yakobsons paradox [305,349] within the scientific community. Several measurement studies using the atomic force microscopy indicate that the thickness of single-layer graphene can vary between 0.4 and 1.8 nm, depending on the type of synthesis [350]. The thickness of single-layer graphene or/and single wall CNT considered by several publications are shown in Table 1. As per this data, the thickness can be as low as 0.066 nm and as high as 0.5 nm. It is important to note that the sheet mechanical properties also influence the results of finite element models, but not only the sheet thickness. The majority of these publications (shown in Table 1) considered 0.34 nm as the nanosheet thickness. Therefore, it

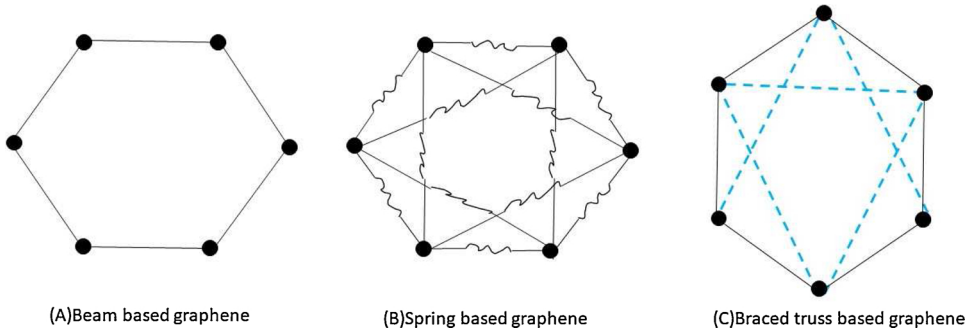

Fig. 5. Beam, spring and truss based models from [323,345].

Table 1
The thickness of graphene as used in literature: few selected publications.

Source	Thickness(nm)
Lee et al. [351]	0.335
Yakobson et al. [352]	0.066
Hernandez et al. [353]	0.34
Pantano et al. [354]	0.34
Pantano et al. [355]	0.075
Pantano et al. [227]	0.075
Lu [356]	0.34
Odegard et al. [245]	0.69
Gupta and Batra [347]	0.34
Wei and Kysar [348]	0.335
Song et al. [357]	0.34
Huang et al. [120]	0.34
Huang et al. [119]	0.34
Zhang and Rodrigue [358]	0.066
Baykasoglu and Mugan [359]	0.34
Baykasoglu and Mugan [360]	0.34
Chen and Liu [327]	0.4
Zhou et al. [69]	0.34
Gil et al. [361]	0.32
Arash et al. [362]	0.34
Niaki et al. [363]	0.34
Hartmann et al. [364]	0.132
Jiang et al. [365]	0.35
Zhu et al. [366]	0.5

can be concluded that the continuum models of graphene and CNT involving shell or plate elements can assume 0.34 nm as the thickness.

4.4. Remarks on continuum mechanics-based models

As commented previously, computational simulations has brought significant progress in relation to the understanding of the mechanical behaviour of graphene and its associated nanostructures. Among the main numerical approaches found extensively in the current literature, the atomistic approach [367,368] enjoys of great popularity. Within this category, classical molecular dynamics [369] is probably one of the most popular techniques. Despite these numerical approaches have achieved great success in capturing complex deformation mechanisms in atomistic problems, they suffer from the inconveniences of excessive overall computational times. Therefore, their use has been restricted to the study of small to moderate size atomistic systems [370]. A second category is the FEM, the approach treated in this paper, which consists of establishing an equivalence between the atomic and mechanical energies at the C−C bond level. In simple terms, FEM provides a way to model the deformation of graphene and general nanostructures within a continuum mechanics-based framework, representing an alternative route to model larger nanostructures at much reduced computational costs and memory requirements.

In particular, the use of unidimensional FE elements provides advantages on bidimensional FE elements due to their inherent capabilities to capture local information at atomic levels. Contrary to continuum shell element formulations, the discrete nature of a two-noded geometric representation enables it to retrieve data from individual atoms and from interatomic forces, and allows the consideration of possible defects or inclusions in the atomic structure. Moreover, when small length scale effects cannot be neglected (for instance, in small atomistic systems), the applicability of continuum shell-type models may become questionable.

We must note that computing times may increase significantly when modelling nanostructures subjected to large levels of deformation. This issue may also restraint the use of molecular dynamics models due to the prohibitive computational times involved in the analyses. Nevertheless, FE models have overcome these limitations when modelling nanostructures subjected to large deformations ([370,371], among many others). We note that the importance of large strains and geometric non-linear effects in graphene has been reported [372], and experimental evidence of the non-linear deformations present in graphene has also been published [351].

In general, the mechanical modelling of graphene and nanostructures relies on the fundamental assumptions implicitly made in continuum mechanics. Here, materials are assumed to be continuum, that is, matter is continuously distributed in the body with a geometry well-known and established, and fills the whole volume it occupies. However, at nanoscale levels, this assumption can be questionable due to the lack of physical representation of covalent bonds between neighbouring atoms. Furthermore, basic concepts like surface forces or stresses can be defined on the surface of a body as long as mechanical contact exists between bodies, or within portions of the body as a result of the mechanical interaction between the parts of the same body. Nevertheless, areas cannot be well-established if the fictitious body associated to the interatomic interaction is not well defined.

The above problem becomes worse when elasticity is adopted as the mathematical framework to describe the relationship between strains and stresses. Here, a classical parameter to describe the deformation of solid materials is the Poisson's ratio, which is defined as the quotient between the lateral contraction of a body subjected to tensile loading and its stretching along the longitudinal direction of loads. In the mechanical modelling of nanostructures, this material parameter does not have any physical interpretation since lateral contraction does not have a physical meaning in a covalent bond. This has resulted in a great variety of Poisson's ratios when modelling atomic systems by means of FE models. Refer, for instance, to Tables 6 and 7 . In spite of the above limitations, continuum mechanics-based modelling approaches have shown remarkable predictive capabilities. This has been noted and accepted widely within the scientific community, probably since Yakobson et al.'s pioneering work [352].

4.5. Multiscale methodologies

As mentioned previously, several authors [82,222–226,373] coupled MM/MD methods with FEM to capture physics at different length

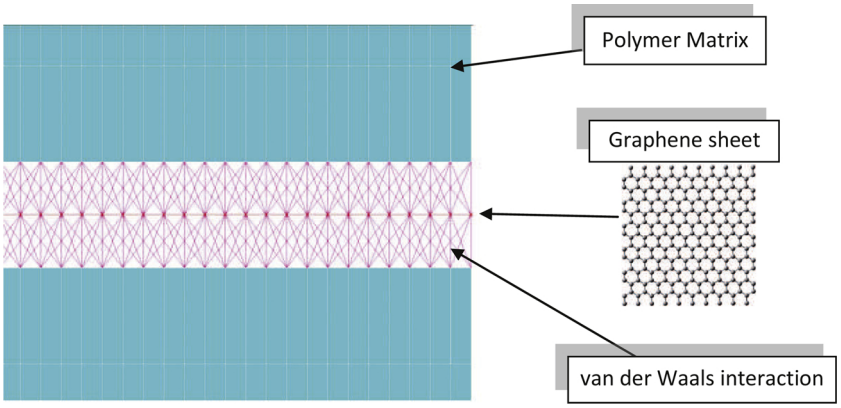

Fig. 6. Multiscale model of GRP: carbon atoms are represented by nodes, covalent bonds are modelled by Timoshenko beams, L-J potential is modelled by spring elements and the polymer matrix is formed by 3D solid elements. The image is taken from Ref. [319].

scales of GANS based materials. However, this section will focus only on the multiscale methods that use FEM purely. Wei and Kyskar [348] used a FEM based multiscale method (within ABAQUS) to link C−C interatomic behaviour with macroscopic deformations of graphene membranes. However, the majority of the researchers who used multiscale FEM used it to model GANS based composite structures [109,233,234,313,318,374]. Capturing nanoscale level physics for all of the constituent materials (matrix, interphase, fibre and filler) in a composite can be computationally expensive. Due to this reason, the problems are being simplified by considering some constituents such as matrix and fibres at the macro-scale level and nanofibres/interphase at the nanoscale level. In the case of carbon nanocomposites, majority of the authors [64,109,233,234,313,318,374] have used methodologies that involve representing graphene/CNT structures as lattice frame structure (shown in the previous section), interphase with a 1D spring element system and the matrix with the continuum 3D solid elements. This procedure has also been referred to a representative volume element method (RVE) or unit cell method. The RVE is shown in Fig. 6 Graphene/CNT nanostructure are connected to the matrix by means of van der Waals interaction forces, that can be defined numerically as:

$$F_{ij} = \frac{\partial V_{ij}}{\partial r} \tag{10}$$

where r is the atomic displacement along **ij** (fibre-matrix length). As per Girifalco et al. [375], the force between the atoms (ij) can also be represented in terms of Lennard Jones (L-J) potentials by

$$F_{ij} = -12\,\epsilon\left[\left(\frac{r_{min}}{y}\right)^{13} - \left(\frac{r_{min}}{y}\right)^{7}\right] \tag{11}$$

where $y = r_{min} + \delta r$, δr is the atomic displacement along the length **ij**. The r_{min} (in Å) is given by $2^{1/6}\sigma$, where $\sigma = (A/B)^{1/6}$. Here, B and A are attractive and repulsive constants associated to the corresponding boundary conditions, with values of 3.4×10^{-4} eV Å^{12} and 5×10^{-7} eV Å^{6}, respectively [375–377]. The constant ϵ is given by the expression $B^2/(4A)$. Within the multiscale models (RVEs), the nonlinear 1D spring elements such as SPRINGA (ABAQUS^{TM}) can be used to simulate this interaction, with an equivalent force-deflection curve given by Eq. (11). A Similar approach has also been used to represent the attractive and repulsive forces between adjacent layers of multi-layer graphene sheets [235]. The interface bonds (spring elements) between the nanofiller and the matrix can be deactivated if the deflection developed is greater than a cut-off distance (0.85 nm in case of polymer matrix) [233,234,318,374]. Also, new interatomic bonds can be regenerated if a displaced carbon atom comes in contact with another atom of the matrix. Saffar et al. [378] presented an alternative model, where all three constituents (matrix, filler and interface) are represented as separate sets of 3D beam elements. Some researchers have also assumed a perfect bonding between the matrix and nanofillers by either modelling a layer of solid 3D elements [95,104] or using shared nodes [70,88,91,92,100,155,237,313,331,379,380] or cohesive zone elements [108,143,328,339]. For example, Lusti and Gusev [63] used a tetrahedral mesh based RVE to represent a CNT/epoxy nanocomposite system, using a finer tetrahedral elements to represent CNT, coarser tetrahedral elements to represent epoxy resin, assuming perfect interface by shared common nodes between CNT/matrix and then enforced a periodic boundary conditions to calculate thermoelastic properties of the nanocomposite. Also, Dai and Liao [140] used hexahedral elements to represent both interface and CNT nanofiller but used tetrahedral and prism elements to represent a matrix. This has resulted in a significant reduction in computation time. Furthermore, Li and Chou [71] modelled entire RVE of wavy SWCNTS embedded in an epoxy matrix with 2D plane elements and predicted the material failure mechanisms. In order to reduce computational expenses, there is also a trend to represent the entire domain of GANS based nanocomposites by a finite element mesh that does not distinguish between nanofiller and matrix and interface [103,105,148,154,381]. This type of approximation becomes a necessity when physics to be simulated is numerically complex, as in the case of explicit dynamic simulation of machining of CNT/polycarbonate composite with a diamond tool [103,381].

Within the context of multiscale methodologies, most of the literature reviewed above use deterministic approaches. However, there exist various types of uncertainties in computational analysis of complex multiscale systems. They include but are not limited to, material parameters, boundary conditions, geometric description, modelling assumptions and numerical discretization techniques. Such uncertainties need to be taken into account for credible predictions arising from multiscale simulations. This can be achieved in a rigorous and mathematically formal manner using probabilistic or stochastic computation methods. In one of the earliest work, Scarpa and Adhikari [382] proposed a probabilistic approach to quantify uncertainty in the natural frequencies of single-wall carbon nanotubes (SWCNTs) arising from the variation in the equivalent material properties. Later the authors highlighted the role of geometric uncertainties in the dynamic analysis of SWCNTs. These works employed the Monte Carlo simulation technique, which can be computationally prohibitively expensive.

The use of computationally efficient surrogate models or metamodels [383] can have a significant impact in reducing the computational cost. One example of an efficient stochastic computational approach is an irregular tessellation technique [384] for carbon nanotube-reinforced polymers. The probabilistic approach has also been extended two-dimensional multiscale systems, where Young's modulus of graphene/polymer composites [385] has been obtained. Stochastic mechanics for multiscale materials is a growing topic and no doubt will play a significant role in the future. Mathematical, analytical and

computational methods for stochastic approaches are, however, fundamentally different from the deterministic methods, and therefore should be thoroughly and rigorously discussed. The readers can refer to [74,303,345,386–390] for more insight on stochastic analysis of nanostructures.

5. Micromechanical modelling of polymer nanocomposites

The multiscale methodology described in the previous section can be computationally intensive for the analysis that will involve large number of nanofillers or particles. Modelling individual atoms and associated covalent bonds under such circumstances will lead to larger numerical run times. Computational micromechanical models combining the concept of a representative volume element (RVE) with a FE technology enable to capture realistic nanocomposite morphologies (i.e. distribution/dispersion of nanoparticles) and provide a full-field resolution for strains and stresses. This section will briefly discuss the ideas and concepts of micromechanical modelling. Although, this section will make references to silicate nano particles, the methodology described here is equally applicable to carbon nano particles.

5.1. Background on micromechanics approaches for polymer nanocomposites

Micromechanical modelling offers a convenient approach for predicting the performance of nanoparticle-based polymer composite systems. That approach typically attempts to capture length and times scales within a wide range: nm-m, and s-min, and link the macroscopic response with underlying the material morphology/structure. In general, one can distinguish analytical and computational micromechanical approaches to predicting macroscopic nanocomposite properties.

Analytical micromechanical models combining Eshelbys single inclusion concept [391] and the Mori-Tanaka theory [392] became popular as efficient predictive means to study linear-elastic properties of polymer nanocomposites. Those approaches enable to account for some morphological features of the nanocomposites such as aspect ratio, volume fraction, or averaged orientation, and thus enable to predict the relationship between nanocomposite morphology and macroscopic properties (linear-elastic in the majority of cases) [393]. Lack of nonlinear effects (e.g. viscous), interactions (e.g. interfacial between polymer and nanoparticle), and accurate descriptions of nanoparticle dispersion and distribution, are some of the major limitations of those models. Some of those limitations can be resolved through relevant modifications such as: (1) averaging of properties of nanoparticle agglomerates [394–396] (see Fig. 7), (2) orientation averaging of the elasticity tensor [396,397] or (3) the application of multi-component models of the Mori-Tanaka type that can account for the presence of an inter-phase surrounding the filler [398].

On the other hand, computational micromechanics approaches typically involve notion of the representative volume element (RVE) concept [399] and computational homogenisation procedure [400] and offer means for performing a numerical analysis across different nanocomposite length scales. For problems involving uniform deformations, it is generally sufficient to predict the macroscopic response from the simulations with an RVE (with multiple realisations). However, when the macroscopic loads lead to non-uniform deformations, then a two-scale procedure (e.g. FE^2) should be used instead [401]. When combined with the FEM-based solution methodology, the RVE-based computational modelling approach can explicitly account for the description of the nanocomposite morphology, both in 2D and 3D [394,402–406]. Additionally, the computational micromechanics approach enables to account for nonlinear, finite strain, time- and temperature-dependent behaviour of the polymer matrix. Furthermore, that approach can be linked with another length and time scale such as molecular [404,405], to account even more accurately for relevant nanoparticle-nanoparticle and nanoparticle-polymer interactions, and results in a truly (sequential) multiscale modelling methodology (see Fig. 8).

Despite the availability of the computational micromechanics approach, only few research works have focused on the prediction of the nonlinear mechanical behaviour of polymer nanocomposites, including small-strain nonlinear mechanical properties [407], or damage processes [408–411]. Even a smaller number of scientific publications and research works has focused on large deformations, in the time-temperature window typical of processing of polymer nanocomposites [401,404–406,412–415]. Strong nonlinearity of those problems requires a robust computational framework to deal with large strains and rotations. Examples of applications of the computational micromechanical approach to polymer nanocomposites are summarised in the two subsections below, with the focus on modelling of large nonlinear deformations.

5.2. Modelling of interface

Currently, three main approaches are generally found in the literature to model the intermediate phase between the nanofillers or nanoparticles and the surrounding polymeric matrix. The first approach consists of modelling the interface through non-linear springs as described earlier. The second alternative consists of modelling the interface by means of an equivalent solid layer with specific thickness and material properties. This modelling procedure is quite straightforward and thus, skipped in the paper. The third modelling option is the use of Cohesive Zone Models (CZMs), normally adopted to describe the fracturing process occurring in the interface. CZMs can be described as a zero thickness interface transferring tractions t from one contact surface to another. These traction forces relate to the displacement jump of the interface $[u]$ by means of an evolution law, which can be expressed by a

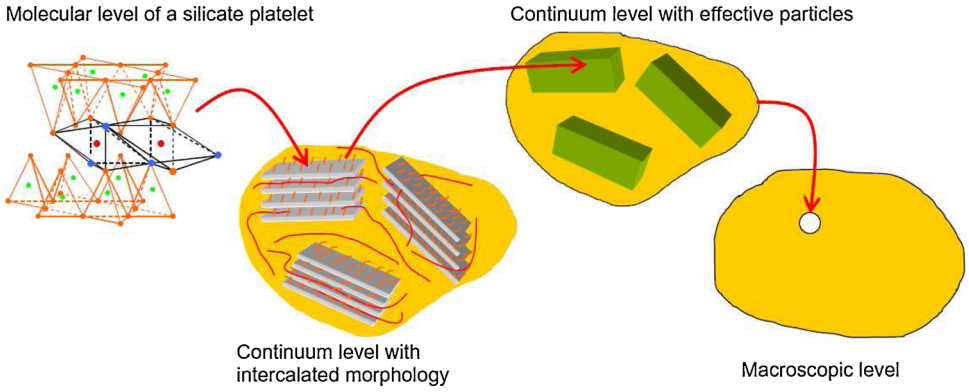

Fig. 7. Modelling methodology and associated scale transitions used in analytical micromechanical approaches for nanoplatelet systems [396].

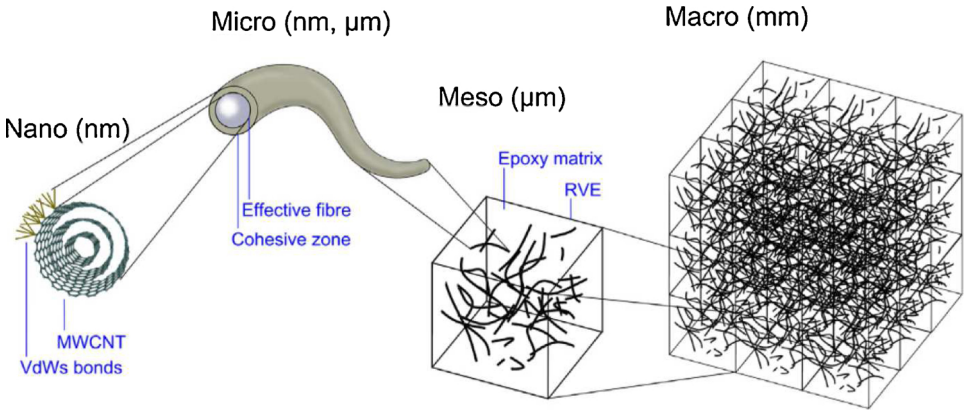

Fig. 8. High-fidelity multiscale modelling methodology [405].

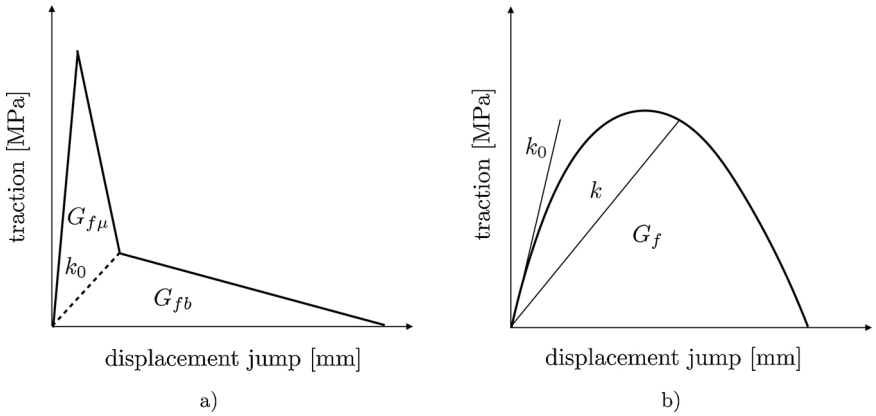

Fig. 9. Stress–displacement jump curves typically used for the modelling of the interface between fillers or particles and the surrounding matrix [416]. (a) Bilinear and (b) power softening laws.

damageable stiffness operator $k([u])$, as $t = k([u])[u]$ [416]. Stress-displacement jump functions typically used in CZMs are bilinear and power softening laws, as shown in Fig. 9. When the nanocomposite is loaded, the cohesive interface opens, and the initial interface stiffness k_0 is assumed to have no damage. Then, the stiffness decreases with respect to the displacement jump and becomes zero at some critical displacement threshold. Furthermore, a damage variable d can be used to represent the stiffness of the interface, i.e., $k = (1 - d)k_0$, with d ranging from 0 (healthy interface point) to 1 (completely damaged interface point) [416]. Further information on CZMs can be found, for instance, in [410,417].

5.3. Nonlinear computational micromechanics for nanoplatelet systems

In [413], the research effort concentrated on predicting the morphology evolution (in terms of nanoparticle reorientation) and strain-induced crystallisation under fast large deformation processes near the glass transition. For this purpose, an advanced computational micromechanics model was developed based on the RVE concept. The model linked a Monte Carlo-based morphology reconstruction tool, with a physically-based nonlinear constitutive model for the PET matrix near the glass transition, and computational homogenisation. Computational experiments predicted significant reorientation (alignment) of the nanofiller, which contributed to the enhanced macroscopic strain stiffening. It was found that the strain stiffening phenomenon was predominantly caused by the strain-induced crystallisation. Although the latter phenomenon also occurs for the unfilled PET, it was significantly enhanced by the presence of nanofiller. For example, the crystallisation phenomenon in the unfilled PET occurs at macroscopic strains equal to around 1.6 at the temperature 95 °C, and strain rate 1 s^{-1}. Additionally, the model predicted the effect of processing conditions (temperature, strain rate) on the morphology changes (see Fig. 10). However, as the relationship between the temperature, strain rate and morphology evolution is quite complex, the changes in morphology were equally attributed to the joint action of those two processing parameters. It is noteworthy to mention that the predicted trends in the macroscopic response of PET-organoclay nanocomposites were in a qualitative agreement with experimental results.

The nanocomposite model [413] was extended by Pisano and Figiel [414] to investigate the effects of nanoparticle agglomeration on the morphology evolution, and the macroscopic response. Hence, the morphology reconstruction procedure was extended to account for the presence of multi-nanoplatelet agglomerates. Based on molecular considerations, it was assumed that spaces between nanoplatelets within each agglomerate contain a mixture of short surfactant chains and bulk polymer chains. Based on experimental observations it was also assumed that the intra-agglomerate response is governed by interparticle slippage. The slippage was then described by a nonlinear traction-separation law within a cohesive zone concept. The law assumed that the intra-agglomerate slippage occurs under constant shear stress through continuously reforming van der Waals interactions. Simulations predicted that the onset of stress-induced crystallisation starts earlier with the decreased number of nanoplatelets in the agglomerate. Although the simulations predicted some significant changes in the agglomerate reorientation, a negligible effect of the agglomerate composition on its reorientation was predicted.

In [415], the computational micromechanics approach was further extended to study the effects of a polymer interphase on the morphology evolution and the macroscopic stress–strain behaviour during processing of polymer-nanoparticle systems. Monte Carlo algorithm

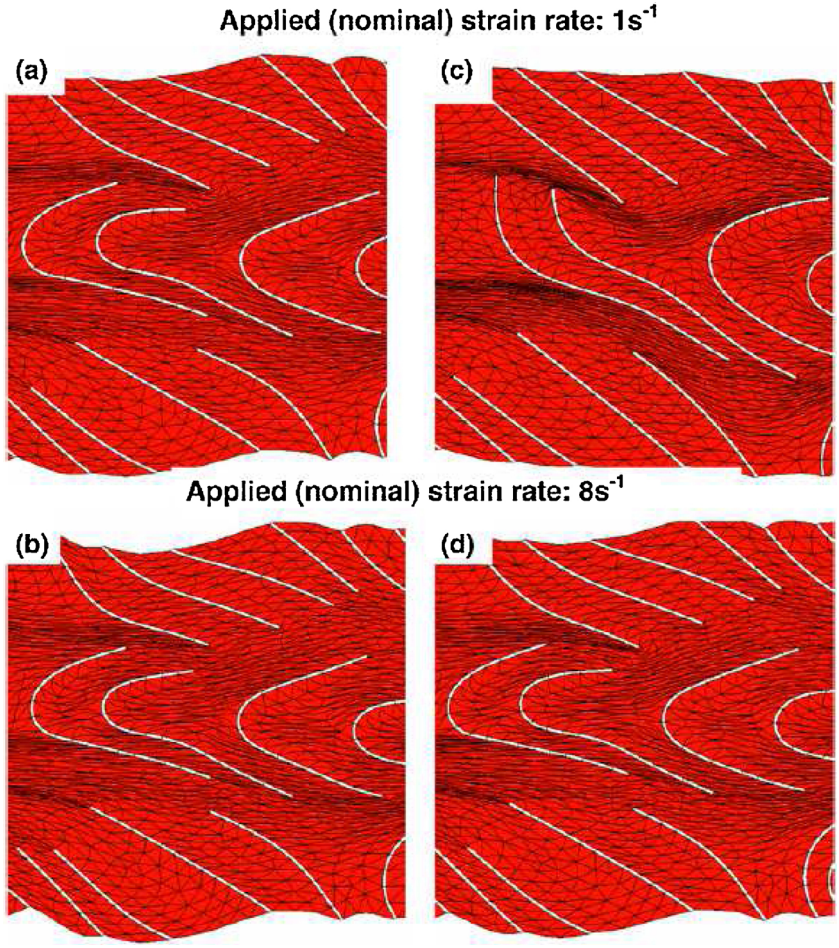

Fig. 10. Predicted impact of temperature and applied (nominal) strain rate on the nanocomposite morphology; volume fraction 5%; particle orientation: random; aspect ratio = 100; (a) and (b) T = 100 °C, and (c) and (d) T = 110 °C; applied (nominal) strain: 1 [413].

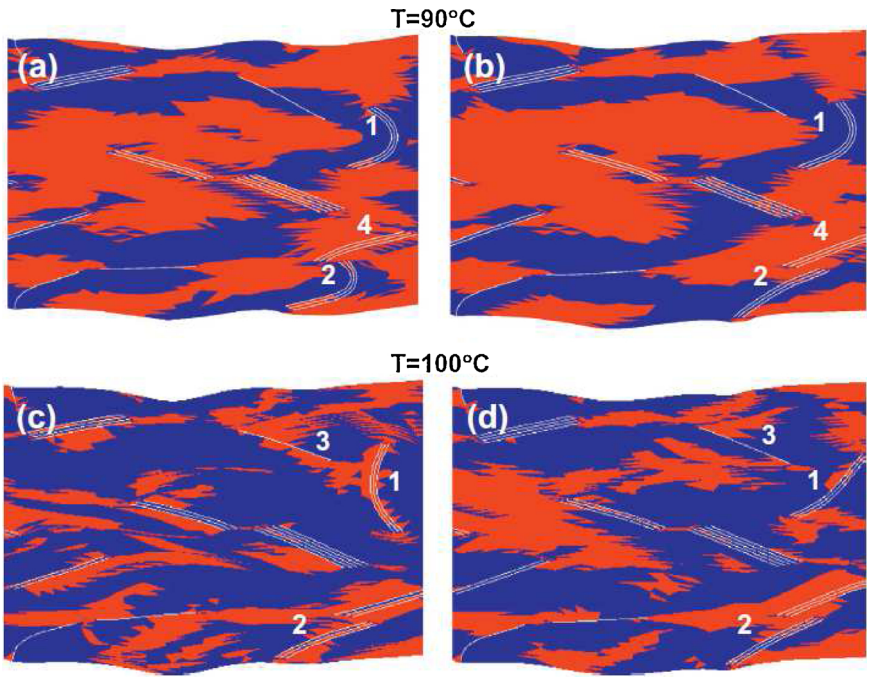

Fig. 11. Effect of the interphase on the size of regions undergoing the lock-up of viscous flow; (1) red colour: lock-up, (2) blue colour: no lock-up; (a) and (c) interphase; (b) and (d) no interphase; applied strain: 1.5 [415]. (For interpretation of the references to color in this figure legend, the reader is referred to the web version of this article.)

was developed to populate nanoparticles with an interphase within an RVE following a skew-Gaussian distribution, based on the experimental data. Physically-based constitutive model for the bulk polymer was modified to account for the change in the polymer mobility near the nanoparticle. Simulation results showed significant influence of the interphase on the overall stress-strain behaviour, and on the local domains undergoing stress-induced crystallisation. Thus, those results confirmed the importance of accounting for the interphase in determining accurately the nanocomposite stresses required for efficient processing. The influence of interphase on the size of regions is shown in Fig. 11.

5.4. Nonlinear computational micromechanics for nanotube systems

In [418] a finite-strain elastoviscoplastic behaviour was combined with an axisymmetric RVE, to predict the effects of the volume fraction and aspect ratio of single wall carbon nanotubes (SWCNT) on the energy absorption characteristics of epoxy-SWCNT systems under macroscopic compression, across the strain rates from quasi-static ($\sim 10^{-3}\ s^{-1}$) to impact ($\sim 10^{3}\ s^{-1}$). Perfect bonding was assumed between the SWCNT and epoxy matrix, so debonding and pull-out of SWCNT from the matrix were excluded as energy dissipation mechanisms. Simulations predicted macroscopic compressive stress-strain curves for different CNT volume fractions and aspect ratios, at different strain rates, and used to calculate the energy absorption characteristics. A significant correlation between the strain energy of the nanocomposite and CNT volume fraction was predicted by the model. The results also showed that the strain hardening of the nanocomposite, which occurs in the post-yield stress–strain regime, has the largest influence on the nanocomposite strain energy.

In [404], a fully 3D computational micromechanical model was developed for epoxy-CNT systems, to compare the effect of spatial orientation of CNTs in epoxy matrix on the nonlinear macroscopic stress-strain response under compression. 3D nanocomposite morphologies were generated using a Monte Carlo simulation tool. The uniform distribution was used for the generation of CNT orientation and dispersion in the epoxy matrix. SWCNTs were modelled as homogenised, straight (non-wavy) solid fibres, which proved to be computationally more efficient than using a tubular representation of SWCNTs. The 3D RVEs were combined with the nonlinear constitutive model for the epoxy, to capture large nonlinear and rate-dependent deformations of the epoxy matrix in compression. Perfect bonding between the SWCNT and epoxy was assumed. A strain hardening behaviour was predicted in the post-yield stress-strain regime for the nanocomposite with aligned CNTs this was in contrast to the results obtained for RVEs containing randomly oriented and distributed CNTs, where strain softening was initially predicted in the post-yield, which then changed to the strain hardening at large strains. The results showed that the CNT alignment has the largest influence on the nanocomposite stress–strain curves. Simulation results for 3D models were also compared with 2D models to reveal possible differences between the two approaches. It was concluded that only 3D models can account accurately for the nanoparticle morphology, and thus nanoparticle shape and orientation. This resulted in a more accurate interactions between the polymer and CNT, and as a result, it led to a more accurate description of the stress transfer from the matrix to CNTs, and thus of the macroscopic stress-strain behaviour.

In [405], a 3D nonlinear computational micromechanics model was proposed to account for the effects of CNT waviness and imperfect bonding at the polymer-CNT interface. The CNTs were modelled as wavy, multi-wall, and their mechanical behaviour was approximated as linear elastic, and transversely isotropic. The van der Waals interactions between the polymer and CNT were described through a bilinear cohesive model, and its parameters were defined based on available results of molecular dynamics simulations, and the Lennard-Jones potential. The finite strain compressive response of epoxy was described by the finite-strain elastoviscoplastic constitutive model. Computational experiments predicted that increasing CNT mass fraction increased the nanocomposite modulus for both, perfectly and imperfectly (van der Waals) bonded CNTs. Those results also showed that the stress transfer across the epoxy-CNT interface is limited in the case of van der Waals interactions. Particularly, the simulations predicted that a threefold increase in Young's modulus can be achieved through modification of the interface properties from imperfect (van der Waals) to perfect bonding. Then, the simulations predicted an increased nanocomposite yield peak with increasing CNT mass fraction. A nonlinear relation between the CNT loading and the yield peak stress was predicted for the van der Waals-driven interfacial interactions. Then, it was found that the effect of van der Waals bonding has the greater magnitude when compared to the effect of CNT waviness. Interestingly, van der Waals bonding did not affect the yield peak by the same magnitude. In terms of energy absorption capabilities, the modelling results suggested to use defect-free and straight CNT, well-bonded to the epoxy matrix this combination is expected to lead to a linear relation between CNT mass fraction and yield peak stress. Generally, the stress-strain curves predicted by the nanocomposite model were in a good qualitative agreement with experimental results. The model with the van der Waals bonding underpredicted the experimental results, while the model with perfect bonding slightly overpredicted experimental data, for both mechanical quantities, i.e. Young's modulus and yield peak stress.

5.5. Issues of agglomeration and extension to macroscale

The majority of the research carried out on multiscale (micro/RVE-to-macro) modelling of CNT systems has focused on well-dispersed systems and uniform distribution of microstructure. This has allowed the researchers to exploit the computational homogenisation approach [400] to predict the macroscopic behaviour of CNT systems. In this framework several assumptions have been made for computational convenience such as global periodicity of the micro/nanostructure, or macroscopically uniform deformations. In these cases, the predictions have been obtained from the study of an RVE problem. However, this can lead to significant inaccuracy if the micro/nanostructure is far from globally periodicity as shown by experimental evidence, where composite domains exhibit a non-uniform microstructure, where the degree of CNT agglomeration can vary throughout the composite system. In those cases, a local periodicity assumption is at least needed, and a fully two-scale (micro/RVE-to-macro) [400] analysis is needed to improve the prediction accuracy. Ultimately, the multiscale procedure should also involve stochastic description of the microstructure [385], thus resulting in an accurate predictive multiscale analysis.

5.6. Issues of perfect bonding in micromechanical analysis

Micromechanical approaches can be used to predict the macroscopic properties of nanoparticle/polymer systems. However, they need to be linked with a nanoscale to include and define model parameters governing relevant phenomena such as molecular structure of nanoparticles, nanoparticle-polymer interactions, or existence of additional phases resulting from reduced/increased mobility of the polymer near the particles, or transcrystalline layers surrounding the nanoparticles. An example of such an approach is a three-scale hierarchical approach linking nano, micro and macro scales [394]. Here, the properties of nanoclay sheets were estimated from MD simulations [419], and were used as input in a micromechanical model based on the Mori-Tanaka theory to predict the macroscopic properties (that were compared with a full-field FE analysis). Further works in the literature are an extension of this framework, and enhance the definition of relevant parameters of analytical or numerical micromechanical models by adding relevant interactions and/or additional phases (e.g. interphase). Some of them extend even further by including stochasticity of the microstructure (e.g. nanoparticle distribution and agglomeration), or variation of

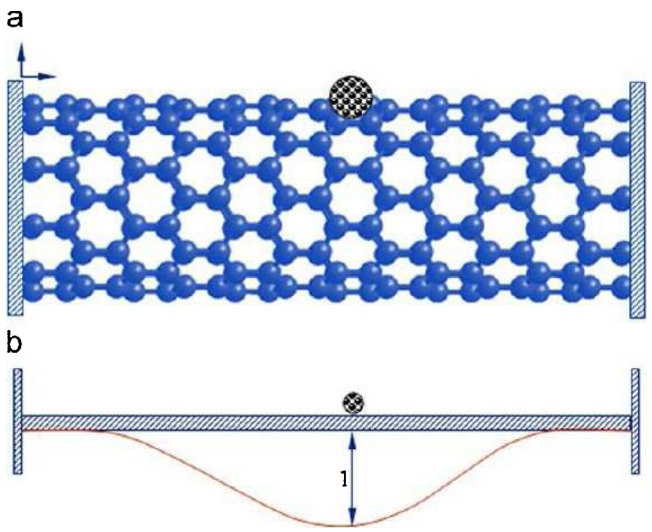

Fig. 12. The CNT based mass sensor developed by the Chowdhury et al. [434]. (a) Suspended mass on SWCNT (b) Approximation of SWCNT into a clamped beam.

elastic constants across the interphase [420]. Such an approach seems to be justified to predict linear elastic properties. However, a major challenge for those hierarchical approaches is that they cannot link various temporal scales, and thus various time-dependent deformation processes such as viscoplasticity. For nanoparticle-entangled polymer systems, this can be a significant challenge given their relatively wide spectrum of relaxation processes, especially when they undergo non-equilibrium processes when approaching their glass transition (see e.g. [415]). The issue of linking the multiple temporal scales and accounting for time-dependent deformation processes has not yet been resolved for nanoparticle-polymer systems, irrespectively of the nanoparticle type, and more research is still needed in this direction. The readers are referred to other relevant articles [385,421].

5.7. The concept of equivalent fibre

An equivalent-continuum approach has been proposed for CNT/polymer systems under small deformations by Odegard et al. [422], and it consists of two steps. In the first step, a relevant nanoscale RVE captures the atomic lattice of a nanostructure along with the interactions occurring at the molecular scale. In particular, an assemblage of discrete masses and corresponding interactions are replaced with a structural mechanics analogue consisting of structural elements (e.g. truss elements), that represent bond-stretching mechanisms. In the second step an equivalent-continuum model represented by an RVE is developed, such that the strain energy in the equivalent-continuum and molecular models are equal under the same loading conditions. Ultimately, the discrete lattice structure is replaced by an effective fibre (cylinder), and used in a micromechanical model and/or in finite-element simulations. A general sketch of the approach is shown in Fig. 3 of [422]. Using this concept, enhanced approaches have been developed for other nanoparticle systems such as graphene, and included van der Waals interactions at the interface and random distribution of microstructures see e.g. [385], and the references therein. However, there is a need to extend these approaches beyond linear elasticity, and time-dependent deformation processes. Readers are also referred to [423] for a comprehensive understanding of this subject.

6. Design of carbon-nano devices using FEM

Very high eigenfrequencies (measured beyond a THz), high stiffness (E measured beyond a TPa), high electron mobility, low electrical noise levels [171], hydrophilicity, mechanical stability, transparency, flexibility, low pull-in voltage [424], chemical stability and ability to adsorb biomolecules (due to π–π stacking) [425], offered by GANS materials, make them ideal candidate materials for sensing/switching applications. All of these properties of GANS based materials can be estimated using FEM, directly or indirectly. GANS based materials can be used in the construction of pressure sensors, strain sensors and mass sensors/resonators. FEM can aid the design and development of these sensors by predicting the behaviour of GANS based materials due to the applied pressure, strain and mass. Li and Chou [426,427] predicted the influence of pressure, mass and strain on natural frequencies of SWCNT using FEM, since a shift in the natural frequency can, in turn, determine the magnitudes of pressure, mass and strain. Similarly, Wu et al. [428] calculated natural frequency shift in SWCNT due to the applied mass in order to design SWCNT based mass sensors. Li and Chou [429] also used the natural frequencies calculated by FEM to justify the use of SWCNT and MWCNT as nano-resonators. Watkins et al. [430] used FEM to determine electric potential and electric conductivity in SWCNT/Ti/Au based electrodes in order to design structural health monitoring nanodevices for aerospace applications. Since MWCNT offers piezoresistability (change in electric resistivity under strain), FEM has been used to determine the deflection in PMMA/MWCNT due to the applied pressure in order to design pressure sensors [431]. Ray and Batra [137] proposed an SWCNT/piezoceramic matrix composite system in order to design an actuator that can control smart structures. The authors used FEM to calculate effective piezoelectric coefficients, effective elastic coefficients and variation of controllability, of SWCNT/piezoceramic matrix and PZT5H/epoxy piezocomposite, in order to prove that SWCNT/piezoceramic matrix offers exceptional damping. Sakhaee-Pour et al. [432,433] also linked natural frequencies (calculated by FEM) of SLGS to its ability to work a mass sensor, atomistic dust detector and strain sensor. Using the FEM, the authors [432] observed mass sensitivity of the SLGS to be as low as 10^{-6} fg and concluded that this sensitivity is highly influenced by the aspect ratio of SLGS, but not by the chirality. Similarly, Chowdhury et al. [434] also used the FEM to calculate natural frequencies of SWCNTs in order to design SWCNT nanoscale mass sensors. This concept the mass sensor is shown in Fig. 12. Li et al. [25] performed similar FEM analysis on the super carbon nanotubes and concluded the mass sensitivity to be as low as 10^{-24} g and strain sensitivity to be as high as 887 Hz/nanostrain. Furthermore, with the aid of FEM, a planar graphene sensor/resonator has been studied under several boundary conditions [435]. This study concluded that a combination of fully clamped boundary condition and the mass being at the centre leads to the optimum design of the resonator. As mentioned in Section 2.3, Li and Chou [145] demonstrated a damage detection technology using a network of CNTs within the glass fibre/epoxy composite, based a change in electrical resistance of CNTs due to damage strains. The authors used FEM to simulate the damage in the composite and also to predict the resulting variation in the electrical resistance of CNTs. Other investigations that made use of FEM to design GANS based devices can be found in [46,50,86,435–450].

7. Mechanical properties of GANS and relevant nanocomposites using FEM

Several researchers have used the FEM to predict mechanical properties of GANS based materials since the year 2003 [92,155]. The researchers have also correlated the numerically (FEM) predicted mechanical properties against those of experimentally and analytically determined values. In this section, we show the values of Young's modulus (E), Poisson's ratio (ν), shear modulus (G), mechanical strength (σ) and strain (ε), buckling strength (λ), vibration characteristics, fracture properties and damping parameters as predicted by various authors up to the year 2018. A subsection has been dedicated to each mechanical property, listing values predicted by authors in tables.

Table 2
Predicted Young's modulus E (TPa) of graphene using finite element method (FEM).

Graphene type	E	Type of FEM	Source
SLGS	1.03	SF	[311]
SLGS	1.17	SF	[316]
SLGS	0.99	SF	[459]
SLGS	1.08	SF	[460]
SLGS	1.04	SF	[461]
SLGS	1.00	SF	[323]
Flakes	1.45	SF	[462]
GO	0.20	Coupled AFM/FEM	[7]
SLGS	1.13	SF	[463]
SLGS	1.07	SF	[464]
Nanoribbon	0.74	SpFEM	[465]
SLGS	0.74	SpFEM	[294]
Nanoribbon	1.05	SpFEM	[466]
Nanoribbon	1.8	SF	[467]
SLGS	1.01	SF	[468]
SLGS	0.35	Coupled MM/FEM	[359]
SLGS (defected)	0.74	SpFEM	[469]
SLGS	1.19	SF	[470]
SLGS	1.0	SF	[471]
Pillared graphene	0.19	SF	[43]
SLGS	1.02	SF	[472]
SLGS (defected)	1.6	SF	[473]
SLGS	1.15	SF	[474]
DLGS	1.00	SF	[475]
SLGS	0.98	Alternative FEM	[452]
MLGS	0.63	SF	[476]
SLGS	0.78	SF	[477]
SLGS	1.20	SpFEM	[478]
TLGS	1.02	combined spring/beam elements	[479]
SLGS	2.90	SF	[451]
GO	0.07	Shell element	[8]
GO	2.60	SF	[480]
SLGS	0.90	AFM-FEA	[481]
Graphyne	0.71	SF	[48]
SLGS	0.86	SpFEM	[295]
SLGS	2.1	SF	[482]
SLGS	0.81	Tersoff–Brenner FEM	[483]
SLGS	0.97	Axisymmetric shell model	[484]
SLGS (polycrystalline)	0.90	Coupled MD-FEM	[485]
SLGS	1.40	SpFEM	[345]
SLGS	0.42	SF	[486]
SLGS	1.4	Shell element	[457]
PGS	0.73	SF	[44]

Table 3
Predicted Young's modulus E (TPa) of CNT using finite element method (FEM).

CNT type	E	Type of FEM	Source
SWCNT	1.00	SF	[311]
MWCNT	1.10	SF	[312]
SWCNT	1.00	Shell	[333]
SWCNT	4.84	Shell	[355]
SWCNT	0.40	SF	[317]
SWCNT	2.40	SF	[320]
DWCNT	1.38	SF	[487]
SWCNT	1.13	SF	[459]
SWCNT	1.35	Coupled MM-FEM	[488]
SWCNT	1.08	SF	[489]
SWCNT	3.51	SF	[490]
SWCNT	1.04	SF	[460]
SWCNT	1.20	SF	[491]
SWCNT junction	0.12	Shell	[492]
SWCNT	5.3	SF	[454]
SWCNT	1.09	SF	[493]
SWCNT	1.32	SpFEM	[292]
SWCNT	2.57	FEM/equivalent beam	[494]
Functionalised SWCNT	0.75	AFEM	[495]
MWCNT	1.19	SF	[24]
MWCNT	1.04	SF	[496]
SWCNT	1.40	SF	[497]
SWCNT	1.04	SF	[498]
SWCNT	1.03	SF	[499]
SWCNT	0.92	SpFEM	[500]
SWCNT	2.90	SF	[501]
CNT-superstructure	1.90	SF	[40]
SWCNT	0.76	SF	[502]
SWCNT	1.03	SF	[503]
SWCNT	1.04	SF	[504]
SWCNT	0.95	SF	[505]
SWCNT	1.1	SF	[77]
SWCNT	1.03	SF	[506]
SWCNT	1.23	SF	[507]
SWCNT	0.95	SF	[79]
SWCNT (defected)	1.13	SF	[463]
SWCNT	2.03	SF	[508]
SWCNT	1.10	SF	[34]
SWCNT	1.06	SF	[470]
DWCNT	0.95	Space frame	[471]
SWCNT	0.86	Spring mass FEM	[509]
SWCNT	1.32	SFEM	[510]
SWCNT	1.05	SF	[511]
MWCNT film	0.0003	Combined FEM-LDV	[453]
SWCNT	0.94	SF	[512]
SWCNT (defected)	1.05	SF	[386]
SWCNT	1.06	SF	[513]
SWCNT	2.15	SF	[514]
SWCNT	0.1(radial)	SF	[455]
SWCNT	1.05	SF	[515]
MWCNT	0.97	SF	[457]
SWCNT	1.05	SF	[458]

For E, ν and G, plots showing scatter of values have also been presented for graphene and CNT. The case of nano-composite is also considered, by showing the type of matrix, type of nano-filler, predicted values of mechanical properties and improvements as compared the matrix's properties. However, no scatter plot has been presented for nano-composites, as various combinations of nanofillers and matrices are possible, and there are very few articles published for each combination. The tables also show the type of FEM used by each publication. The publications present a range of values of mechanical properties based on the parameters such as the size of nanostructures, number of walls/sheets for CNT/graphene and degree of functionalization. Within this range, the current paper has selected the maximum value to show the highest possible values of the mechanical properties for a GANS material. In the future, the data presented in the tables will aid researchers that are attempting the mechanical determine mechanical properties of GANS materials, to compare and make engineering judgement on the input data for computer models.

7.1. Young's modulus E

The values of E for graphene and CNT predicted in various publications are shown in Tables 2 and 3 respectively. Tables 4 and 5 show the E predicted by various authors in nanocomposites. We have identified 43 publications predicting (using FEM) the values of E, for various forms of graphene such as SLGS, MLGS, GO, nanoribbons, flakes, polycrystalline graphene, graphyne and pillared graphene. Shi et al. [451] presented the highest value (i.e. 2.9 TPa) for an MLGS system using SF (space frame) approach. Wang et al. [8] presented the lowest value (i.e. 0.07 TPa) for a system of GO involving functionalised groups, by a combination of MD and FEM. Pillared graphene is a nanostructure formed by supporting graphene sheets with CNT pillars. For pillared graphene, We have found two publications that predict the values of E to be 0.19 TPa [43] and 0.73 TPa [44]. The plot showing the scatter of E for SLGS can be seen in Fig. 13. The lowest value of E for SLGS found is 0.35 TPa and is from a coupled MM/FEM model [359]. The highest value of E for SLGS found is 2.9 TPa [451] (mentioned previously). In Table 2, SF indicates the method of the space frame, AFM/FEM indicates a method that involves combining atomic force microscopy with FEM, SpFEM indicates the method of spring based FEM, MM/FEM indicates a method that combines molecular mechanics method with FEM, alternative FEM indicates a homogenised FEM

Table 4
Predicted enhancement in Young's modulus E (%) of nanocomposites using finite element method (FEM).

Filler type	Matrix type	E_m in GPa	E_C in GPa	% Enhancement	FEM type	Source
MWCNT	Poly(vinyl alcohol)	1	45	440	MSOFSO	[91]
MWCNT	poly(vinyl alcohol)	1	40	390	MSOFSO	[92]
SWCNT	Polymer	2.41	36.12	1500	MSOFSP	[313]
SWCNT	Polymer	5	53.5	1070	Axisymmetric	[331]
SWCNT	Polymer	100	144	44	MSOFSO	[327]
SWCNT	Epoxy	3	45	1400	MSOFSO	[63]
SWCNT	Polystyrene	3	4.2	40	MSOFSP	[95]
SWCNT	Polymer	5	65	1200	Axisymmetric	[332]
MWCNT	Polystyrene	1	300	2990	MPFP	[93]
CNT array	LaRC-SI	3.8	250	6480	MPFP	[98]
MWCNT	Polymer	3.07	700	2270	MSOFSO/analytical	[65]
SWCNT	Polymer	1.21	4.8	297	CVFEM	[66]
SWCNT	Epoxy	3.07	600	1944	MSOFSO	[67]
SWCNT	polymer	5	53.46	969	Axisymmetric	[516]
SWCNT	polymer	3.8	2400	590	MSOFSO	[517]
SWCNT	LaRC-SI	3.8	9.5	150	MSOFSP	[99]
SWCNT	Epoxy	N/A	N/A	430	MSOFSO	[68]
MWCNT	Polymer	1.9	2.15	13	MSOFSH	[339]
SWCNT	Polymer	130	220	69	MSOFSP	[378]
SWCNT	Polymer	3.11	131.7	41	MSOFSH	[108]
SWCNT	Polymer	100	134	34	MSOFBE	[341]
SWCNT	Rubber	1.5×10^{-3}	39.04	25,489	MSOFSP	[114]
SWCNT	Epoxy	3.89	30.2	776	MSOFSO	[70]
SWCNT	Epoxy	3.7	10.5	84	MPFP	[71]
MWCNT	polycarbonate	4.66	5.08	9	MSOFSO	[104]
SWCNT	Polyethylene	2.7	5.00	85	MSOFSP	[96]
MWCNT	PMMA	2.5	225	8900	MSOFSP	[72]
SWCNT	Epoxy	3.0	55.2	1740	MSOFSP	[73]
SWCNT	Polymer	5.0	41.0	720	MSOFSO	[379]
SWCNT	Polymer	3.0	23.5	716	Axisymmetric	[143]
SWCNT	PMMA	2.5	225.4	8916	MSOFSO	[109]
SWCNT	PET	2.6	2.95	13.46	FEM/analytical	[116]
SWCNT	Polymer	10	45	350	MSOFSO	[376]
SWCNT	Epoxy	10	12.7	27	MSOFSP	[74]
SWCNT	Polymer	10	56	460	MSOFSP	[518]
SWCNT	Epoxy	10	56	460	MSOFSP	[75]
SWCNT	Polyimide	N/A	92.9	N/A	FE-MD	[101]
SWCNT	Polymer	2	28	1300	MSOFSO	[77]
MWCNT	Polymer	3.15	4	27	FE-EX	[76]
SWCNT	Polymer	5	55.35	1027	MSOFSO	[380]
DLGS	Polymer	2.5	59.5	2300	MSOFSP	[110]
SWCNT	Epoxy	4.6	45.45	888	MSOFSP	[79]
SWCNT	LaRC-SI	3.8	28.80	658	MSOFBE	[100]
SLGS	Chitosan	1.4	5.6	300	OE(Tet)	[133]
SWCNT	Polymer	5	52.5	950	MSOFSO	[519]
SWCNT	Rubber	1×10^{-3}	65.0	6.4×10^{6}	MSOFSO	[115]
SLGS	Epoxy	3.66	10.2	180	MSOFP	[520]
MWCNT	Al	72.03	83.96	16.60	MSOFSO	[151]
SLGS	Polymer	10	75.0	740	MSOFSP	[521]
SWCNT	Epoxy	10	16.1	60	MSOFSP	[388]
SLGS	Epoxy	2.0	11.25	462	MSOFSP	[318]
SLGS	polypropylene	1.5	3.9	160	MSOFSP	[119]
SWCNT	Epoxy	3.5	10.5	200	MSOFSO	[522]
EG	PLA	3.1	2.6	19.23	MSOFSO	[126]
MLGS	Polymer	N/A	N/A	36	MSOFSO	[523]
SWCNT	Polymer	10	11.24	12.4	N/S	[389]
SLGS	Epoxy	2.13	6	182	MSOFSO	[411]
SLGS	Epoxy	3	100	3233	MSOFSP	[83]

adopted by [452], combined spring/beam elements indicates a method that connected nodes of carbon atoms with both beam and spring elements, Tersoff–Brenner FEM indicates a method that involves representing covalent bonds by Tersoff–Brenner potentials, axisymmetric shell model indicates a method of modelling SLGS by axisymmetric FEs and coupled MD-FEM indicates a method that couples molecular dynamics with FEM.

Fifty-two publications have been identified, that present the numerically (FEM) predicted values of E for CNTs. These publications cover various forms of CNTs such as SWCNT, MWCNT, defected CNTs, SWCNT junction, functionalized CNTs, CNT superstructure, and CNT film. The lowest value found in the table is 0.0003 TPa, for a film of MWCNT, using a method that involves a combination of LDV (laser Doppler vibrometer) and FEM [453]. The highest value found is 5.3 TPa for a system of SWCNT using FE SF structure to represent the wall [454]. This value of 5.3 TPa is based on a large zigzag (14,0) armchair SWCNT structure. The plot showing the scatter of E for SWCNT can be seen in Fig. 13. The lowest value of E for an SWCNT found in the table is 0.1 TPa [455]. This value is measured in the radial direction of SWCNT using SF FEM approach. Ninety-one publications have been identified, that use FEM to predict the E of GANS based composite materials. All of these publications used polymer-based matrix systems, except the authors [151,456] using Al matrix and carbon matrix, respectively. Exceptionally, the authors [457] used Si as fibre and SLGS as

Table 5
Predicted enhancement in Young's modulus E (%) of nanocomposites using finite element method (FEM)-Continued.

Filler type	Matrix type	E_m in GPa	E_C in GPa	% Enhancement	FEM type	Source
SWCNT	Epoxy	3.62	158	4264	MSOFSO	[112]
SWCNT	Polypropylene	1.5	3	100	MSOFSH	[524]
RGO	Polycarbonate	1.8	2	10	FE-EX	[107]
MWCNT	Polymer	5	52.65	953	MSOFSO	[525]
SWCNT	Polypropylene	1.98	3.52	78	MSOFSO	[121]
SWCNT	Polymer	3.0	56.61	1787	MSOFSP	[526]
SWCNT	Polypropylene	1.6	2.6	62.5	MSOFSO	[122]
SWCNT	Polyurethene	3.75	19.13	410	FE-EX	[527]
SLGS	Chitosan	1.4	5.8	314	OE(Tet)	[134]
SWCNT	Polymer	3.0	41.62	1287	MSOFSP	[390]
GNP	HDPE	1.1	2	82	MSOFSP	[130]
MLGS	Polypropylene	1.4	1.5	7.1	MSOFSO	[123]
SLGS	Polymer	3.9	10	156	MSOFSP	[528]
MWCNT	Carbon	N/A	N/A	9.4	FE-EX	[456]
SWCNT	Polymer	10	54.47	445	MSOFSP	[84]
SWCNT	Polymer	2.41	38.12	1481	MSOFSP	[529]
SWCNT	Polymer	N/A	150	N/A	MSOFSP	[530]
Coiled-CNT	Polypropylene	1.98	3.4	81	MSOFSO	[33]
rGO	Polypropylene	1.8	2.2	22	FE-EX	[11]
GPN	GF/PA6	54.1	100	84.5	MSOFSO	[142]
MWCNT	Epoxy	1	5.1	410	MSOFSO	[531]
SWCNT	Epoxy	3	34	3100	MSOFSP	[85]
SLGS	Epoxy	3	4.7	57	MSOFSP	[532]
GNP	Epoxy	2.9	3.4	17.24	MSOFSO	[13]
SWCNT	Polymer	5	21	320	MSOFSO	[533]
Si	SLGS	133	592	345	MSPFSH	[457]
SWCNT	Polymer	3	100	9700	MSOFSO	[534]
SWCNT	T300/epoxy	129.5	132	1.9	MSOFSO	[387]
SWCNT	Epoxy	2	47	2250	MSOFSP	[535]
SWCNT	Epoxy	3.5	29.85	753	MSOFSP	[536]
SWCNT	Epoxy	3.24	4.2	30	MSOFSO	[537]
SWCNT	Polyethylene	3.4	5.9	75	MSOFSO	[97]
SWCNT	Polymer	5×10^{-4}	5.25×10^{-4}	5	MSOFSO	[458]

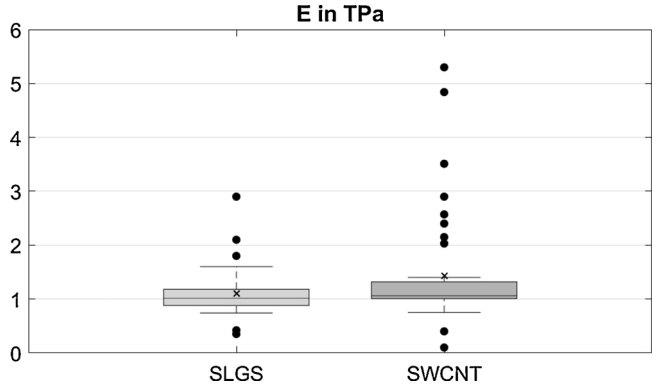

Fig. 13. Scatter of Young's modulus (E) for SWCNT and SLGS.

a matrix. These publications listed in Tables 4 and 5 used various types of carbon nanofillers including SWCNT, MWCNT, SLGS, DLGS, EG (expanded graphite), MLGS, CNT array, rGO, GNP and coiled-CNT. These tables also show the values of E for the matrix materials and the enhancement in E due to the addition of nanofillers. Some publications have not presented the values of E_m and/or enhancement in E; these are marked as N/A (not available) in the tables. The highest E enhancement predicted is 6.4×10^6% by the publication [115]. In this publication, the researchers used SWCNT to reinforce rubber matrix. The numerical model involved the representation of rubber matrix and SWCNT filler with solid FE elements. Such a large enhancement in E (6.4×10^6%), can be due to the end to end presence of SWCNT within the RVE. The other higher value of E enhancement predicted is 25,489% by the publication [114]. These researches also used SWCNT to reinforce rubber matrix. The numerical model involved the representation of rubber matrix with solid materials, an SF FE model to represent SWCNT and spring elements to represent the vdw interactions between matrix and filler. Such a large enhancement in E (25,489%), can be due to the end to end presence of SWCNT within the RVE. The least value of enhancement predicted is 5% by the researchers [458]. The authors used very soft polymer (5×10^{-3} GPa) as matrix material. In this publication, both matrix and filler have been represented by solid type finite elements in the RVE FE model. The lower value of enhancement can be due to the random distribution of SWCNT fillers within the RVE.

Table 6
Predicted Poisson's ratio ν of graphene using finite element method (FEM).

Graphene type	ν	Type of FEM	Source
SLGS	0.5	SF	[316]
SLGS	1.4	SF	[461]
SLGS	0.29	SF	[323]
Flakes	0.72	SF	[462]
SLGS	0.22	SpFEM	[294]
Nanoribbon	0.54	SpFEM	[466]
Graphane	0.68	SF	[37]
Nanoribbon	0.46	SF	[467]
SLGS	0.23	SF	[539]
SLGS	0.11	SF	[468]
Pillared Graphene RAPHENE	0.03	SF	[43]
DLGS	0.09	SF	[475]
MLGS (defected)	0.45	SF	[476]
SLGS	0.5	SF	[477]
SLGS	0.05	SF	[478]
GO	0.06	SF	[480]
SLGS	0.08	SF	[540]
Graphyne	0.4	SF	[48]
SLGS	0.52	SpFEM	[295]
SLGS	−0.001	SF	[482]

Table 7
Predicted Poisson's ratio ν of carbon nanotube (CNT) using finite element method (FEM).

CNT type	ν	Type of FEM	Source
SWCNT	0.35	SF	[317]
SWCNT Junction	1.45	Shell	[492]
SWCNT	0.65	SF	[454]
MWCNT	0.45	SF	[24]
SWCNT	0.96	SF	[538]
SWCNT	0.66	SF	[506]
SWCNT	0.28	SF	[539]
SWCNT	0.06	SF	[513]
SWCNT	0.32	Solid element	[458]

Table 8
Predicted change in Poisson's ratio (ν) of nanocomposites using finite element method (FEM).

Filler type	Matrix type	ν_m	ν_C	% Change	FEM type	Source
SWCNT	polymer	0.3	0.49	63	Axisymmetric	[331]
SWCNT	polymer	0.3	0.38	27	MSOFSO	[327]
SWCNT	polystyrene	0.33	0.44	33	MSOFSP	[95]
CNT Array	LaRC-SI	0.39	0.33	15.4	MPFP	[98]
MWCNT	Polymer	0.3	0.15	50	MSOFSO/ analytical	[65]
SWCNT	Epoxy	0.3	0.27	10	MSOFSO	[67]
SWCNT	polymer	0.3	0.47	57	Axisymmetric	[516]
SWCNT	LaRC-SI	0.43	0.405	5.8	MSOFSP	[99]
MWCNT	polycarbonate	0.38	0.374	1.6	MSOFSO	[104]
SWCNT	Polymer	0.3	1.644	448	MSOFSO	[379]
SWCNT	Polymer	0.28	0.16	42.9	Axisymmetric	[143]
SWCNT	PET	0.438	0.43	1.8	FEM/ analytical	[116]
SWCNT	Epoxy	0.3	0.29	3.3	MSOFSP	[74]
SWCNT	LaRC-SI	0.4	0.42	5	MSOFBE	[100]
SWCNT	Rubber	0.5	0.45	10	MSOFSO	[115]
SLGS	Epoxy	0.36	0.19	47.22	MSOFP	[520]
SWCNT	Epoxy	0.3	0.286	4.7	MSOFSP	[388]
SLGS	Epoxy	0.34	0.54	59	MSOFSP	[83]
SWCNT	Epoxy	0.34	0.29	14.7	MSOFSO	[112]
MWCNT	Polymer	0.3	0.31	3.3	MSOFSO	[525]
SWCNT	Polypropylene	0.3	0.38	27	MSOFSO	[122]
SWCNT	Polymer	0.3	0.26	13	MSOFSP	[84]
SWCNT	T300/Epoxy	0.25	0.092	63.2	MSOFSO	[387]

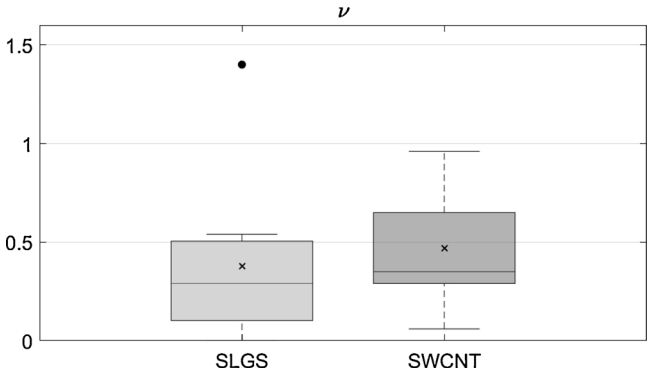

Fig. 14. Scatter of Poisson's ratio ν for SWCNT and SLGS.

7.2. Poisson's ratio (ν)

The values of ν for graphene, CNT and nanocomposites predicted in various publications are shown in Tables 6–8respectively. We have identified 20 publications predicting (using FEM) the values of ν, for various of forms of graphene such as SLGS, DLGS, MLGS, flakes, nanoribbon, graphane, pillared graphene, GO and graphyne. The authors of each publication mentioned in the table have presented a range of values. In each publication, the current article has selected the lowest value within the range, in order to identify the stiffest possible nanostructure. The lowest value predicted ($^{-}0.001$) is for an SLGS system in the publication [482], using Morse potentials. The negative value indicates that the SLGS structures can behave as auxetic materials. These authors used an SF FE model to simulate SLGS, introducing 1nN/nm force along the armchair direction at both edges and constraining the atoms at the centre of the SLGS sheet. For the graphene, the highest value of ν predicted is 1.4, by the authors [461]. These authors also used SF FE model to predict the E and G of the SLGS and then calculated ν using the Hooke's law equation ($\nu = (E/G) - 1$). This value of 1.4 for ν has been obtained by constraining one end and applying shear and normal force to the other end of an armchair SLGS (size = 6.4 nm × 4.2 nm). The lower dimension of SLGS can be responsible for such a large value of ν (1.4). The scatter of ν values for SLGS can be seen in Fig. 14, which shows an average value of 0.3. 9 papers that numerically predict ν values of CNTs using FEM, have been identified in Table 7. All of these articles considered cylindrical-SWCNTs except [492], which considered junction-SWCNT. Among the values in the table, the value 0.06, presented by authors [513], is found to be the lowest. These authors used an SF FE model to represent an armchair SWCNT (9,9) and constrained one edge and applied force on the other edge to calculate mechanical properties. Such a lower value of ν (0.06) can be due to the length (24.6 nm) of SWCNT used in the publication. As per this table, the highest value of ν predicted [492] is for a junction type SWCNT and is 1.45. These authors used shell finite element to represent the SWCNT junction, applied constraints at tube edge atoms and then applied tensile strain. The value of ν equal to 1.45 is measured at an applied tensile strain of 0.035. The scatter of ν values for SWCNT can be seen in Fig. 14. The scatter shows an average value of 0.5. The highest value of ν found for SWCNT is 0.96 by the authors [538]. These authors used a SF FE model to represent an armchair SWCNT with 30° chirality angle. This chirality angle can be the influencing factor behind a higher value of ν (0.96). Twenty-three publications that predict the ν for nanocomposites have been identified and shown in Table 8. The types of nanofillers considered by the publications are also shown in the table, and these include SWCNT, MWCNT, SLGS and CNT array, and all the matrices are polymer types. The least enhancement in ν presented is 1.6% by the authors [104]. These authors used solid finite elements to represent both polycarbonate matrix and MWCNT filler and measured ν at 77 K. The presence of temperature can be the factor that is leading to lower enhancement in ν. The highest enhancement in ν predicted is 448% by the authors [379]. These authors used a square-shaped RVE involving solid FE elements to represent both SWCNT filler and polymer matrix. The absence of interphase in the model can be the reason for such a large enhancement of ν.

7.3. Fluctuation of Poisson's ratio in nanocomposites

It can be observed that the value of Poisson's ratio of each nanocomposite is different as compared to other nanocomposites, as shown in Table 8, with an exception for two cases [122,327]. There can be various factors that govern such fluctuations. Such variations are also observed in nanomaterials as shown in Tables 6 and 7 . In the case of nanomaterials, the fluctuation can be due to the nature of the nanomaterial type. Another factor that needs attention is the direction of loads while measuring Poisson's ratio. Sun and Zhao [317] showed a decrease in the Poisson's ratio as a result of increasing the SWCNT diameter. In contrast, Zhang et al. [24] showed growth in Poisson's ratio when increasing the DWCNT diameter. An increase in the length of SWCNT has led to a decrease in its Poisson's ratio [513]. This means that the dimensions of nanomaterials also contribute towards the fluctuations of their Poisson's ratios. Furthermore, Avila et al. [454,506] assessed the influence of chirality on the Poisson's ratio of SWCNT, wherein the chiral configuration offered the highest value and the zigzag configuration offered the lowest values of Poisson's ratio. The

density of the defects in nanomaterials significantly influences their Poisson's ratio [538]. As per [482], the choice of force field models also influences the numerically measured Poisson's ratio of a nanosheet. The range within which the Poisson's ratio of nanomaterials has fluctuated/scattered has been depicted in Fig. 14. These nanomaterials act as nanofillers within the nanocomposites. The characteristics of these nanofillers along with those of host resin materials act as source of fluctuations in Poisson's ratios of nanocomposites shown in Table 8. To further clarify the sources of fluctuations of Poisson's ratio in nanocomposites, the sources are listed below:

1. Geometrical properties of fillers: The geometric properties such as CNT diameter, CNT length, CNT wall numbers, graphene length, and graphene width will influence the Poisson's ratio of nanocomposites.
2. Chirality of fillers: The filler configurations such as zigzag, armchair and chiral will influence the Poisson's ratio of nanocomposites.
3. Filler defects: The defects such as vacancies and Stone Wales, and the density of these defects within the filler, will influence the Poisson's ratio of the nanocomposite.
4. Resin type: The choice of host materials such as polymers, ceramics, and metals will influence the Poisson's ratio of nanocomposites.
5. Interfacial effects: The choice of interface models such as the assumption of perfect bonding or detailed functional group model will influence the value of numerically predicted Poisson's ratio.
6. Modelling strategy: The choice of modelling parameters such as those of force field constants (Amber or Morse), atomistic models (spring-based or beam based) and shape of RVE will influence the value of the numerically predicted Poisson's ratio.
7. Filler content: The filler content determined by volume fraction or by weight fraction will influence the value of numerically predicted Poisson's ratio of the nanocomposites.

7.4. Tensile strength

The predicted tensile strength (σ_T) and maximum strain (ϵ_T) by various authors on graphene, CNT and nanocomposites are shown in Tables 9–11 > , respectively. Twenty-five publications that use FEM to predict σ_T and ϵ_T of graphene have been identified and listed in Table 9. Various forms of graphene such as SLGS, TLGS, MLGS, nanoribbon, GO, and ruga have been considered by the authors shown in this table. The highest (σ_T) predicted is 425 GPa for a system of MLGS by the authors [541]. In this publication, the authors used a shell element model to represent the armchair and zigzag MLGS system. The value 425 GPa has been taken from the analysis of the zigzag MLGS system within the publication. The lowest value of σ_T predicted is 0.62 GPa and is from the authors [479]. These authors used an SF FE model to represent a molecule of TLGS. In the table, the lowest ϵ_T predicted is 0.1, and this value is shown by two publications [357,542]. The authors [357] used a method that combines MD with FEM to predict the stress–strain behaviour of an MLGS system. Whereas the other authors [542] used an SF FEM to model SLGS and develop its stress–strain plots. Twenty-two publications that predicted the σ_T and ϵ_T of CNTs have been identified. The highest value of σ_T predicted is 270 GPa by the authors [508]. These authors used an SF FEM to develop the stress–strain behaviour of SWCNT. For CNTs, the lowest value of σ_T predicted is 3.5 GPA by the authors [492]. These authors used a shell element based FE model to represent a junction type SWCNT. This publication [492] is also the one that quotes the highest ϵ_T (0.35). In Table 10, the lowest quoted ϵ_T is 0.08 [543]. These authors used a shell element model to represent an SWCNT system. In Table 11, there are 38 publications that present the σ_{TC} (nanocomposite tensile strength) values and ϵ_{TC} (nanocomposite maximum strain) values. The publications listed in this table have considered various types of fillers such as SWCNT, SLGS, MWCNT, MLGS, GNP, and GO. All the matrices are polymer types, except the publications by Eftekhari et al. [162] and Gangele and Pandey [457]. The authors [162] considered cement matrix and SWCNT filler and the authors [457] considered SLGS matrix and Si filler. This publication [457] presented the highest σ_{TC} (77 GPa), by using shell FEs to represent filler and SF FEs to a matrix. In Table 11, the lowest σ_{TC} is 0.24×10^{-3} GPa [136]. These authors [136] used an axisymmetric FE to represent nanocomposite system of polyacrylic/acid/gelatin matrix and GO filler. The ϵ_{TC} presented by these authors [136] is the highest (0.52) in the table. The least value of ϵ_{TC} presented in the table is 2.5×10^{-3} [162]. These authors [162] considered plate FEs to represent the matrix and the filler. The RVE to represent short fibre and long fibre nanocomposites used in the article [318] is shown in Fig. 15. This figure also shows stress-strain ($\sigma - \epsilon$) curves computed by RVE's of three different lengths and validated against the rule of mixtures.

Table 9
Predicted tensile strength σ_T (GPa) of graphene using finite element method (FEM).

Graphene type	σ_T (GPa)	ϵ_T	Type of FEM	Source
SLGS	57.6	0.17	SF	[543]
Nanoribbon	142	0.35	SpFEM	[465]
SLGS	121	0.27	SpFEM	[294]
SLGS	122	0.19	SF	[372]
SLGS	96	0.14	Coupled MM/FEM	[359]
SLGS	129	0.28	SpFEM	[469]
SLGS	120	0.2	FEM-DFT	[544]
SLGS	125	0.2	SF	[471]
SLGS	117	0.18	Hexagonal Elements	[363]
SLGS	165	0.26	SF	[473]
MLGS	425	0.2	Shell Elements	[541]
DLGS	60	0.085	SF	[475]
SLGS	122	0.2	Alternative FEM	[452]
MLGS	80	0.1	MD-FE	[357]
SLGS	35	0.1	SF	[542]
TLGS	0.62	0.6	SF	[479]
GO	5	0.15	FE-EX	[8]
Ruga	20	0.12	FEM-MD	[52]
GO	34	N/A	Solid Element	[545]
TLGS	0.64	0.6	Combined spring/beam elements	[546]
SLGS	0.4	0.2	SF	[547]
SLGS	110	0.13	SF	[540]
SLGS	85	0.13	Tersoff–Brenner FEM	[483]
SLGS	81.2	0.125	Coupled MD-FEM	[485]
SLGS	93.6	0.161	SBFEM	[303]

Table 10
Predicted tensile strength σ_T (GPa) of CNT using finite element method (FEM).

CNT type	σ_T (GPa)	ϵ_T	Type of FEM	Source
SWCNT	101	0.3	SF	[317]
SWCNT	65	0.09	Coupled MM-MD-FEM	[317]
SWCNT	120	0.22	SF (Spring elements)	[459]
SWCNT	200	0.24	Coupled MM-FEM	[488]
SWCNT	112	0.17	SF	[548]
SWCNT	119	0.19	SF (Spring elements)	[549]
SWCNT	120	0.2	SF	[550]
SWCNT Junction	3.5	0.35	Shell	[492]
SWCNT	65	0.08	Shell elements	[543]
SWCNT	88	0.17	AFEM	[495]
SWCNT	120	0.22	SpFEM	[500]
CNT-Superstructure	85	0.6	SF	[40]
SWCNT	125	0.23	SF	[551]
SWCNT	114	0.2	SF	[505]
SWCNT	85	0.09	SF	[463]
SWCNT	120	0.2	SF	[77]
SWCNT	270	0.21	SF	[508]
SWCNT	115	0.2	SF	[79]
SWCNT	115	0.22	SF	[471]
SLGS	121	0.21	Hexagonal element	[363]
SWCNT-Coiled	115	0.21	MDFEM	[552]
MWCNT	104	0.16	SF	[457]

Table 11
Predicted enhancements in tensile strength σ_T (GPa) and tensile strain ε_{TC} of nanocomposites using finite element method (FEM).

Filler type	Matrix type	σ_{TM} (GPa)	σ_{TC} (GPa)	ε_{TM}	ε_{TC}	FEM type	Source
SWCNT	Polymer	0.5	11	0.11	0.25	MSOFBE	[341]
SWCNT	Rubber	1.5e10^{-3}	4.5	0.35	0.21	MSOFSP	[114]
SWCNT	Epoxy	38×10^{-3}	68×10^{-3}	N/A	0.65	MPFP	[71]
MWCNT	polycarbonate	61×10^{-3}	65×10^{-3}	0.058	0.058	MSOFSO	[104]
SWCNT	Polymer	0.5	2.5	0.05	0.05	MSOFSO	[376]
SWCNT	Polymer	0.3	2.8	0.05	0.05	MSOFSP	[518]
SWCNT	Epoxy	0.25	2.4	0.05	0.05	MSOFSP	[75]
SWCNT	Polymer	4	5	0.2	0.2	MSOFSO	[77]
MWCNT	Polymer	71×10^{-3}	78×10^{-3}	0.03	0.03	FE-EX	[76]
SWCNT	Polymer	N/A	2.4	N/A	N/A	MSOFSO	[380]
SWCNT	Epoxy	38×10^{-3}	10	0.009	0.22	MSOFSP	[79]
SWCNT	LaRC-SI	N/A	115×10^{-3}	N/A	0.017	MSOFBE	[100]
SLGS	Chitosan	0.14	0.22	0.7	0.3	OE	[133]
SWCNT	Rubber	0.7×10^{-3}	7	0.8	0.2	MSOFSO	[115]
SLGS	Polymer	0.18	1.5	0.02	0.02	MSOFSP	[521]
SLGS	PEEK	0.02	0.3	0.05	0.05	MSOFBE	[124]
SLGS	Epoxy	62e10^{-3}	1	0.04	0.08	MSOFSP	[318]
SLGS	polypropylene	20×10^{-3}	200×10^{-3}	0.016	0.016	MSOFSP	[119]
SLGS	Epoxy	50	135×10^{-3}	N/A	0.038	MSOFSO	[411]
SWCNT	Cement	2.2×10^{-3}	2.9×10^{-3}	1e10^{-4}	2.5×10^{-3}	MPFP	[162]
GO	polyacrylic/acid/gelatin	0.14×10^{-3}	0.24×10^{-3}	0.25	0.52	Axisymmetric	[136]
SWCNT	Polypropylene	30×10^{-3}	82×10^{-3}	0.06	0.06	MSOFSH	[524]
SWCNT	Polypropylene	25.8×10^{-3}	40×10^{-3}	0.06	0.05	MSOFSO	[121]
GO	Gelatin	N/A	4×10^{-3}	N/A	0.16	MPFP	[129]
SWCNT	Polyurethene	25e10^{-3}	48e10^{-3}	1.5	0.7	FE-EX	[527]
SLGS	Chitosan	N/A	0.22	N/A	0.4	OE	[134]
SWCNT	Polymer	0.5	1.6	0.05	0.05	MSOFSP	[390]
GNP	HDPE	30×10^{-3}	40×10^{-3}	0.15	0.16	MSOFSP	[130]
MLGS	Polypropylene	34	55	0.1	0.2	MSOFSO	[123]
SWCNT	Epoxy	N/A	12.5×10^{-3}	N/A	0.03	MSOFSO	[553]
SWCNT	Epoxy	38×10^{-3}	49×10^{-3}	0.03	0.03	MSOFSO	[531]
GPN	GF/PA6	0.4	2.3	0.25	0.5	MSOFSO	[142]
SWCNT	Epoxy	0.06	1.13	0.035	0.035	MSOFSP	[85]
GNP	Epoxy	65×10^{-3}	70×10^{-3}	0.035	0.03	MSOFSO	[13]
SLGS	Si	17	77	0.11	0.16	MSHFSP	[457]
SWCNT	Epoxy	55×10^{-3}	2.8	0.06	0.06	MSOFSP	[535]
SWCNT	Epoxy	0.2	0.9	0.2	0.03	MSOFSO	[537]
SWCNT	Polymer	N/A	7	N/A	0.1	MSOFSP	[554]

7.5. Shear modulus G

The predicted shear modulus G by various authors for graphene, CNT and nanocomposites are shown in Tables 12, 13 and 14 , respectively. Twenty-three publications that predict the G of graphene using FEM, have been identified. The authors listed in Table 12 have considered various types of graphene, such as SLGS, TLGS, DLGS, MLGS, polycrystalline graphene, flakes, pillared graphene and nanoribbons. Within this table, the highest predicted G is 2.1 TPa by the authors [323]. The authors [323] used an SF FE model to predict mechanical properties of SLGS. The authors arrived at this value of 2.1 TPa, by assuming very large values for two Morse constants ($k_b \rightarrow \infty$ & $k_s \rightarrow \infty$). In Table 12, the lowest value of G predicted is 0.01 TPa by the authors [555]. These authors used SF FE model to represent a BLGS system of size 7.99 nm × 0.92 nm. The presence of weak van der Waal's interaction between two SLGS can the reason for such a small value. The scatter of G for SLGS is shown in Fig. 16and shows an average value of 0.63 TPa for G. Twenty-five publications that predict G of CNTs have been identified and shown in Table 13. Various types of CNTs in the listed publications are SWCNT, DWCNT and MWCNT. As per the table, the largest value of G is 1.4 TPa and is presented by the authors [494]. These authors modelled an SWCNT using SF FEM and extracted tensile, bending and torsional rigidities. With the aid of these rigidities, an analytical beam model has been constructed to predict the mechanical properties. Such a higher value of G (1.4 TPa) can be due to the use of continuous beam structures, rather than SF discrete structures used by other authors. In Table 12, another large value of G is 1.25 TPa, presented by the authors [34]. These authors used an SF FE model to represent coiled SWCNTs and calculate mechanical properties. The value of 1.25 TPa is taken from an armchair coiled SWCNT of size (18,18). Such a higher value of G (1.25 TPa) indicate that coiled SWCNT's offer higher stiffness in shear as compared to straight SWCNTs. The lowest value found is 0.32 TPa, presented by the authors [509]. These authors used spring elements to model C– bonds of the SWCNT and such a lower value of G (0.32 TPa) can be due to the lower directional stiffness associated with the spring elements, as compared to the beam elements used in typical SF structures. The scatter of G values in TPa for SWCNTs can be seen in Fig. 16 and the average value is 0.5 TPa. Twenty publications that predict the G of nanocomposites have been identified and shown in Table 14. The nanofillers considered by the authors include SWCNT, MWCNT, SLGS, MLGS, coiled-CNT and CNT arrays. All the matrices in the table are polymer types except the matrix used by the author [152]. These authors used SnBi a matrix (reinforced by MLGS fillers). The highest predicted enhancement in G due to nano-reinforcement is 28,000% [65]. These authors [65] used a method that combined FEM with analytical equations in order to predict the mechanical properties of polymer reinforced by MWCNT fillers. An 80% drop in G has been observed in the publication by authors [143]. In this publication, the authors modelled CNT reinforced IM7 carbon fibre reinforced embedded in an epoxy system using axisymmetric FEs.

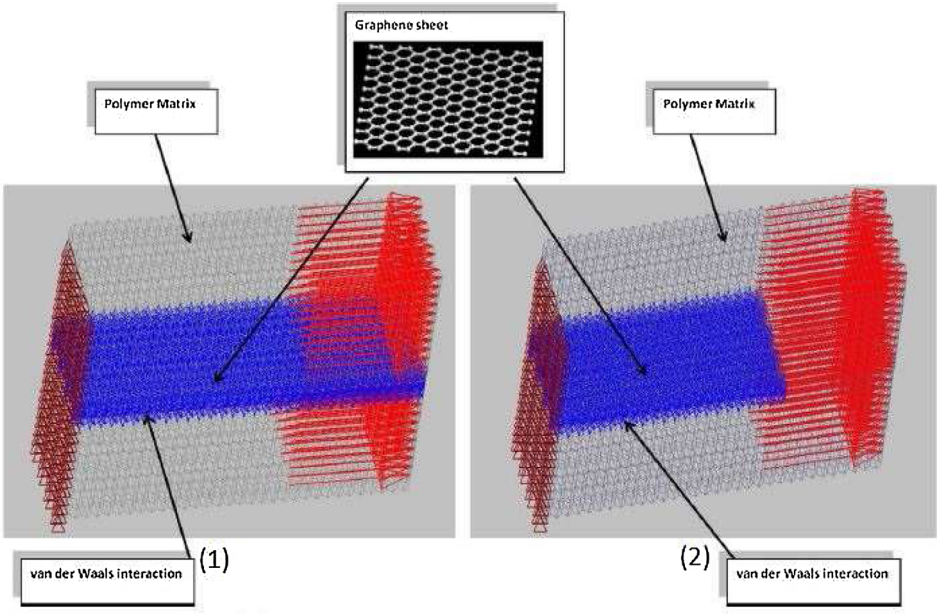

(a) Continuous fibre (1) and Short fibre RVE (2)

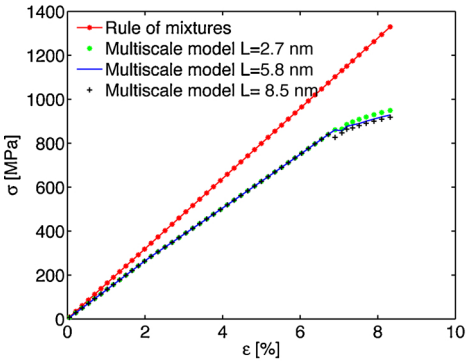

(b) $\sigma - \epsilon$ curve for continuous fibre RVE

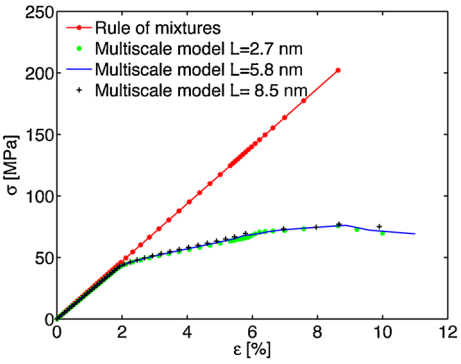

(c) $\sigma - \epsilon$ curve curve for short fibre GSRP

Fig. 15. RVEs and stress-strain curves developed in the article [318].

Table 12
Predicted shear modulus G (TPa) of graphene using finite element method (FEM).

Graphene type	G (TPa)	Type of FEM	Source
SLGS	0.49	SF	[311]
SLGS	0.4	SF	[95]
SLGS	0.3	SF	[316]
SLGS	0.23	SF	[461]
SLGS	2.1	SF	[323]
Flakes	0.41	SF	[462]
BLGS	0.01	SF	[555]
SLGS	0.5	SF	[556]
SLGS	0.4	SpFEM	[294]
Nanoribbon	0.49	SpFEM	[466]
SLGS	0.5	Coupled MM/FEM	[359]
SLGS	0.4	SpFEM	[469]
SLGS	1.8	SF	[557]
SLGS	0.21	SF	[472]
Pillared Graphene	0.06	SF	[43]
MLGS	0.21	SF	[474]
DLGS	0.42	SF	[475]
SLGS	0.45	SF	[83]
Polycrystalline TLGS	0.23	SF	[546]
Graphyne	.07	SF	[48]
SLGS	0.44	SpFEM	[295]
SLGS	0.72	SF	[482]
Pillared graphene	0.23	SF	[44]

7.6. Buckling strength

Using FEM, the predicted buckling strength (λ) by various authors can be found in Tables 15–17. Nine publications that use FEM to predict the λ of graphene have been identified and shown in Table 15. Various forms of graphene considered by the authors include SLGS, MLGS, nanoribbon and graphyne. It is evident from the table that the buckling strength has been presented in various units such as N/nm, nN and also in terms of non-dimensional parameters. Majority of these authors [235,559–561] developed space frame (SF) based FE models to represent SLGS and performed eigenvalue analysis to calculate the buckling strength. The authors [562] used 3D solid elements within the FE tool ABAQUS, to calculate the non-dimensional buckling parameter ($N_B = \mathrm{NR}^2/D$), where N is radial compressive load, R is the radius of the circular SLGS and D is the flexural rigidity. The authors [47] developed an equivalent shell element based sheet to represent SLGS and calculate eigenvalue-buckling strength under clamped and clamped-free boundary conditions. The buckling strength (5.5 nN) shown in the table is taken from a sheet (10 nm × 10 nm) that was clamped. The space frame FE representation of BLGS used by the article [235] is shown in Fig. 17. The figure also shows the boundary conditions used to simulate buckling. Twenty-eight publications that predict the buckling strength of CNTs have been shown in Table 16. The authors have considered various types of CNTs, such as SWCNT, DWCNT, MWCNT, SWSiCNT (single wall silicon carbide nanotube) and SWCNT-VA (SWCNT-

Table 13
Predicted shear modulus G (TPa) of CNT using finite element method (FEM).

CNT type	G (TPa)	Type of FEM	Source
SWCNT	0.49	SF	[311]
MWCNT	0.49	SF	[312]
SWCNT	0.4	SF	[95]
SWCNT	0.5	SF	[320]
DWCNT	0.5	SF	[487]
SWCNT	0.47	SF	[558]
SWCNT	0.48	SF	[460]
SWCNT	0.5	SF	[493]
SWCNT	0.43	SpFEM	[292]
SWCNT	0.14	FEM/equivalent beam	[494]
DWCNT	0.42	SF	[496]
SWCNT	0.5	SF	[497]
SWCNT	0.46	SF	[498]
SWCNT	0.41	SF	[376]
SWCNT	0.42	SF	[518]
SWCNT	0.5	SF	[77]
SWCNT	0.5	SF	[506]
SWCNT	0.34	SF	[505]
SWCNT	0.34	SF	[79]
SWCNT (Coiled)	1.25	SF	[34]
SWCNT	0.47	SF	[470]
SWCNT	0.32	Spring mass FEM	[509]
SWCNT	0.51	SF	[511]
SWCNT	0.5	SF	[344]
SWCNT	0.9	Solid elements	[458]

vertically aligned). Similar to the case of graphene as previously mentioned, the majority of these publications [497,498,563–565] considered an eigenvalue analysis to predict the buckling strength of SF CNT models. The authors [566] performed a post-buckling analysis using an SF FE models of SWCNT and DWCNT. These authors termed their method as AFEM (atomistic finite element method) and concluded that the AFEM solution process is faster as compared to other methods. The authors deployed AFEM within the FE package ABAQUS, calculated strain energies and reaction forces in SWCNT and DWCNT, in order to simulate the buckling behaviour. Other authors [296] used a combination of analytical nonlocal formulas and FEM to predicting the critical temperature and the critical stress at which the buckling will initiate in an MWCNT system. The critical temperature 4144 K shown in the table is taken from a system of TWCNT ($r = 8.5$ nm & $h = 0.34$ nm). The authors [567] considered a system of SWCNT subjected to axial compressive loading, transverse bending loading and temperature variation. These authors used nonlocal-based FEM to calculate non-dimensional buckling strength given by $\lambda_{nd} = \lambda_{cr}/P$, where λ_{cr} is the critical buckling load and P is the applied axial compressive load. Six publications that predict the buckling strength of nanocomposites using FEM have been identified and shown in Table 17. Various types of fillers considered by the listed authors are SWCNT, SLGS, MLGS and GNP. The matrix is found to a polymer type in all of the publications. The highest enhancement in the buckling strength predicted due to nanoreinforcement is 568% by the authors [238]. This publication developed a plate model based on the combination of Bodyanski analytical equation and FEM. This plate has been subjected to various edge boundary conditions such as simply supported, clamped and fully fixed. Other authors [568] used an isogeometric to predict the critical buckling temperature of 487 K for an MLGS/PMMA functionally graded composite system.

7.7. Vibrational characteristics

Using FEM, the predicted natural frequencies (ω) by various authors can be found in Tables 18–20. 26 publications that use FEM to predict ω of graphene (ω_G) have been identified and shown in Table 18. Various forms of graphene considered by the authors include SLGS, TLGS, MLGS, nanoribbon, SLGS-SWCNT junction and DLGS-DWCNT junction. The highest natural frequency suggested for graphene (ω_G) is 185 THz, by the authors [464]. These authors used SF FE method to predict ω_G in a fully clamped circular SLGS. The lowest ω_G predicted is 5.1×10^{-5} THz [584] and is for an SLGS system used to design a resonator. Another value of ω_G that needs attention is 0.075 THz by the authors [585]. These authors used an SF FE method to model wrinkled SLGS. The first four mode shapes of SLGS computed in the publication [236] is shown in Fig. 18. Forty-one publications that use FEM to predict the natural frequencies of CNT (ω_{CNT}) have been identified and shown in Table 19. Various forms of CNT considered by the authors include SWCNT, DWCNT, MWCNT and super-CNT structure. The highest ω_{CNT} identified is 30 THz by the authors [586]. These authors used a beam element based FE method to predict the dynamic behaviour of SWCNT. The lowest ω_{CNT} found is 1×10^{-12} THz presented by the authors [587]. These authors also used an equivalent beam element model to represent SWCNT. Although the majority of the publications listed in Table 19 considered SWCNTs, the publication [25] considered a super-CNT involving a cylinder constructed by joining a hexagonal array of SWCNTs. These authors proposed a mass and strain sensor using super-CNT. The SWCNTs within the super-CNTs were constructed as FE SF structures, and maximum ω_{CNT} presented in this publication is 0.28 THz. This

Table 14
Predicted enhancement in shear modulus G (%) of nanocomposites using finite element method(FEM).

Filler type	Matrix type	G_m (GPa)	G_C (GPa)	% Enhancement	FEM type	Source
CNT array	LaRC-SI	1.6	10	119	MPFP	[98]
MWCNT	Polymer	0.8	225	28,000	MSOFSO/analytical	[65]
SWCNT	Epoxy	2.4	18.5	670	MSOFSO	[67]
SWCNT	polymer	1.4	2.1	55	MSOFSO	[517]
SWCNT	LaRC-SI	1.4	3.3	140	MSOFSP	[99]
SWCNT	Epoxy	47	9.4	−80	Axisymmetric	[143]
SWCNT	Polymer	3.8	5.1	34	MSOFSP	[518]
SWCNT	Polymer	1.92	2.2	14.6	MSOFSO	[77]
SWCNT	Epoxy	1.8	13.52	651	MSOFSP	[79]
SWCNT	Epoxy	5.89	36.43	518	XFEM	[162]
SLGS	Epoxy	1.12	54	4400	MSOFSP	[83]
SLGS	Epoxy	1.32	2.8	112	MSOFSO	[112]
SWCNT	Polypropylene	0.6	0.78	30	MSOFSO	[122]
MLGS	SnBi	12	23	91	MSOFSO	[152]
SLGS	Polymer	1.4	4.3	207	MSOFSP	[528]
Coiled-CNT	Polypropylene	0.7	1.05	50	MSOFSO	[33]
SWCNT	Epoxy	1	3.2	220	MSOFSP	[85]
SWCNT	Polymer	0.8	2	150	MSOFSO	[534]
SWCNT	T300/Epoxy	3	9	200	MSOFSO	[387]
SWCNT	Polyethylene	N/A	1.54	N/A	MSOFSO	[97]

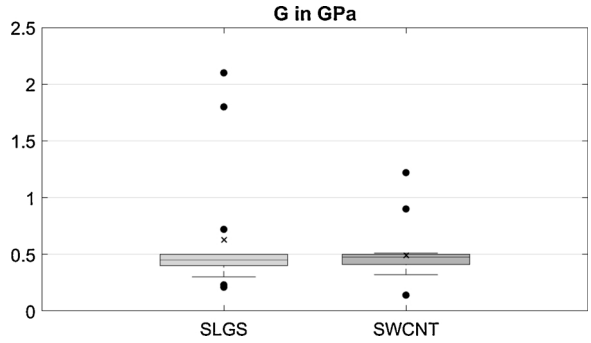

Fig. 16. Scatter of shear modulus G for SWCNT and SLGS.

Table 15
Predicted buckling capacity λ of graphene using finite element method(FEM).

Graphene type	λ_{cr}	Type of FEM	Source
SLGS	50 N/nm	SF	[559]
SLGS	190 N/nm	SF	[235]
Nanoribbon	0.2×10^{-9} N/nm	SF	[560]
SLGS	33 nN	SF	[561]
MLGS	1000×10^{-9} N/nm	Nonlocal FEA	[298]
SLGS	58 (non-dimensional)	Solid elements	[562]
Graphyne	5.5 nN	Shell elements	[47]
SLGS	15 nN/nm	Nonlocal isogeometric FEM	[569]
SLGS	1.13 N/m	SF	[486]

Table 16
Predicted buckling capacity λ of CNT using finite element method(FEM).

CNT type	λ_{cr}	Type of FEM	Source
DWCNT	200 nN	SF	[563]
MWCNT	612 nN	Shell	[354]
MWCNT	750 eV/nm	SF	[566]
DWCNT	2.21×10^{-7} N	Shell elements	[570]
SWCNT	0.08 (strain)	Shell elements	[336]
SWCNT	0.1 (strain)	SF	[571]
SWCNT	0.07 (strain)	AFEM	[572]
SWCNT	190 nN	Beam element	[564]
SWCNT	60 nN	SF	[493]
SWCNT	49.12 GPa	Shell element	[573]
SWCNT	22 eV (strain energy)	AFEM	[574]
SWCNT	140 nN nm (flexural moment)	Shell element	[575]
MWCNT	100 nN	SF	[497]
SWCNT	190 nN	SF	[498]
SWCNT	700 nN	SF	[576]
SWCNT	0.018 (strain)	SF	[577]
SWCNT	4144 K (temperature)	Semi analytical FEM	[296]
SWCNT	0.16 (strain)	SF	[578]
SWCNT	0.16 eV/atom (strain energy)	SF	[370]
SWCNT	3.7 nN	SF	[565]
SWSiCNT	650 nN	SF	[579]
MWCNT	202.6 nN	SF	[580]
SWCNT	10 (λ_{nd})	Non-local FEM	[567]
SWCNT (hetero-junction)	18 nN	SF	[60]
SWCNT	13,000 nN	SF	[581]
SWCNT	11 nN	SF	[582]
SWCNT (hetero-junction)	20 nN	SF	[59]
SWCNT-VA	7000 nN	SF	[457]

maximum value has been taken from a (6,0) super-CNT which was subjected to bridged boundary condition. 15 publications that numerically predict the natural frequencies of nanocomposites (ω_{COMP}) using FEM have been identified and shown in Table 20. Various types of fillers used by the authors are SLGS, SWCNT and GNP. All of the publications considered polymer type matrices, except [165,443,588], that considered Si/SiO_2, cement/prepeg and piezoelectric material as matrices, respectively. Among the 15 publications, three publications presented natural frequencies of the neat matrix ω_m. In Table 20, the enhancement in natural frequency due to nanoreinforcement varies from 4.8% to 90%. Some of the publications [589–594] presented ω_{COMP} as non-dimensional. For further information, readers are suggested to refer to these references [589–594].

7.8. Fracture parameters

Apart from predicting maximum σ and ϵ as shown in Section 7.4, several publications predicted other fracture parameters such as strain energy release rate (SERR), stress intensity factor (SIF), fracture energy, J-integral, filler pullout force. The values of these fracture parameters as predicted by several authors are shown in Tables 21 and 22 . All the publications that presented fracture parameters for graphene, shown in Table 21, considered SLGS. The authors [540,626,627] used the most popular SF FE method to represent SLGS and calculated SERR and SIF. The publication [302] deployed a novel method that couples quantum mechanics with FEM. This involved predicting C—C bond breakage using quantum mechanics based density function theory (DFT) and then simulating crack propagation by XFEM. Other authors [628] introduced a crack in a shell-based FE model of the SLGS and calculated stress field at the crack tip. This stress field has been used to calculate SIF and SERR. The publication [629] predicted fracture energy (0.025 eV/atom) using a novel MM based FE method to represent C—C bonds. This novel method involved representing each C—C bond in the SLGS by three separate elements. The element 1 referred to as $U2$ represented bond stretching, and element 2 referred to as $U3$ represented angle bending and element 3 referred to as $U4$ represented dihedral angle. These novel element types have been introduced in ABAQUS as user-defined elements in order to model mode I, mode II and mode III fracture behaviour of SLGS. Nineteen publications that predict fracture properties of nanocomposites have been identified and shown in Table 22. Various types of fillers considered by the authors are SWCNT, MWCNT, SLGS and GNP. Various host materials considered are epoxy, Al, polycarbonate, polyethylene, Si_3N_4, SiO_2, cement, concrete and Cu. The authors [105] predicted a 7% increase in J-Integral by reinforcing polycarbonate matrix with MWCNT. These authors developed FE models that involved using 3D solid FEs to represent filler and the host material. The publications [76,78,154,158] calculated toughness of nanocomposites. Other publications [80,96,233,630,631] simulated the pulling behaviour of filler from the host material and reported force required for a complete pullout. Several publications [142,632,633] shown in the table, calculate SERR of nanocomposites. The authors [76,78] used FEM to determine the optimum dimensions of an epoxy/MWCNT specimen and the optimum location a crack in the specimen. This specimen has then been used to experimentally determine E, σ_T, ϵ_T, mode I toughness and mode II toughness of the nanocomposite, using ASTM test setups. Other authors [142] reinforced PA6 resin with GNP and then reinforced this GNP/PA6 composite with short S-glass fibres. In this publication, the micro/nano level mechanical properties have been determined by the multiscale modelling tool DIGIMAT, and then these properties have been called into the LS-DYNA software, to simulate the fracture behaviour of a GNP/PA6/S-Glass composite automotive crash box. The maximum SERR (4200 J/m^2) predicted by these authors, for the composite specimen has been shown in Table 22.

The current authors developed RVEs that considered various combinations of nanofibres, such as SLGS-SLGS, SWCNT-SWCNT, SLGS-SWCNT and SWCNT-SLGS to compute pullout forces, and the analysis results are presented in the publication [233]. These RVEs and the boundary conditions adopted to simulate the nanofibre pullout are shown in Fig. 19. The pullout force is used as an indicator of interfacial strength between nanofibre and resin matrix. This numerical simulation considered several types of chemical interlinkers between two

Table 17
Predicted enhancement in buckling capacity λ of nanocomposites using finite element method (FEM).

Filler type	Matrix type	λ_{crm}	λ_{crc}	% Enhancement	FEM type	Source
SWCNT	Polymer	N/A	16 nN	N/A	MSOFSP	[64]
SWCNT	Polystyrene	109 kN	728 kN	568	Bodyanski FEM	[238]
SLGS	Epoxy	3.7×10^{-2} nN	4.7×10^{-2} nN	27	MSOFSF	[583]
SLGS	Epoxy	40.1 N	68 N	70	MSOFSF	[234]
MLGS	PMMA	N/A	487 K (temperature)	N/A	Isogeometric FEM	[568]
GNP	Epoxy	1 (normalised)	5.3 (normalised)	430	MSOFSO	[15]

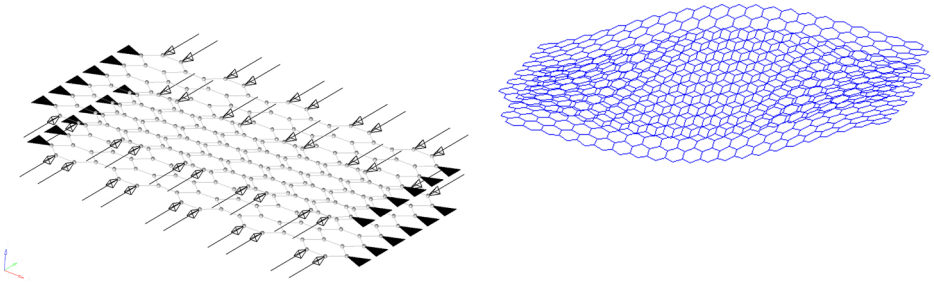

(a) Bridged boundary conditions on BLGS

(b) First buckling mode shape of BLGS under bridged boundary conditions

Fig. 17. The buckling mode shape computed in Ref. [235].

Table 18
Predicted natural frequency ω of graphene using finite element method(FEM).

Graphene type	ω_g in THz	Type of FEM	Source
SLGS	2.9	SF	[432]
SLGS	5.8	SF	[595]
SLGS	5.5	SF	[433]
MLGS (resonator)	5.1×10^{-5}	N/A	[584]
SLGS	2.8	SF	[596]
TLGS	32.5	Non Local FEM	[576]
SLGS	0.375	SF	[597]
SLGS	0.38	SF	[598]
SLGS	185	SF	[464]
MLGS	0.15	SF	[506]
BLGS	7.5	SF	[236]
SLGS	0.38	SF	[599]
Nanoribbon	0.325	SF	[560]
SLGS	7.2	SF	[600]
SLGS	1.3	SF	[360]
SLGS	0.1	SF	[601]
SLGS	1.2	PE	[365]
SLGS	5	SpFEM	[602]
SLGS	0.075	SF	[585]
SLGS	25	SpFEM	[446]
MLGS	8.5	SF	[547]
SLGS-SWCNT junction	2.5	SF	[62]
SLGS	1.2	SGFEM	[603]
DLGS-DWCNT junction	0.75	SF	[58]
SLGS	0.4	SF	[486]
SLGS	0.7	SF	[604]

Table 19
Predicted natural frequency ω of CNT using finite element method(FEM).

Graphene type	ω_{CNT} in THz	Type of FEM	Source
MWCNT	1.65	SF	[605]
SWCNT	0.5	SF	[426]
SWCNT	2.02×10^{-6}	Solid elements	[428]
SWCNT	5	SF	[432]
SWCNT	1.5	SF	[606]
SWCNT	0.27	SF	[493]
Super-CNT	0.28	SF	[25]
SWCNT	1×10^{-3}	SF	[607]
SWCNT	5	SpFEM	[608]
DWCNT	0.25	SF	[498]
MWCNT	1.7	SpFEM	[293]
SWCNT	2.7	SF	[609]
SWCNT	2.7	SF	[497]
SWCNT	10	SF	[596]
SWCNT	4×10^{-3}	Displacement FEM	[610]
MWCNT	0.73	Shell elements	[321]
SWCNT	0.5	SpFEM	[437]
SWCNT	8.5×10^{-5}	Solid Elements	[440]
SWCNT	0.09	Solid elements	[439]
SWCNT	0.1	Solid elements	[438]
SWCNT	5.8×10^{-3}	Displacement FEM	[611]
SWCNT	2.8×10^{-3}	SF	[612]
SWCNT	0.15	SF	[565]
SWCNT	1.91	SF	[506]
SWCNT	7.0	SF	[613]
SWCNT	0.28	SF	[441]
SWCNT	2.5×10^{-4}	Non-local FEM	[614]
SWCNT	5.6	Beam elements	[615]
SWCNT	0.89	SF	[616]
SWCNT	0.95	SF	[18]
SWCNT	0.76	SF	[61]
SWCNT	8.5	SF	[617]
SWCNT	30	Beam elements	[586]
DWCNT	8	Solid elements	[618]
SWCNT	26×10^{-3}	SF	[619]
DWCNT	55×10^{-3}	SF	[344]
SWCNC	2	SF	[620]
SWCNT	2.3	SF	[621]
SWCNT	1×10^{-12}	Beam elements	[587]
SWCNT	1.5	SpFEM	[622]
SWCNT	28×10^{-3}	Shell elements	[623]

nanofibres, namely aliphatic diamines $(CH_2)_3N_2H_4$ and $(CH_2)_{10}N_2H_4$, and aromatic phenylenediamine. The influence of these interlinkers on the nanofibre pullout force is shown in Fig. 20. The presence of interlinkers increased the pullout force as the fibre reached a certain distance. This publication [233] demonstrated that an auxetic behaviour of SWCNT contributed towards the increase in pullout force.

7.9. Damping properties

Four publications that predict enhancement in loss factor of a material, due to nanoreinforcement, have been shown in Table 23. The publications have presented a range of values of damping loss factors

Table 20
Predicted enhancement in natural frequency ω of nanocomposites using finite element method (FEM).

Filler type	Matrix type	ω_m	ω_{COMP}	% Enhancement	FEM type	Source
SLGS	Polymer	N/A	0.72 THz	N/A	MSOFSP	[319]
SWCNT	Polymer	N/A	21.4 (ND)	N/A	MBFB	[589]
SWCNT	PmPV	N/A	136 (ND)	N/A	MSHFSH	[590]
SWCNT	PmPV	N/A	6.16×10^4 rad/s	N/A	MSHFSH	[125]
SWCNT	Polymer	175.33 GHz	242 GHz	38.3	MSOFSP	[624]
SWCNT	Polymer	N/A	134.27 (ND)	N/A	MSHFSH	[591]
SLGS	Si/SiO_2	N/A	50 MHz	N/A	MSHFSH	[443]
SWCNT	PmPV	N/A	124.0 (ND)	N/A	9 noded elements	[592]
GNP	Cement/Prepeg	N/A	46 Hz	N/A	MSOFSO	[165]
SWCNT	PMMA	N/A	226.0 (ND)	N/A	MSHFSH	[593]
SWCNT	Polymer	N/A	3767.39 Hz	N/A	Strong Formulation-FEM	[625]
GNP	Polymer	N/A	991.00 Hz	N/A	MSOFSO	[14]
GNP	Epoxy	0.43 (ND)	0.83 (ND)	93	MSOFSO	[594]
SWCNT	PEEK	2.1 GHz	2.2 GHz	4.8	MSOFSO	[623]
SWCNT	Piezoelectric	N/A	18×10^5 rad/s	N/A	MSHFSH	[588]

depending upon filler volume/weight fraction, temperature, strain, filler dimensions and interfacial shear strength (ISS). The loss factor values shown in Table 23, are the maximum values taken from the range of values shown within each publication. Fillers considered by the publications are SWCNT and MWCNT. The host materials considered are polymer types such as epoxy and PEEK. From the table, it is evident that, if the host matrix is epoxy, MWCNT filler offers higher loss factor (0.3) as compared to SWCNT fillers. The combination involving SWCNT and PEEK offers the highest loss factor as compared to other combinations. Koratkar et al. [155] modelled a nanocomposite of MWCNT filler and cyanoacrylate epoxy matrix using FE beam elements. With the aid of these beam elements, the authors obtained an equation of motion with complex and real terms in order to develop an element stiffness matrix and determine the damping ratio/loss factor. Other authors [69] constructed a 2D shell element based FE model to represent an epoxy/SWCNT nanocomposite RVE. Using this RVE, the authors determined the variation of damping ratio and damping loss factor with respect to the applied strain. Dai and Liao [140] modelled an RVE capsule consisting SWCNT, interface layer and epoxy resin. All three constituents have been discretized by 3D solid elements (SOLID185) within ANSYS. Using this RVE capsule, the variation of the loss factor and damping ratio with respect to the applied strain have been calculated. Savvas et al. [124] developed an SF based FE model to represent an SWCNT. Based on the behaviour of this SF FE model, an equivalent beam has been developed to represent the SWCNT within a cube of PEEK matrix (modelled by continuum solid 3D FE elements). Using this RVE, the authors [124] calculated the variation of the damping loss factor with respect to the variation of ILSS.

8. Thermal properties of GANS and relevant nanocomposites using FEM

It is a well-known fact that the GANS based materials offer superior thermal properties such as thermal conductivity (K), melting point, specific heat, coefficient of thermal expansion (CTE), thermal stability, glass transition temperature and thermal diffusivity, as compared to other materials. For example, the K of graphene can be up to 5300 W/mK [635] and the K of CNT can be up to 6600 W/mK [636]. Reinforcing epoxy resin with SWCNT can enhance the CTE of the resin by 90,954%. But, the majority of the publications gathered in the current survey, focused on determining the mechanical properties of GANS based materials. A Minority of the publications focused on determining the thermal properties of graphene, CNT and nanocomposites. Twenty-one publications that predict thermal properties of GANS have been identified and shown in Sections 8.1 and 8.2. These publications used FEM to determine the CTE and K of graphene, CNT and nanocomposites. Some publications deployed altered FEMs such as Object-Oriented FEM (OOFEM) and Control Volume FEM (CVFEM). Readers can make use of the thermal property values and references present in this section to develop numerical thermal models of GANS based materials.

Table 21
Predicted fracture property of graphene using finite element method(FEM).

Graphene type	Fracture property	Type of FEM	Source
SLGS	0.8 J/m^2 (SERR)	Shell Element	[628]
SLGS	4.3 MPa m$^{1/2}$ (SIF)	XFEM-QM	[302]
SLGS	2100 kJ/m^2 (SERR)	SF	[626]
SLGS	120 (normailised SERR)	SF	[627]
SLGS	0.025 eV/atom (energy)	MM-FEM	[629]
SLGS	3.7 MPa m$^{1/2}$ (SIF)	SF	[540]

8.1. Thermal conductivity (K)

Tables 24 and 25 show the numerically predicted thermal conductivity (K) of graphene and nanocomposites, respectively. Four

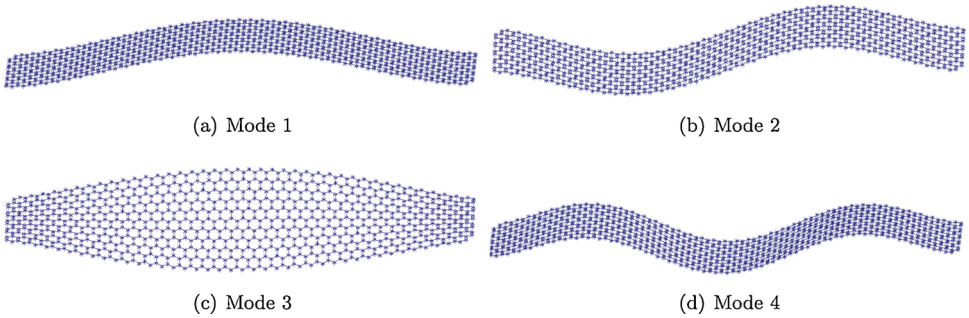

(a) Mode 1 (b) Mode 2

(c) Mode 3 (d) Mode 4

Fig. 18. The first four mode shapes of SLGS computed in the article [236].

Table 22
Predicted fracture property of nanocomposites using finite element method (FEM).

Filler type	Matrix type	Fracture property	FEM type	Source
MWCNT	Al_2O_3	5.5 MPa $m^{1/2}$ (toughness)	MSOFSO	[158]
MWCNT	Polycarbonate	3.2×10^4 (matrix-3 $\times 10^4$)(J integral (N/m))	MSOFSO	[105]
SWCNT	Polyethylene	80 nN (pullout)	MSOFSO	[96]
MWCNT	Epoxy	2.43 (matrix-1.64) (MPa $m^{1/2}$) (toughness)	FE-EX	[76]
MWCNT	Epoxy	2.43 (matrix-1.64) (MPa $m^{1/2}$) (toughness)	FE-EX	[78]
SWCNT	Polymer	3.5 (normalised J-Integral)	MSOFSF	[521]
MWCNT	Si_3N_4	5.6 (MPa $m^{1/2}$ toughness)	MSOFSO	[154]
SLGS	Polymer	20 (normalised SERR)	MSOFSF	[632]
SWCNT	Epoxy	1.6 (pullout nN)	MSOFSF	[80]
SWCNT	Epoxy	1.0 (matrix- 0.65) (MPa $m^{1/2}$) (SIF))	MSOFSF	[81]
SLGS	Epoxy	1.9 (normalised SERR))	MSOFSF	[634]
SWCNT	Cement	36 (N/m energy)	XFEM	[162]
MLGS	SiO_2	1.1 (normalised pullout)	N/A	[630]
SWCNT	Epoxy	80 (μN pullout)	MSHFME	[631]
SWCNT	Concrete	22 (N/m energy)	MSHFBE	[163]
SLGS	Epoxy	360 (nN pullout)	MSOFSP	[233]
SWCNT	Epoxy	2.5 (/m^2 SERR)	MSOFSO	[633]
SWCNT	Cu	0.8 (J/m^2 SERR)	MSOFSO	[633]
GNP	GFRPA6	4200 (J/m^2 SERR)	MSHFSH	[142]

publications that use FEM to predict the K of graphene are shown in Table 24. The types of graphene considered by the publications are graphite, SLGS and MLGS. According to this table, SLGS offers the highest K and graphite offers the lowest K. Among the four publications, only one publication completely relied on FEM to predict K, whereas the other three relied on either the FE–MD or FE–analytical combinations. The authors in the publication [49], modelled a porous graphite foam specimen with 3D tetrahedral FEs using the tool ALGOR. The authors considered 92.5% porosity in the foam and calculated temperature and heat flux in the graphite foam specimen. Then the bulk K of the specimen (K_b) has then been calculated by the equation:

$$K_b = \frac{1/A \sum_{n_{sp}} (q_z)/(\Delta T/\Delta z)}{n_{sp}} \tag{12}$$

where q_z is heat flux calculated from FEM, ΔT is the temperature difference calculated from FEM, A is the cross-section area, n_{sp} is the number of the sample point, and Δz is the distance between the sample points. Then the effective K of the porous graphite has been calculated by $K_{eff} = K_b/K_{sol}$, where, K_{sol} is the intrinsic K of graphite. Jang et al. [637], used a coupled FEM-least square method to predict the temperature in an MLGS system and then calculate K. In the publication [638], the authors used an equilibrium molecular dynamics method (EBM) to predict K in polycrystalline graphene with a small sized grains and then performed a multiscale coupling with FEM to predict K for larger grains. In [639], the authors used a non-equilibrium molecular dynamics method (EBM) to predict K in BLGS with small sized grains and then performed a multiscale coupling with FEM to predict K for laminated graphene sheets the macroscopic level. No publication that predicts K of the CNT using FEM has been identified. Ten publications that predict K of nanocomposites have been identified and shown in Table 25. Various types of fillers considered by the authors are SWCNT, MWCNT, MLGS and GNP. Considered host materials are polymers, water, Cu and Al. Sihn et al. [146] used FEM to determine the optimum K of transition zone (TZ) between epoxy and MWCNT. Based on the FEM results, the researchers fabricated TZ using layers of metals and also by functionalizing MWCNT. In the next step, a laser flash technique has been used to measure K. The measured K of the composite is found to be 90,954% of the K of the matrix. In Table 25, least enhancement of K shown is 23% and is by the authors [640]. The authors used a coupled MD-FE method to determine the enhancement (23%) at 10% MWCNT V_f (volume fraction).

8.2. Coefficient of thermal expansion (CTE)

In the survey conducted here, four research publications that predict CTE of graphene, CNT and nanocomposites have identified and shown in Tables 26 and 27 . Table 26 shows CTE of both graphene and CNT. In Table 26, the type of CNT and graphene used by the authors are SWCNT and SLGS. Cao et al. [337] used a combination of MD and FEM to predict thermal vibrational characteristics and CTE of SWCNT, whereas the other authors [460] used the well-known SF based FEM to predict CTE of SWCNT and SLGS. These authors constrained one end of the SWCNT and SLGS, introduced uniformed temperature on all nodes/atoms and then calculated CTE based on the deflection of nodes/atoms. The value 2.2×10^{-6} °C shown in the table is taken from an armchair SWCNT with a diameter 3.2 nm. The other value 2.31×10^{-6} °C is taken from an armchair SLGS with height of 4.5 nm. Two publications that predict CTE of nanocomposite have been identified and shown in Table 27. The fillers considered in both publications are SWCNT. A drop in CTE due to nanoreinforcement has been considered as enhancement.

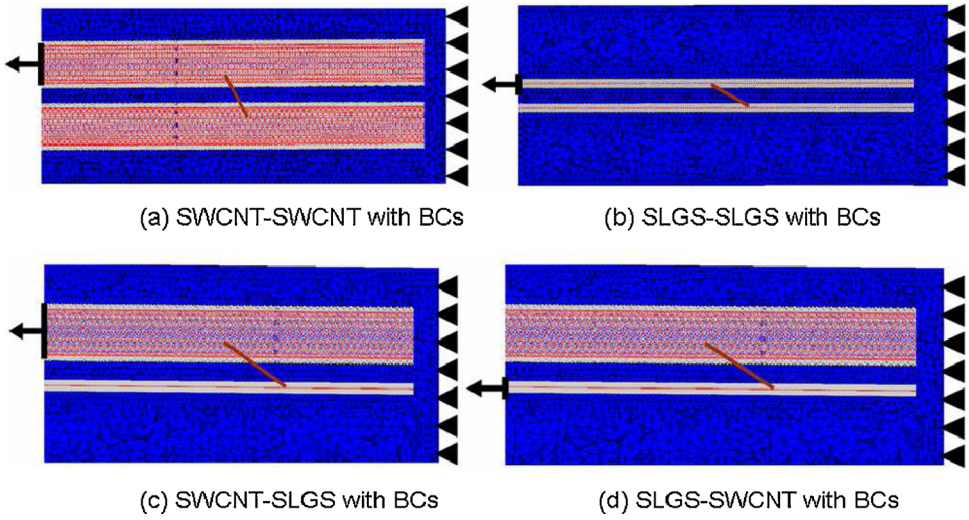

Fig. 19. RVEs developed in Ref. [233] to simulate fibre pullout.

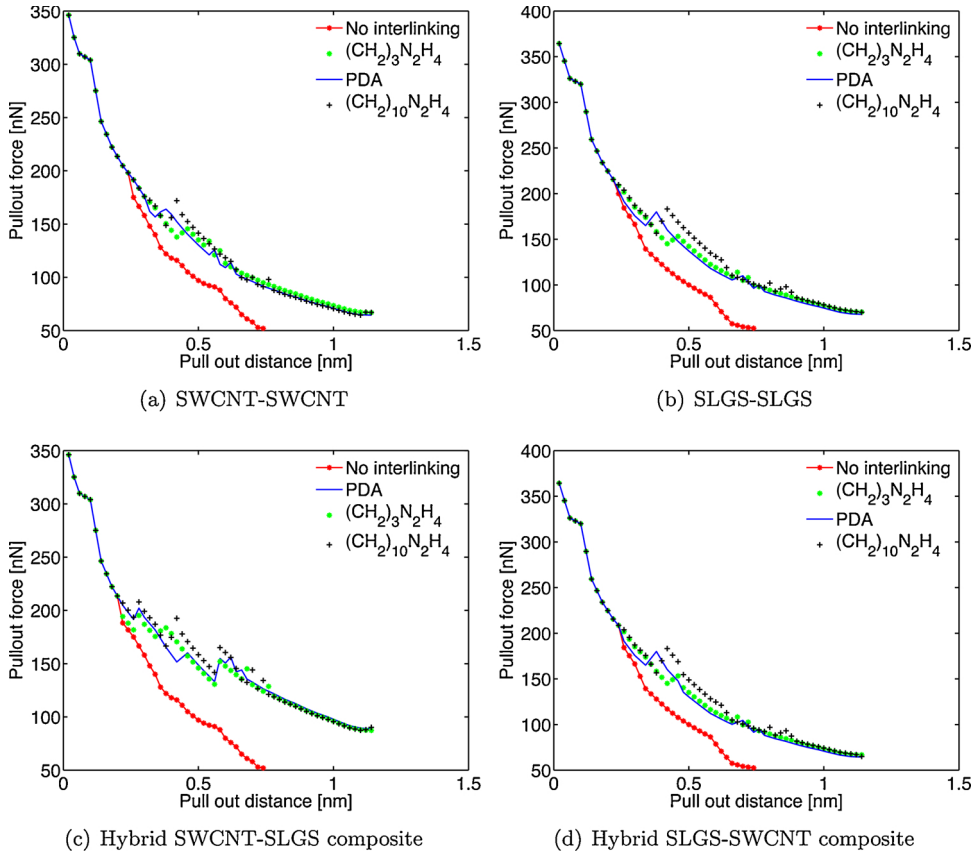

Fig. 20. Force required to pull out the fibre from the nanocomposites [233].

Table 23
Predicted damping of nanocomposite using finite element method(FEM).

Filler type	Matrix type	Loss factor	FEM type	Source
MWCNT	Cyanoacrylate epoxy	0.3	MBFB	[155]
SWCNT	Epoxy	0.1	MSHFSH	[69]
SWCNT	Epoxy	0.24	MSOFSO	[140]
SWCNT	PEEK	0.42	MSOFBE	[124]

Table 24
Predicted thermal conductivity K of graphene using finite element method (FEM).

Graphene type	Thermal conductivity	Type of FEM	Source
Graphite	0.042 W/m°C	Solid element	[49]
MLGS	2000 W/m K	FE–analytical	[637]
SLGS	3000 W/m K	FE–MD	[638]
MLGS	455.0 W/m K	FE–MD	[639]

Table 26
Predicted coefficient of thermal expansion of GANS using finite element method (FEM).

Type	*CTE*	Type of FEM	Source
SWCNT	$-0.55 \times 10^{-6}\,K^{-1}$	FE–MD	[337]
SWCNT	2.2×10^{-6} °C	SF	[460]
SLGS	2.31×10^{-6} °C	SF	[460]

The authors [63] represented SWCNT/epoxy nanocomposite with 3D solid FEs and predicted an 11.4% enhancement in CTE, due to nanoreinforcement. This is the lowest predicted enhancement in Table 27. The other authors [70] considered four types of host materials, namely epoxy, Pb, Ti and steel. These authors also represented both matrix and filler with 3D solid FEs. As per these authors [70], epoxy benefits from the highest CTE (91%) enhancement due to nanoreinforcement. Whereas the host material steel attains the lowest enhancement (15%) due to nanoreinforcement.

Table 25
Predicted enhancement in thermal conductivity K W/mK of nanocomposites using finite element method (FEM).

Filler type	Matrix type	K_m in W/mK	K_c in W/mK	% Enhancement	FEM type	Source
MWCNT	Water	N/A	N/A	40	FE-EX	[641]
SWCNT	Epoxy	0.122	0.6	392	CVFEM	[66]
SWCNT	Epoxy	0.275	250.4	90,954	FE-EX	[146]
MWCNT	AlSi	150	272	81	OOFEM	[147]
MWCNT/GNP	Epoxy	0.225	0.5	122	MSOFSO	[12]
MLGS	PLA	0.125	0.29	132	MSOFSO	[126]
MLGS	Epoxy	N/A	N/A	23	MSOFSO	[640]
MLGS	PDMS	0.2	0.9	350	MSOFSO	[131]
MLGS	Cu	390	221	43	MSOFSH	[149]
SWCNT	AL	240	475	98	MSOFSO	[150]

Table 27
Predicted enhancement in coefficient of thermal expansion of nanocomposites using finite element method (FEM).

Filler type	Matrix type	CTE_m	CTE_{comp}	% Enhancement	FEM type	Source
SWCNT	Epoxy	7×10^{-5} K^{-1}	6.2×10^{-5} K^{-1}	11.4	MSOFSO	[63]
SWCNT	Epoxy	58×10^{-6} K^{-1}	5.2×10^{-6} K^{-1}	91	MSOFSO	[70]
SWCNT	Pb	29×10^{-6} K^{-1}	8.7×10^{-6} K^{-1}	69	MSOFSO	[70]
SWCNT	Ti	8.6×10^{-6} K^{-1}	6.45×10^{-6} K^{-1}	25	MSOFSO	[70]
SWCNT	Steel	12×10^{-6} K^{-1}	10.2×10^{-6} K^{-1}	15	MSOFSO	[70]

9. Future directions of FEM in the analysis of GANS and relevant nanocomposites

Most of the research carried out in the field of GANS, and their composites is currently focused on the prediction of their mechanical properties using the finite element method. This is probably attributed to the traditional use of FEM in the solution of mechanical problems over the past few decades. Its widespread understanding within engineering and scientific community has allowed rapid dissemination into several branches of mechanics, such as the nanomechanics of GANS and GANS reinforced composite materials. After a comprehensive review of over six hundred research papers, several omissions in the FE modelling of GANS and their nanocomposites have been identified. Therefore, recommendations future research directions to address these gaps are given in the following.

From the publications reviewed here, no research works have been identified discussing the influence of temperature on the Poisson's ratio ν of graphene, CNT or nanocomposites by means of FE techniques. Thus, it is recommended to explore the computation of ν under different thermal conditions. To achieve this objective, the development of new thermo-mechanical FE atomistic models will constitute an unavoidable task. Moreover, few authors have predicted the Young's modulus E and shear modulus G of graphane and graphyne. Similarly, no literature about the FE predictions of their σ_T, ϵ_T and ω values has been found. Therefore, in the future, this gap needs to addressed. In addition, novel FE based atomistic models must be developed in order to predict σ_T, ϵ_T, λ and ω of pillared graphene. There is also a need to model advanced architectures (such as, super-CNT and pillared graphene) of nanoreinforcements by means of FE atomistic based simulations. These nano reinforcements are expected to enhance the mechanical and thermal properties of the host materials significantly. Values of G and λ for graphane and super-CNT have not been widely reported in the literature. This lack of data needs to be addressed. Publications that have predicted numerically the values of G of nanocomposites numerically have not considered popular host materials such as PEEK, Al, polyurethane, polycarbonate, rubber and glass matrices. The development of FE based atomistic models to simulate these host materials and nanoreinforcements is required and must be addressed in the future. Furthermore, the computational development of space frame atomistic FE models of super-CNT and pillared graphene is expensive. However, these nanostructures can also be simulated by equivalent beams. Therefore, simplified models are also required in order to capture the response of large atomistic/molecular systems. On the other hand, very limited data about λ values for nanocomposites exists in the literature. Here, only six publications have been identified. This gap needs to be filled by future works by predicting λ for various possible combinations of nanofillers and host materials. The majority of the research works that have predicted ω_{COMP} values have not presented ω_m. Therefore; researchers are recommended to present in their future works ω_{COMP} values in conjunction with ω_m. The fracture properties such as SERR and SIF available in the literature have been limited to SLGS. Then, numerical simulations must be extended to determine fracture properties for MLGS, SWCNT, MWCNT, super-CNT and pillared graphene. The nanoreinforcement pull out force presented in the literature is restricted to few host materials, namely epoxy, polyethylene and SiO_2. Therefore, future publications need to consider other possible host materials. The publications that predicted damping in the nanocomposites considered either SWCNT or MWCNT. There is a need to consider the influence of other nanofiller types such as SLGS and MLGS on the damping properties of nanocomposites. When compared to the number of publications dealing with the mechanical properties of nanomaterials, the number of publications predicting thermal properties is somewhat limited. This lack of research is even more pronounced in other areas involving acoustic, electric, chemical or coupled physical fields, among others. Therefore, urgent attention is required to close this gap.

Multiscale analyses have been limited the simplified physical behaviour of RVEs. There is a need to include more complex microscopic features in the future, such as debonding between adjacent microphases, crack opening/closure, size effects or softening damage, among others. The simultaneous description of several length scales is also required and needs immediate attention. Multiscale FE simulations must be extended to describe the fully coupled physical behaviour of material scales, from molecular levels to engineering components. To date, this task seems to be unfeasible due to the excessive computational times and memory requirements involved in the FE simulations. This challenge must be addressed in order to solve real problems found the industry. If all of the above-mentioned challenges are overcome, then GANS and their composites can be successfully adopted in all industries including aerospace, automotive and biomedical.

10. Research subjects that are mature and the challenges that require attention

The current review suggests that many aspects of the finite element modelling of GANS have evolved since the last two decades and have reached the stage of full maturity. The fidelity and the complexity of the finite element models are ever-increasing. However, there are many issues still in their infancy that need more attention in the future. Although such issues have been mentioned in the previous section, the most important mature aspects and future challenges will be highlighted in the next subsections for the sake of clarity.

10.1. Matured aspects

1. Atomistic modelling: The fundamentals of atomistic model development, based on interatomic potentials, have been fully established.
2. FEM as an established tool: FEM as a tool to study the nanoscale behaviour of GANS has been widely accepted within academia.
3. Validation: Within the GANS research community, FEM has been validated against experimental, theoretical and other numerical methods.
4. Basic mechanical properties: Currently, FEM can predict the mechanical properties of GANS with reasonable accuracy. The properties include Young's modulus, Poisson's ratio, shear modulus, natural frequency, and buckling strength, among others.
5. Basic thermal properties: Currently, FEM can predict basic thermal properties of GANS with reasonable accuracy. These properties include thermal conductivity and coefficient of thermal expansion.

6. Idealized geometries: The GANS research community is making use of FEM as an efficient and reliable tool to understand the specimens of GANS with idealized geometries.
7. Design of nanodevices: FEM has been successfully deployed to aid the design of nanodevices using GANS. The nanodevices include pressure sensors, strain sensors, mass sensors/resonators, structural health monitoring devices, and atomic dust detectors.
8. Successful customization: FEM was initially developed to solve problems in civil engineering. However, in the later era, FEM has been successfully customized to solve problems in GANS research community. The customization includes the development of element types, material models and solution procedures.

10.2. Aspects requiring attention

1. Macroscopic considerations: Most of FEM investigations have focused on the understanding of the nanoscale behaviour of GANS and their composites. It is required to extend the FEM based studies to understand the macroscopic influence of these nanomaterials.
2. Beyond academia: There is a need to transfer the FE modelling of GANS from academia to industry.
3. Beyond idealized geometries: The extension of FEM strategies developed for square sheets of graphene and cube-shaped nanocomposite RVEs to futuristic GANS based products are urgently required, such as aircraft fuselage and wind turbines.
4. Thermal influence on Poisson's ratio: As per the articles reviewed here, FEM has not been utilized to understand the influence of temperature on Poisson's ratio of GANS and their composites. There is a need to fill this gap.
5. Other variants of GANS: In the context of FEM, literature has not paid full attention to other variants of graphene such as super CNT, pillared graphene, graphane, and graphyne. The mechanical and thermal properties of these nanomaterials are required to be studied employing FEM.
6. Wider range of host materials: In the context of FEM, literature has mainly focused on a limited number of host materials with carbon nano reinforcements. It is required to study the interaction of carbon nano reinforcements with a wider range of host polymers, ceramics, and metals with the aid of FEM.
7. Expensive simulation: The atomistic finite element simulations of large realistic structures can be computationally expensive and time-consuming. As a result, there is a need to explore condensed modelling approaches such as substructuring and sub modelling within GANS research community.
8. Multiphysics simulation: The mainstream research in the computational GANS research community has not considered the interaction of liquids and gas with these nanomaterials, except a few isolated publications. There is a need to open up a new arena of finite element based fluid-structure interaction research in the GANS research community.
9. Pull out simulations: In the finite element based literature, the pullout simulations have considered a limited number of filler and resin types. It is needed to consider various types of nanofillers and resins in nanofibre pull out simulations. This will pave the way for a comprehensive understanding of the interfacial characteristics of nano reinforcements.

11. Conclusions

In this article, a comprehensive review of finite element techniques applied to the study of graphene and its associated nanostructures has been presented. Various derivatives of graphene and carbon nanotubes have been described along with the relevant nanocomposites, with an insight into combinations of host materials and fillers. Numerical methods other than the finite element method, that are available to analyse graphene-based materials have also been presented briefly. The most popular finite element strategy to represent graphene-based nanostructures by means of beam lattice finite elements has been discussed in detail, followed by an overview of the associated multiscale methods. A review on the representative volume element based micromechanical modelling has been introduced. The role of the finite element method in the design of carbon-based nanodevices such as nanosensors and nanoresonators has also been presented.

Reported values of Young's modulus for graphene, carbon nanotube and nanocomposites using finite element method, have been listed and discussed. The data obtained by finite element simulations suggests that Young's modulus for graphene and carbon nanotube can be as high as 2.9 and 4.84 TPa, respectively. For the shear modulus of graphene and carbon nanotube, the reported values are up to 1.8 and 1.25 TPa, respectively. Numerical predictions for the Poisson's ratio have also been presented. For graphene and carbon nanotube, their values can be as low as -0.001 and 0.06, respectively. The scatter of Young's moduli, shear moduli and Poisson's ratios for single-layer graphene, and single-wall carbon nanotube have been discussed using tabular and graphical approaches. The atomistic finite element predictions of the tensile strength and the tensile strain have been reviewed. Tensile strengths up to 425 and 270 GPa have been predicted for graphene and carbon nanotube, respectively. A tensile strain up to 60% has been predicted for graphene and carbon nanotube. The tensile strength and tensile strain of nanocomposites have also been listed and compared with those of host materials.

Another aspect discussed in details in this paper is the possibility of enhancement of mechanical properties using nanoreinforcements. The enhancement in the Young's modulus, Poisson's ratio and shear modulus of a host material due to nanoreinforcement has been presented. Their enhancements have been reported up to 6.4×10^6, 448 and 28,000%, respectively. The enhancement in the Poisson's ratio of a host material due to nanoreinforcement can be up to 448%. The enhancement in the shear modulus of a host material due to nanoreinforcement can be up to 28,000%. A literature survey on the buckling behaviour of graphene-based nanostructures and nanocomposites has shown an increase of up to 568% in the buckling strength when including nanoreinforcements. The natural frequencies of graphene and carbon nanotubes can be up to 185 and 30 THz, respectively. The increase in natural frequency due to the inclusion of nanoreinforcements can be as high as 93%. As per the literature survey conducted here, it can be concluded that, by using GANS based materials as nanoreinforcements, they can significantly enhance both mechanical and thermal properties of host materials. However, the numerical analysis performed in the literature considered idealistic geometries using RVEs. The predicted properties will significantly differ if realistic geometries are to be considered. Therefore, such large enhancements numerically predicted in terms of an order of magnitudes higher than that of host materials, are unlikely to be achievable in practice.

The fracture properties of graphene-based nanostructures and relevant nanocomposites such as strain energy release rate, stress intensity factor, J-Integral and fibre pullout force have been listed and discussed in the current article. Furthermore, very limited data about the damping properties of nanocomposites has been found in the literature. Based on the gathered data, it can be concluded that the loss factor can be up to 0.43 for a polymer/carbon nanotube nanocomposite.

Thermal properties of graphene-based nanostructures and relevant nanocomposites have also been reviewed. The thermal conductivity of graphene can be up to 3000 W/mK. The thermal conductivity enhancement due to nanoreinforcements can be up to 90,954%. Within the literature, coefficient thermal expansion of carbon nanotube has been presented in both negative and positive. For the case of nanocomposites, an increase the coefficient of thermal expansion of up to 91% can be achieved by the use of nanoreinforcements.

Several important aspects of the computational modelling of nanostructures and nanocomposites appear to have been overlooked in

the literature. It is expected that the present paper will guide researchers to address these important issues in the near future.

Conflict of interest

None declared.

References

[1] R. Courant, Bull. Am. Math. Soc. 49 (1943) 1–23, https://doi.org/10.1090/s0002-9904-1943-07818-4.
[2] W. Ritz, J. für die Reine und Angew. Math. 135 (1909) 1–61.
[3] B. Galerkin, Vestnik Inzh 19 (1915) 897–908.
[4] R. Clough, The Finite Element Method in Plane Stress Analysis, American Society of Civil Engineers, 1960, p. 35.
[5] O.C. Zienkiewicz, R.L. Taylor, D.D. Fox, The Finite Element Method for Solid and Structural Mechanics, 1st ed., McGraw-Hill, Great Britain, 1967.
[6] N. Gokhale, S. Deshpande, S. Bedekar, A. Thite, Practical Finite Element Analysis, Book, (2007).
[7] J.W. Suk, R.D. Piner, J. An, R.S. Ruoff, ACS Nano 4 (11) (2010) 6557–6564, https://doi.org/10.1021/nn101781v pMID: 20942443.
[8] C. Wang, Q. Peng, J. Wu, X. He, L. Tong, Q. Luo, J. Li, S. Moody, H. Liu, R. Wang, S. Du, Y. Li, Carbon 80 (2014) 279–289, https://doi.org/10.1016/j.carbon.2014.08.066.
[9] D. Han, Y. Zhao, Y. Zhang, S. Bai, RSC Adv. 5 (2015) 94426–94435, https://doi.org/10.1039/C5RA16780A.
[10] H. Moon, D. Kumar, H. Kim, C. Sim, J. Chang, J. Chang, H. Kim, H. Kim, D. Lim, ACS Nano 9 (3) (2015) 2711–2719, https://doi.org/10.1021/nn506516p.
[11] M. Sadigh, G. Marami, Mater. Des. 92 (2016) 36–43, https://doi.org/10.1016/j.matdes.2015.12.006.
[12] M. Safdari, M. Al-Haik, Carbon 64 (2013) 111–121, https://doi.org/10.1016/j.carbon.2013.07.042.
[13] K.A. Zarasvand, H. Golestanian, Compos. Sci. Technol. 139 (2017) 117–126, https://doi.org/10.1016/j.compscitech.2016.12.024 http://www.sciencedirect.com/science/article/pii/S0266353816313276.
[14] Z. Zhao, C. Feng, Y. Wang, J. Yang, Compos. Struct. 180 (2017) 799–808, https://doi.org/10.1016/j.compstruct.2017.08.044 http://www.sciencedirect.com/science/article/pii/S026382231731783X.
[15] Y. Wang, C. Feng, Z. Zhao, J. Yang, Compos. Struct. 202 (2018) 38–46, https://doi.org/10.1016/j.compstruct.2017.10.005.
[16] S. Subrina, D. Kotchetkov, J. Nanoelectron. Optoelectron. 3 (3) (2008) 249–269, https://doi.org/10.1166/jno.2008.303 https://www.ingentaconnect.com/content/asp/jno/2008/00000003/00000003/art00003.
[17] H. Han, Y. Zhang, N. Wang, M. Samani, Y. Ni, Z. Mijbil, M. Edwards, S. Xiong, K. Saaskilahti, M. Murugesan, Y. Fu, L. Ye, H. Sadeghi, S. Bailey, Y. Kosevich1, C. Lambert, J. Liu, S. Volz, Nat. Commun. 7 (2016) 1–9, https://doi.org/10.1038/ncomms11281.
[18] J. Lee, B. Lee, Comput. Mater. Sci. 51 (1) (2012) 30–42, https://doi.org/10.1016/j.commatsci.2011.06.041 http://www.sciencedirect.com/science/article/pii/S0927025611003831.
[19] B. Dittrich, K. Wartig, D. Hofmann, R. Mülhaupt, B. Schartel, Polym. Adv. Technol. 24 (2013) 916–926, https://doi.org/10.1002/pat.3165.
[20] W. Lee, S. Tsoi1, K. Whitener, R. Stine, J. Robinson, J. Tobin, A. Weerasinghe, P. Sheehan, S. Lyuksyutov, Robust Reduction of Graphene Fluoride Using an Electrostatically Biased Scanning Probe 6 Springer, 2013, pp. 767–774, https://doi.org/10.1007/s12274-013-0355-1.
[21] A. Manjavacas, S. Thongrattanasiri, F. Abajo, Nanophotonics 2 (2013) 1–12, https://doi.org/10.1515/nanoph-2012-0035.
[22] C. Li, T.-W. Chou, Phys. Rev. B 68 (2003) 73405, https://doi.org/10.1103/PhysRevB.68.073405.
[23] M. Arroyo, T. Belytschko, Phys. Rev. Lett. 91 (2003) 215505, https://doi.org/10.1103/PhysRevLett.91.215505.
[24] Y. Zhang, X. Chen, X. Wang, Compos. Sci. Technol. 68 (2) (2008) 572–581, https://doi.org/10.1016/j.compscitech.2007.03.012 http://www.sciencedirect.com/science/article/pii/S0266353807001066.
[25] Y. Li, X. Qiu, F. Yang, X.-S. Wang, Y. Yin, Nanotechnology 19 (2008) 165502, https://doi.org/10.1088/0957-4484/19/16/165502.
[26] J.G. Park, S. Li, R. Liang, X. Fan, C. Zhang, B. Wang, Nanotechnology 19 (18) (2008) 185710 http://stacks.iop.org/0957-4484/19/i=18/a=185710.
[27] M. Upmanyu, H. Wang, H. Liang, R. Mahajan, J. R. Soc. Interface 5 (20) (2008) 303–310, https://doi.org/10.1098/rsif.2007 http://rsif.royalsocietypublishing.org/content/5/20/303.full.pdf.
[28] K. Tserpes, C. Kora, Aerospace 5 (4) (2018), https://doi.org/10.3390/aerospace5040106 http://www.mdpi.com/2226-4310/5/4/106.
[29] J. Guo, Y. Yoon, Y. Ouyang, Nano Lett. 7 (7) (2007) 1935–1940, https://doi.org/10.1021/nl0706190 pMID: 17552571.
[30] Y. Yoon, J. Guo, Appl. Phys. Lett. 91 (7) (2007) 73103, https://doi.org/10.1063/1.2769764.
[31] V.B. Shenoy, C.D. Reddy, A. Ramasubramaniam, Y.W. Zhang, Phys. Rev. Lett. 101 (2008) 245501, https://doi.org/10.1103/PhysRevLett.101.245501.
[32] K. Kim, A. Sussman, A. Zettl, ACS Nano 4 (3) (2010) 1362–1366, https://doi.org/10.1021/nn901782 pMID: 20131856.
[33] N. Khani, M. Yildiz, B. Koc, Mater. Des. 109 (2016) 123–132, https://doi.org/10.1016/j.matdes.2016.06.126.
[34] S.H. Ghaderi, E. Hajiesmaili, Comput. Mater. Sci. 55 (2012) 344–349, https://doi.org/10.1016/j.commatsci.2011.11.016 http://www.sciencedirect.com/science/article/pii/S0927025611006306.
[35] L. Pan, Y. Konishi, H. Tanaka, O. Suekane, T. Nosaka, Y. Nakayama, Jpn. J. Appl. Phys. 44 (4R) (2005) 1652.
[36] C.D. Reddy, Q.H. Cheng, V.B. Shenoy, Y.W. Zhang, J. Appl. Phys. 109 (5) (2011) 54314, https://doi.org/10.1063/1.3555612.
[37] F. Scarpa, R. Chowdhury, S. Adhikari, Phys. Lett. A 375 (20) (2011) 2071–2074, https://doi.org/10.1016/j.physleta.2011.03.050 http://www.sciencedirect.com/science/article/pii/S0375960111003987.
[38] J. Lee, C. Shim, B. Lee, Int. J. Mater. Sci. Appl. 2 (2013) 209–220, https://doi.org/10.11648/j.ijmsa.2013020617.
[39] M. Shi, Q. Li, B. Liu, X. Feng, Y. Huang, Int. J. Solids Struct. 46 (25) (2009) 4342–4360, https://doi.org/10.1016/j.ijsolstr.2009.08.024 http://www.sciencedirect.com/science/article/pii/S0020768309003321.
[40] K.I. Tserpes, P. Papanikos, Compos. Struct. 91 (2) (2009) 131–137, https://doi.org/10.1016/j.compstruct.2009.04.039 http://www.sciencedirect.com/science/article/pii/S0263822309001640.
[41] C.-L. Wong, M. Annamalai, Z.-Q. Wang, M. Palaniapan, J. Micromech. Microeng. 20 (11) (2010) 115029 http://stacks.iop.org/0960-1317/20/i=11/a=115029.
[42] D. Davidovikj, J. Slim, S. Cartamil-Bueno, H. Zant, P. Steeneken, W. Venstra1, Nano Lett. 16 (2016) 2768–2773, https://doi.org/10.1021/acs.nanolett.6b00477.
[43] S. Sihn, V. Varshney, A.K. Roy, B.L. Farmer, Carbon 50 (2) (2012) 603–611, https://doi.org/10.1016/j.carbon.2011.09.019 http://www.sciencedirect.com/science/article/pii/S0008622311007536.
[44] L. Song, Z. Guo, C. Chai, Z. Wang, Y. Li, Y. Luan, Carbon 140 (2018) 210–217, https://doi.org/10.1016/j.carbon.2018.08.058.
[45] S. Duan, K. Yang, Z. Wang, M. Chen, L. Zhang, H. Zhang, C. Li, ACS Appl. Mater. Interfaces 8 (2016) 2187–2192, https://doi.org/10.1021/acsami.5b10791.
[46] J. Shi, X. Li, H. Cheng, Z. Liu, L. Zhao, T. Yang, Z. Dai, Z. Cheng, Z. Shi, L. Yang, Z. Zhang, A. Cao, H. Zhu, Y. Fang, Adv. Funct. Mater. 26 (2016) 2078–2084, https://doi.org/10.1002/adfm.201504804.
[47] S. Rouhi, T. Reza, B. Ramzani, S. Mehran, Proc. Inst. Mech. Eng. Part C: J. Mech. Eng. Sci. 231 (6) (2016) 1162–1178, https://doi.org/10.1177/0954406216631574.
[48] R. Couto, N. Silvestre, J. Nanomater. 2016 (2016) 1–15, https://doi.org/10.1155/2016/7487049.
[49] M.K. Alam, A.M. Druma, C. Druma, J. Compos. Mater. 38 (22) (2004) 1993–2006, https://doi.org/10.1177/0021998304044772.
[50] T. Yang, Y. Wang, X. Li, Y. Zhang, X. Li, K. Wang, D. Wue, H. Jinf, Z. Li, H. Zhu, Nanoscale 6 (2014) 1–6 doi:13053–13059.
[51] T. Yang, W. Wang, H. Zhang, X. Li, J. Shi, Y. He, Q. Zheng, Z. Li, H. Zhu, ACS Nano 9 (2015) 10867–10875, https://doi.org/10.1021/acsnano.5b03851.
[52] T. Zhang, X. Li, H. Gao, Extreme Mech. Lett. 1 (2014) 3–8, https://doi.org/10.1016/j.eml.2014.12.007.
[53] B. Nam, S. Bae, S. Park, Y. Yoo, J. Lee, J. Han, J. Yi, Sci. Direct 15 (2015) 33–42, https://doi.org/10.1016/j.nanoen.2015.04.001.
[54] K. Cai, J. Luo, Y. Ling, J. Wan, Q. Qin, Sci. Rep. 6 (2016) 1–10, https://doi.org/10.1038/srep35157.
[55] R. Poelma, X. Fan, Z. Hu, G. Tendeloo, H. Zeijl, G. Zhang, Adv. Funct. Mater. 26 (2016) 1233–1242, https://doi.org/10.1002/adfm.201503673.
[56] A. Gangele, S. Garala, A. Pandey, Int. J. Mech. Sci. 146–147 (2018) 191–199, https://doi.org/10.1016/j.ijmecsci.2018.07.032.
[57] N. Ginga, W. Chen, S. Sitaraman, Sci. Direct J. 66 (2014) 57–66, https://doi.org/10.1016/j.carbon.2013.08.042.
[58] R. Ansari, S. Rouhi, A. Shahnazari, Mech. Adv. Mater. Struct. (2017), https://doi.org/10.1080/15376494.2016.1255813.
[59] J. Bocko, P. Lengvarsky, J. Sarlozi, J. Mech. Eng. 68 (2) (2018) 9–16, https://doi.org/10.2478/scjme-2018-0013.
[60] S. Yengejeh, M. Zadeh, A. Ochsner, Appl. Phys. A 115 (2013) 1335–1344, https://doi.org/10.1007/s00339-013-7999-2.
[61] M. Fakhrabadi, A. Amini, A. Rastgoo, Comput. Mater. Sci. 65 (2012) 411–425, https://doi.org/10.1016/j.commatsci.2012.08.002.
[62] R. Ansari, S. Rouhi, A. Shahnazari, Eur. Phys. J. Appl. Phys. 76 (2) (2016) 20402, https://doi.org/10.1051/epjap/2016160173.
[63] H.R. Lusti, A.A. Gusev, Model. Simul. Mater. Sci. Eng. 12 (3) (2004) S107 http://stacks.iop.org/0965-0393/12/i=3/a=S05.
[64] C. Li, T.-W. Chou, Compos. Sci. Technol. 66 (14) (2006) 2409–2414, https://doi.org/10.1016/j.compscitech.2006.01.013 special Issue in Honour of Professor C.T. Sun, http://www.sciencedirect.com/science/article/pii/S0266353806000285.
[65] G.D. Seidel, D.C. Lagoudas, Mech. Mater. 38 (8) (2006) 884–907, https://doi.org/10.1016/j.mechmat.2005.06.029 advances in Disordered Materials, http://www.sciencedirect.com/science/article/pii/S0167663605001699.
[66] Y.S. Song, J.R. Youn, Carbon 44 (4) (2006) 710–717, https://doi.org/10.1016/j.carbon.2005.09.034 http://www.sciencedirect.com/science/article/pii/S0008622305005609.
[67] D.C. Hammerand, G.D. Seidel, D.C. Lagoudas, Mech. Adv. Mater. Struct. 14 (4) (2007) 277–294, https://doi.org/10.1080/15376490600817370.
[68] A. Fereidoon, E. Saeedi, B. Ahmadimoghadam, Proceedings of the World Congress on Engineering 2008, vol. II, (2008).
[69] X. Zhou, E. Shin, K. Wang, C. Bakis, Compos. Sci. Technol. 64 (15) (2004) 2425–2437, https://doi.org/10.1016/j.compscitech.2004.06.001 developments in carbon nanotube and nanofibre reinforced polymers http://www.sciencedirect.com/science/article/pii/S0266353804001319.
[70] S. Kirtania, D. Chakraborty, Int. Conf. Mech. Eng. 13 (2009), https://pdfs.

semanticscholar.org/8218/9521929a75b8c8863a40c06a047f260cb367.pdf.
[71] C. Li, T.-W. Chou, Compos. Part A: Appl. Sci. Manuf. 40 (10) (2009) 1580–1586, https://doi.org/10.1016/j.compositesa.2009.07.002 http://www.sciencedirect.com/science/article/pii/S1359835X09001924.
[72] S. Georgantzinos, G. Giannopoulos, N. Anifantis, J. Comput. Theor. Nanosci. 7 (8) (2010) 1436–1442, https://doi.org/10.1166/jctn.2010.1500 https://www.ingentaconnect.com/content/asp/jctn/2010/00000007/00000008/art00014.
[73] G. Giannopoulos, S. Georgantzinos, N. Anifantis, Compos. Part B: Eng. 41 (8) (2010) 594–601, https://doi.org/10.1016/j.compositesb.2010.09.023 http://www.sciencedirect.com/science/article/pii/S1359836810001642.
[74] M.M. Shokrieh, R. Rafiee, Comput. Mater. Sci. 50 (2) (2010) 437–446, https://doi.org/10.1016/j.commatsci.2010.08.036 http://www.sciencedirect.com/science/article/pii/S0927025610005057.
[75] M.M. Shokrieh, R. Rafiee, Compos. Struct. 92 (10) (2010) 2415–2420, https://doi.org/10.1016/j.compstruct.2010.02.018 http://www.sciencedirect.com/science/article/pii/S0263822310000802.
[76] M. Ayatollahi, S. Shadlou, M. Shokrieh, Eng. Fract. Mech. 78 (14) (2011) 2620–2632, https://doi.org/10.1016/j.engfracmech.2011.06.021 http://www.sciencedirect.com/science/article/pii/S0013794411002451.
[77] M. Ayatollahi, S. Shadlou, M. Shokrieh, Compos. Struct. 93 (9) (2011) 2250–2259, https://doi.org/10.1016/j.compstruct.2011.03.013 http://www.sciencedirect.com/science/article/pii/S0263822311000973.
[78] M. Ayatollahi, S. Shadlou, M. Shokrieh, Mater. Des. 32 (2011) 2115–2124, https://doi.org/10.1016/j.matdes.2010.11.034.
[79] J. Wernik, S. Meguid, Acta Mech. 217 (1) (2011) 1–16, https://doi.org/10.1007/s00707-010-0377-7.
[80] J. Wernik, B. Cornwell-Mott, S. Meguid, Int. J. Solids Struct. 49 (2012) 1852–1863, https://doi.org/10.1016/j.ijsolstr.2012.03.024.
[81] A. Fereidoon, M. Rajabpour, H. Hemmatian, Sci. Direct 54 (2013) 400–408, https://doi.org/10.1016/j.compositesb.2013.05.020.
[82] B. Mortazavi, O. Benzerara, H. Meyer, J. Bardon, S. Ahzi1, Sci. Direct 60 (2013) 356–365, https://doi.org/10.1016/j.carbon.2013.04.048.
[83] G. Giannopoulos, I. Kallivokas, Finite Elem. Anal. Des. 90 (2014) 31–40, https://doi.org/10.1016/j.finel.2014.06.008.
[84] M. Zuberi, V. Esat, Compos.: Part B Eng. 71 (2015) 1–9, https://doi.org/10.1016/j.compositesb.2014.11.020.
[85] M. Karimi, A. Montazeri, R. Ghajar, Compos. Struct. 160 (2017) 782–791, https://doi.org/10.1016/j.compstruct.2016.10.053 http://www.sciencedirect.com/science/article/pii/S0263822316315276.
[86] M. Rein, O. Breuer, H. Wagner, Compos. Sci. Technol. 71 (3) (2011) 373–381, https://doi.org/10.1016/j.compscitech.2010.12.008 http://www.sciencedirect.com/science/article/pii/S0266353810004768.
[87] G. Gallo, E. Thostenson, Mater. Today Commun. 3 (2015) 17–26, https://doi.org/10.1016/j.mtcomm.2015.01.009.
[88] P. Lakshmi, P. Reddy, Int. J. Eng. Res. Appl. (IJERA) 2 (2012) 1–10 http://citeseerx.ist.psu.edu/viewdoc/download?doi=10.1.1.446.8731&rep=rep1&type=pdf.
[89] H. Ning, J. Li, N. Hu, C. Yan, Y. Liu, L. Wu, F. Liud, J. Zhang, Sci. Direct 91 (2015) 224–233, https://doi.org/10.1016/j.carbon.2015.04.054.
[90] H. Zhou, H. Yi, Y. Liu, X. Hu, A. Warrier, G. Dai, Compos. Part B 88 (2016) 201–211, https://doi.org/10.1016/j.compositesb.2015.10.035.
[91] F. Fisher, R. Bradshaw, L. Brinson, Appl. Phys. Lett. 80 (24) (2002) 4647–4649, https://doi.org/10.1063/1.1487900.
[92] F. Fisher, R. Bradshaw, L. Brinson, Compos. Sci. Technol. 63 (11) (2003) 1689–1703, https://doi.org/10.1016/S0266-3538(03)00069-1 modeling and Characterization of Nanostructured Materials http://www.sciencedirect.com/science/article/pii/S0266353803000691.
[93] V. Anumandla, R.F. Gibson, Compos. Part A: Appl. Sci. Manuf. 37 (12) (2006) 2178–2185, https://doi.org/10.1016/j.compositesa.2005.09.016 the 11th US – Japan Conference on Composite Materials http://www.sciencedirect.com/science/article/pii/S1359835X05003830.
[94] M. Heshmati, M. Yas, Mater. Des. 49 (2013) 894–904, https://doi.org/10.1016/j.matdes.2013.01.073.
[95] N. Hu, H. Fukunaga, C. Lu, M. Kameyama, B. Yan, Proc. R. Soc. Lond. A: Math. Phys. Eng. Sci. 461 (2058) (2005) 1685–1710, https://doi.org/10.1098/rspa.2004.1422 http://rspa.royalsocietypublishing.org/content/461/2058/1685.full.pdf.
[96] Y. Chen, B. Liu, X. He, Y. Huang, K. Hwang, Compos. Sci. Technol. 70 (9) (2010) 1360–1367, https://doi.org/10.1016/j.compscitech.2010.04.015 http://www.sciencedirect.com/science/article/pii/S0266353810001600.
[97] A. Srivastava, V. Pathak, M. Dixit, National Conference on Advanced Materials, Manufacturing and Metrology, (2018), pp. 74–79 ISBN: 978-93-87480-56-8.
[98] B. Ashrafi, P. Hubert, Compos. Sci. Technol. 66 (3) (2006) 387–396, https://doi.org/10.1016/j.compscitech.2005.07.020 http://www.sciencedirect.com/science/article/pii/S0266353805002848.
[99] A. Selmi, C. Friebel, I. Doghri, H. Hassis, Compos. Sci. Technol. 67 (10) (2007) 2071–2084, https://doi.org/10.1016/j.compscitech.2006.11.016 http://www.sciencedirect.com/science/article/pii/S0266353806004453.
[100] I. Afrooz, A. Ochsner, M. Rahmandoust, Comput. Mater. Sci. 51 (2012) 422–429, https://doi.org/10.1016/j.commatsci.2011.08.003.
[101] J.-L. Tsai, S.-H. Tzeng, Y.-T. Chiu, Compos. Part B: Eng. 41 (1) (2010) 106–115, https://doi.org/10.1016/j.compositesb.2009.
[102] F. Dalmas, R. Dendievel, L. Chazeau, J.-Y. Cavaillé, C. Gauthier, Acta Mater. 54 (11) (2006) 2923–2931, https://doi.org/10.1016/j.actamat.2006.02.028 http://www.sciencedirect.com/science/article/pii/S1359645406001662.
[103] A. Dikshit, J. Samuel, R.E. DeVor, S.G. Kapoor, J. Manuf. Sci. Eng 130 (3) (2008) 031115–031122, https://doi.org/10.1115/1.2927431 https://manufacturingscience.asmedigitalcollection.asme.org/article.aspx?articleid=1452066.
[104] T. Takeda, Y. Shindo, F. Narita, Y. Mito, Mater. Trans. 50 (3) (2009) 436–445, https://doi.org/10.2320/matertrans.MBW200817.
[105] Y. Kuronuma, Y. Shindo, T. Takeda, F. Narita, Fatigue Fract. Eng. Mater. Struct. 33 (2) (2010) 87–93, https://doi.org/10.1111/j.1460-2695.2009.01419.x.
[106] Y. Shindo, T. Kuronuma, F. Yand Takeda, S. Narita, Fu, Compos.: Part B 43 (2012) 39–43, https://doi.org/10.1016/j.compositesb.2011.04.028.
[107] H. Jang, H. Kim, T. Dodge, P. Sun, H. Zhu, J. Nam, J. Suhr, Carbon 77 (2014) 390–397, https://doi.org/10.1016/j.carbon.2014.05.042.
[108] A. Pantano, F. Cappello, Meccanica 43 (2008) 263–270.
[109] A. Montazeri, R. Naghdabadi, J. Appl. Polym. Sci. 117 (1) (2010) 361–367, https://doi.org/10.1002/app.31460.
[110] A. Montazeri, H. Rafii-Tabar, Phys. Lett. A 375 (45) (2011) 4034–4040, https://doi.org/10.1016/j.physleta.2011.08.073 http://www.sciencedirect.com/science/article/pii/S0375960111011364.
[111] P. Spanos, A. Kontsos, Probab. Eng. Mech. 23 (4) (2008) 456–470, https://doi.org/10.1016/j.probengmech.2007.09.002 dedicated to Professor Ove Ditlevsen http://www.sciencedirect.com/science/article/pii/S0266892008000271.
[112] S. Herasati, L. Zhang, H. Ruan, Int. J. Solids Struct. 51 (2014) 1781–1791, https://doi.org/10.1016/j.ijsolstr.2014.01.019.
[113] E.D. Yildirim, X. Yin, K. Nair, W. Sun, J. Biomed. Mater. Res. Part B: Appl. Biomater. 87B (2) (2008) 579–590, https://doi.org/10.1002/jbm.b.31118.
[114] S. Georgantzinos, G. Giannopoulos, N. Anifantis, Theor. Appl. Fract. Mech. 52 (3) (2009) 158–164, https://doi.org/10.1016/j.tafmec.2009.09.005 http://www.sciencedirect.com/science/article/pii/S0167844209000925.
[115] M. Motamedi, M. Eskandari, M. Yeganeh, Mater. Des. 34 (2012) 603–608, https://doi.org/10.1016/j.matdes.2011.05.013.
[116] T.G. del Río, P. Poza, J. Rodríguez, M. García-Gutiérrez, J. Hernández, T. Ezquerra, Compos. Sci. Technol. 70 (2) (2010) 284–290, https://doi.org/10.1016/j.compscitech.2009.10.019 http://www.sciencedirect.com/science/article/pii/S0266353809003820.
[117] G. Guo, Y. Zhu, J. Appl. Mech. 82 (2015), https://doi.org/10.1115/1.4029635 031005-1-031005-7.
[118] I. Alig, D. Lellinger, S.M. Dudkin, P. Pötschke, Polymer 48 (4) (2007) 1020–1029, https://doi.org/10.1016/j.polymer.2006.12.035 http://www.sciencedirect.com/science/article/pii/S0032386106013723.
[119] J. Huang, D. Rodrigue, Mater. Des. 50 (2013) 936–945, https://doi.org/10.1016/j.matdes.2013.03.095.
[120] Z. Huang, L. Wang, B. Sun, M. He, J. Liu, H. Li, X. Zhai, J. Optics 16 (2014) 1–7, https://doi.org/10.1088/2040-8978/16/10/105004.
[121] E. Mohammadpour, M. Awang, S. Kakooei, H. Akil, Mater. Des. 58 (2014) 36–42, https://doi.org/10.1016/j.matdes.2014.01.007.
[122] A. Chanteli, K. Tserpes, Compos. Struct. 132 (2015) 1141–1148, https://doi.org/10.1016/j.compstruct.2015.07.033.
[123] M. Shokrieh, V.A. Joneidi, J. Compos. Mater. 49 (2015) 2317–2328, https://doi.org/10.1177/0021998314545191.
[124] D. Savvas, V. Papadopoulos, M. Papadrakakis, Int. J. Solids Struct. 49 (2012) 3823–3837, https://doi.org/10.1016/j.ijsolstr.2012.08.031.
[125] B. Thomas, T. Roy, Acta Mech. 227 (2015) 581–599, https://doi.org/10.1007/s00707-015-1479-z.
[126] B. Mortazavi, F. Hassouna, A. Laachachi, A. Rajabpour, S. Ahzi, D. Chapron, V. Toniazzo, D. Ruch, Thermochim. Acta 552 (2013) 106–113, https://doi.org/10.1016/j.tca.2012.11.017.
[127] H. Yao, J. Ge, C. Wang, X. Wang, W. Hu, Z. Zheng, Y. Ni, S. Yu, Adv. Mater. 30 (2013) 1–7, https://doi.org/10.1002/adma.201303041.
[128] Q. Jing, Q. Liu, L. Li, Z. Dong, V. Silberschmidt, Compos. Part B Eng. 89 (2016) 1–8, https://doi.org/10.1016/j.compositesb.2015.11.033.
[129] S. Panzavolta, B. Bracci, C. Gualandi, M. Focarete, Carbon 78 (2014) 566–577, https://doi.org/10.1016/j.carbon.2014.07.040.
[130] M. Safaei, A. Sheidaei, M. Baniassadi, S. Ahzi, M. Mashhadi, F. Pourboghrat, Comput. Mater. Sci. 96 (2015) 191–199, https://doi.org/10.1016/j.commatsci.2014.08.036.
[131] Y. Zhang, Y. Zhao, S. Bai, X. Yuan, Compos. Part B 106 (2016) 324–331, https://doi.org/10.1016/j.compositesb.2016.09.052.
[132] A. Manta, M. Gresil, C. Soutis, Appl. Compos. Mater. 24 (2) (2017) 281–300, https://doi.org/10.1007/s10443-016-9557-5.
[133] S. Ebrahimi, K. Ghafoori-Tabrizi, H. Rafii-Tabar, Comput. Mater. Sci. 53 (2012) 347–353, https://doi.org/10.1016/j.commatsci.2011.08.034.
[134] S. Ebrahimi, H. Rafii-Tabar, Comput. Mater. Sci. 101 (2015) 189–193, https://doi.org/10.1016/j.commatsci.2015.01.036.
[135] T.-C. Hou, K.J. Loh, J.P. Lynch, Nanotechnology 18 (31) (2007) 315501 http://stacks.iop.org/0957-4484/18/i=31/a=315501.
[136] S. Faghihi, A. Karimi, M. Jamadi, R. Imani, R. Salarian, Mater. Sci. Eng. C 38 (2014) 299–305, https://doi.org/10.1016/j.msec.2014.02.015.
[137] M.C. Ray, R.C. Batra, Smart Mater. Struct. 16 (5) (2007) 1936 http://stacks.iop.org/0964-1726/16/i=5/a=051.
[138] J.T. Wescott, P. Kung, A. Maiti, Appl. Phys. Lett. 90 (3) (2007) 33116, https://doi.org/10.1063/1.2432237.
[139] I. Alig, D. Lellinger, M. Engel, T. Skipa, P. Pötschke, Polymer 49 (7) (2008) 1902–1909, https://doi.org/10.1016/j.polymer.2008.01.073 http://www.sciencedirect.com/science/article/pii/S0032386108001341.
[140] R.H. Dai, W.H. Liao, MicroNano2008-70165 70165 (2008) 333–339, https://doi.org/10.1115/MicroNano2008-70165 http://proceedings.asmedigitalcollection.asme.org/proceeding.aspx?articleid=1622896.

[141] Z. Fan, M.H. Santare, S.G. Advani, Compos. Part A: Appl. Sci. Manuf. 39 (3) (2008) 540–554, https://doi.org/10.1016/j.compositesa.2007.11.013 http://www.sciencedirect.com/science/article/pii/S1359835X07002631.
[142] A. Elmarakbi, W. Azoti, M. Serry, Appl. Mater. Today 6 (2017) 1–8, https://doi.org/10.1016/j.apmt.2016.11.003 http://www.sciencedirect.com/science/article/pii/S2352940716302189.
[143] M. Kulkarni, D. Carnahan, K. Kulkarni, D. Qian, J.L. Abot, Compos. Part B: Eng. 41 (5) (2010) 414–421, https://doi.org/10.1016/j.compositesb.2009.09.003 http://www.sciencedirect.com/science/article/pii/S1359836809001826.
[144] N. Nguyen, A. Hao, J. Park, R. Liang, Res. Gate 18 (2016) 1906–1912, https://doi.org/10.1002/adem.201600307.
[145] C. Li, T.-W. Chou, Compos. Sci. Technol. 68 (15) (2008) 3373–3379, https://doi.org/10.1016/j.compscitech.2008.09.025 http://www.sciencedirect.com/science/article/pii/S0266353808003503.
[146] S. Sihn, S. Ganguli, A.K. Roy, L. Qu, L. Dai, Compos. Sci. Technol. 68 (3) (2008) 658–665, https://doi.org/10.1016/j.compscitech.2007.09.016 http://www.sciencedirect.com/science/article/pii/S0266353807003648.
[147] S.R. Bakshi, R.R. Patel, A. Agarwal, Comput. Mater. Sci. 50 (2) (2010) 419–428, https://doi.org/10.1016/j.commatsci.2010.08.034 http://www.sciencedirect.com/science/article/pii/S0927025610005033.
[148] A. Morka, B. Jackowska, Comput. Mater. Sci. 50 (4) (2011) 1244–1249, https://doi.org/10.1016/j.commatsci.2010.03.046 proceedings of the 19th International Workshop on Computational Mechanics of Materials http://www.sciencedirect.com/science/article/pii/S0927025610001977.
[149] T. Wejrzanowski, M. Grybczuk, M. Chmielewski, K. Pietrzak, K. Kurzydlowski, A. Strojny-Nedza, Mater. Des. 99 (2016) 163–173, https://doi.org/10.1016/j.matdes.2016.03.069.
[150] S. Rouhi, R. Ansari, M. Ahmadi, Mod. Phys. Lett. B 31 (6) (2017) 1750053, https://doi.org/10.1142/S0217984917500531.
[151] N. Nouri, S. Ziaei-Rad, S. Adibi, F. Karimzadeh, Mater. Des. 34 (2012) 1–14, https://doi.org/10.1016/j.matdes.2011.07.047.
[152] Y. Peng, K. Deng, J. Alloys Compd. 625 (2015) 44–51, https://doi.org/10.1016/j.jallcom.2014.11.110.
[153] D. Ma, P. Wu, J. Alloys Compd. 671 (2016) 127–136, https://doi.org/10.1016/j.jallcom.2016.02.093.
[154] A. Kothari, S. Hub, Z. Xia, E. Konca, B. Sheldon, Acta Mater. 60 (2012) 3333–3339, https://doi.org/10.1016/j.actamat.2012.02.046.
[155] N.A. Koratkar, B. Wei, P.M. Ajayan, Compos. Sci. Technol. 63 (11) (2003) 1525–1531, https://doi.org/10.1016/S0266-3538(03)00065-4 modeling and Characterization of Nanostructured Materials http://www.sciencedirect.com/science/article/pii/S0266353803000654.
[156] B. Roman-Manso, F. Figueiredo, B. Achiaga, R. Barea, D. Perez-Coll, A. Morelos-Gomez, M. Terrones, M. Osendi, M. Belmonte, P. Miranzo, IEEE Photonics J. 100 (2016) 318–328, https://doi.org/10.1016/j.carbon.2015.12.103.
[157] Z. Xia, L. Riester, W. Curtin, H. Li, B. Sheldon, J. Liang, B. Chang, J. Xu, Acta Mater. 52 (4) (2004) 931–944, https://doi.org/10.1016/j.actamat.2003.10.050 http://www.sciencedirect.com/science/article/pii/S1359645403006608.
[158] Z. Xia, W. Curtin, B. Sheldon, J. Eng. Mater. Technol. 126 (3) (2004) 238–244, https://doi.org/10.1115/1.1751179 http://materialstechnology.asmedigitalcollection.asme.org/article.aspx?articleid=1427200.
[159] I. Alfonso, O. Navarro, J. Vargas, A. Beltrán, C. Aguilar, G. González, I. Figueroa, Compos. Struct. 127 (2015) 420–425, https://doi.org/10.1016/j.compstruct.2015.03.032.
[160] L.Y. Chan, B. Andrawes, Comput. Mater. Sci. 47 (4) (2010) 994–1004, https://doi.org/10.1016/j.commatsci.2009.11.035 http://www.sciencedirect.com/science/article/pii/S0927025609004467.
[161] G. Formica, W. Lacarbonara, R. Alessi, J. Sound Vib. 329 (10) (2010) 1875–1889, https://doi.org/10.1016/j.jsv.2009.11.020 http://www.sciencedirect.com/science/article/pii/S0022460X09009328.
[162] M. Eftekhari, S. Ardakani, S. Mohammadi, Theor. Appl. Fract. Mech. 72 (2014) 64–75, https://doi.org/10.1016/j.tafmec.2014.06.005.
[163] M. Eftekhari, S. Mohammadi, Int. J. Impact Eng. 87 (2016) 55–64, https://doi.org/10.1016/j.ijimpeng.2015.06.023.
[164] J. Le, H. Du, S. Pang, Compos. Part B 67 (2014) 555–563, https://doi.org/10.1016/j.compositesb.2014.08.005.
[165] H. Cakir, F. Uysal, V. Acar, Measurement 90 (2016) 233–241, https://doi.org/10.1016/j.measurement.2016.04.061.
[166] W. Pan, J. Xiao, J. Zhu1, C. Yu, G. Zhang, Z. Ni, K. Watanabe, T. Taniguchi, Y. Shi, X. Wang, Sci. Rep. 2 (2012) 1–6, https://doi.org/10.1038/srep00893.
[167] H. Park, H. Ha, R. Ruoff, A. Bard, J. Electroanal. Chem. 716 (2014) 8–15, https://doi.org/10.1016/j.carbon.2014.07.040.
[168] H. Qian, Y. Ma, Q. Yang, B. Chen, Y. Liu, X. Guo, S. Lin, J. Ruan, X. Liu, L. Tong, Z. Wang, Nanoscale N (2014) 1–6 https://pubs.acs.org/sharingguidelines.
[169] R. Major, M. Sanak, A. Mzyk, L. Lipinska, M. Kot, P. Lacki, F. Bruckert, B. Major, Orig. Res. Article 14 (2014) 540–549, https://doi.org/10.1016/j.acme.2014.04.012.
[170] M. Kammoun, S. Berg, H. Ardebili, Nanoscale 7 (2015) 17516–17522, https://doi.org/10.1039/x0xx00000x.
[171] J. Wang, S. Rathi, S. Singh, I. Lee, S. Maeng, H. Joh, G. Kim, Sci. Direct 220 (2015) 755–761, https://doi.org/10.1016/j.snb.2015.05.133.
[172] Z. Xu, L. Chen, X. Shi, Q. Zhang, A. Mohamed, M. Ibrahim, W. Zhai, J. Yao, Q. Zhu, Y. Xiao, Tribol. Trans. 58 (2015) 668–678, https://doi.org/10.1080/10402004.2014.1002596.
[173] X. Yin, T. Zhang, L. Chen, X. Li, Optics Lett. 40 (2015) 1733–1736, https://doi.org/10.1364/OL.40.001733.
[174] Y. Zhao, W. Zeng, Z. Tao, P. Xiong, Y. Qu, Y. Zhu, R. Soc. Chem. 51 (2015) 866–869, https://doi.org/10.1039/c4cc07937j.
[175] Y. Zhao, D. Yang, X. Li, X. Hu, D. Zhou, Y. Lu, Nanoscale 10 (2016) 19233–19642, https://doi.org/10.1039/C8NR06471G.
[176] G. Gallo, E. Thostenson, Compos. Struct. 141 (2016) 14–23, https://doi.org/10.1016/j.compstruct.2015.07.082.
[177] S. Liu, Q. Liao, S. Lu, Z. Zhang, G. Zhang, y Zhang, Adv. Funct. Mater. 26 (2016) 1347–1353, https://doi.org/10.1002/adfm.201503905.
[178] A. Rifat, G. Mahdiraji, R. Ahmed, D. Chow, Y. Sua, Y. Shee, F. Adikan, IEEE Photonics J. 8 (1) (2016) 1–8, https://doi.org/10.1109/JPHOT.2015.2510632.
[179] M.A. Rafiee, J. Rafiee, I. Srivastava, Z. Wang, H. Song, Z.-Z. Yu, N. Koratkar, Small 6 (2) (2010) 179–183, https://doi.org/10.1002/smll.200901480.
[180] M.A. Rafiee, J. Rafiee, Z. Wang, H. Song, Z.-Z. Yu, N. Koratkar, ACS Nano 3 (12) (2009) 3884–3890 pMID: 19957928. 10.1021/nn9010472.
[181] Q. Liu, X. Zhou, X. Fan, C. Zhu, X. Yao, Z. Liu, Polym.-Plast. Technol. Eng. 51 (3) (2012) 251–256, https://doi.org/10.1080/03602559.2011.625381.
[182] T. Ramanathan, A. Abdala, S. Stankovich, D. Dikin, M. Herrera-Alonso, R. Piner, D. Adamson, H. Schniepp, X. Chen, R. Ruoff, S. Nguyen, I. Aksay, R. Prud'Homme, L. Brinson, Nat. Nanotechnol. 3 (6) (2008) 327–331, https://doi.org/10.1038/nnano.2008.96.
[183] D. Qian, G. Wagner, W. Liu, M. Yu, R. Ruoff, Appl. Mech. Rev. 55 (6) (2002) 495–533, https://doi.org/10.1115/1.1490129 http://appliedmechanicsreviews.asmedigitalcollection.asme.org/article.aspx?articleid=1397363.
[184] S. Kitipornchai, X.Q. He, K.M. Liew, Phys. Rev. B 72 (2005), https://doi.org/10.1103/PhysRevB.72.075443.
[185] C.Y. Wang, L.C. Zhang, Nanotechnology 19 (19) (2008) 195704 http://stacks.iop.org/0957-4484/19/i=19/a=195704.
[186] Y.-G. Hu, K. Liew, Q. Wang, Proc. Eng. 31 (2012) 343–347, https://doi.org/10.1016/j.proeng.2012.01.1034 international Conference on Advances in Computational Modeling and Simulation http://www.sciencedirect.com/science/article/pii/S1877705812010582.
[187] N. Silvestre, C. Wang, Y. Zhang, Y. Xiang, Compos. Struct. 93 (7) (2011) 1683–1691, https://doi.org/10.1016/j.compstruct.2011.01.004 http://www.sciencedirect.com/science/article/pii/S0263822311000183.
[188] Y. Sun, K. Liew, Comput. Methods Appl. Mech. Eng. 197 (33) (2008) 3001–3013, https://doi.org/10.1016/j.cma.2008.02.003 http://www.sciencedirect.com/science/article/pii/S0045782508000480.
[189] S. Adhikari, R. Chowdhury, J. Appl. Phys. 107 (12) (2010) 124322, https://doi.org/10.1063/1.3435316.
[190] R. Chowdhury, S. Adhikari, C. Wang, F. Scarpa, Comput. Mater. Sci. 48 (4) (2010) 730–735, https://doi.org/10.1016/j.commatsci.2010.03.020 http://www.sciencedirect.com/science/article/pii/S0927025610001382.
[191] M.L. Contreras, D. Ávila, J. Alvarez, R. Rozas, J. Mol. Graphics Model. 38 (2012) 389–395, https://doi.org/10.1016/j.jmgm.2012.05.001 http://www.sciencedirect.com/science/article/pii/S1093326312000538.
[192] K. Liew, X. He, C. Wong, Acta Mater. 52 (9) (2004) 2521–2527, https://doi.org/10.1016/j.actamat.2004.01.043 http://www.sciencedirect.com/science/article/pii/S1359645404000771.
[193] H. Rafii-Tabar, Phys. Rep. 390 (4) (2004) 235–452, https://doi.org/10.1016/j.physrep.2003.10.012 http://www.sciencedirect.com/science/article/pii/S0370157303004356.
[194] D. Qian, W.K. Liu, R.S. Ruoff, J. Phys. Chem. B 105 (44) (2001) 10753–10758, https://doi.org/10.1021/jp0120108.
[195] R. Batra, A. Sears, Int. J. Solids Struct. 44 (22) (2007) 7577–7596, https://doi.org/10.1016/j.ijsolstr.2007.04.029 http://www.sciencedirect.com/science/article/pii/S0020768307002119.
[196] T. Belytschko, S.P. Xiao, G.C. Schatz, R.S. Ruoff, Phys. Rev. B 65 (2002) 235430.
[197] K.N. Kudin, G.E. Scuseria, B.I. Yakobson, Phys. Rev. B 64 (2001) 235406, https://doi.org/10.1103/PhysRevB.64.235406.
[198] V.V. Mokashi, D. Qian, Y. Liu, Compos. Sci. Technol. 67 (3) (2007) 530–540, https://doi.org/10.1016/j.compscitech.2006.08.014 http://www.sciencedirect.com/science/article/pii/S0266353806003010.
[199] C. Feng, S. Kitipornchai, J. Yang, Compos. Part B: Eng. 110 (2017) 132–140, https://doi.org/10.1016/j.compositesb.2016.11.024 http://www.sciencedirect.com/science/article/pii/S1359836816312550.
[200] Z. Lei, K. Liew, J. Yu, Compos. Struct. 98 (2013) 160–168, https://doi.org/10.1016/j.compstruct.2012.11.006 http://www.sciencedirect.com/science/article/pii/S0263822312005582.
[201] Y. Zhang, Z. Lei, L. Zhang, K. Liew, J. Yu, Eng. Anal. Bound. Elem. 56 (2015) 90–97, https://doi.org/10.1016/j.enganabound.2015.01.020 http://www.sciencedirect.com/science/article/pii/S0955799715000478.
[202] A. Marini, I. Silveiro, F.J. García de Abajo, ACS Photonics 2 (7) (2015) 876–882, https://doi.org/10.1021/acsphotonics.5b00067.
[203] Y. Liu, N. Nishimura, Y. Otani, Comput. Mater. Sci. 34 (2) (2005) 173–187, https://doi.org/10.1016/j.commatsci.2004.11.003 http://www.sciencedirect.com/science/article/pii/S0927025605000108.
[204] P. Li, L.J. Jiang, H. Bagcl, IEEE Trans. Antennas Propag. 63 (7) (2015) 3065–3076, https://doi.org/10.1109/TAP.2015.2426198.
[205] P. Li, L.J. Jiang, IEEE Trans. Antennas Propag. 63 (10) (2015) 4458–4467, https://doi.org/10.1109/TAP.2015.2456977.
[206] M. Mohammadi, A. Farajpour, A. Moradi, M. Ghayour, Compos. Part B: Eng. 56 (2014) 629–637, https://doi.org/10.1016/j.compositesb.2013.08.060 http://www.sciencedirect.com/science/article/pii/S135983681300468X.
[207] C. Wang, V. Tan, Y. Zhang, J. Sound Vib. 294 (4) (2006) 1060–1072, https://doi.org/10.1016/j.jsv.2006.01.005 http://www.sciencedirect.com/science/article/pii/S0022460X06000356.
[208] I. Ostanin, R. Ballarini, D. Potyondy, T. Dumitrică, J. Mech. Phys. Solids 61 (3)

(2013) 762–782, https://doi.org/10.1016/j.jmps.2012.10.016 http://www.sciencedirect.com/science/article/pii/S0022509612002372.
[209] C. Demir, O. Civalek, B. Akgoz, Math. Comput. Appl. 15 (1) (2010) 57–65, https://doi.org/10.3390/mca15010057 http://www.mdpi.com/2297-8747/15/1/57.
[210] W.H. Duan, C.M. Wang, Nanotechnology 20 (7) (2009) 75702 http://stacks.iop.org/0957-4484/20/i=7/a=075702.
[211] G. Kovacevic, S. Yamashita, Opt. Express 24 (4) (2016) 3584–3591, https://doi.org/10.1364/OE.24.003584 http://www.opticsexpress.org/abstract.cfm?URI=oe-24-4-3584.
[212] A.G. Arani, E. Haghparast, H.B. Zarei, Phys. B: Condens. Matter 495 (2016) 35–49, https://doi.org/10.1016/j.physb.2016.04.039 http://www.sciencedirect.com/science/article/pii/S0921452616301648.
[213] Y. Fu, J. Hong, X. Wang, J. Sound Vib. 296 (4) (2006) 746–756, https://doi.org/10.1016/j.jsv.2006.02.024 http://www.sciencedirect.com/science/article/pii/S0022460X06002513.
[214] R.W. Jiang, Z.B. Shen, G.J. Tang, Acta Mech. 227 (10) (2016) 2899–2910, https://doi.org/10.1007/s00707-016-1649-7.
[215] X.-L. Gao, K. Li, Int. J. Solids Struct. 42 (5) (2005) 1649–1667, https://doi.org/10.1016/j.ijsolstr.2004.08.020 http://www.sciencedirect.com/science/article/pii/S0020768304004688.
[216] T. Murmu, S. Adhikari, M. McCarthy, J. Comput. Theor. Nanosci. 11 (5) (2014) 1230–1236, https://doi.org/10.1166/jctn.2014.3487 https://www.ingentaconnect.com/content/asp/jctn/2014/00000011/00000005/art00002.
[217] K.M. Liew, Y. Zhang, L. Zhang, J. Model. Mech. Mater. 1 (1) (2007), https://doi.org/10.1515/jmmm-2016-0159 https://www.degruyter.com/view/j/jmmm.2017.1.issue-1/jmmm-2016-0159/jmmm-2016-0159.xml.
[218] R. Rasuli, A.I. zad, M.M. Ahadian, Nanotechnology 21 (18) (2010) 185503 http://stacks.iop.org/0957-4484/21/i=18/a=185503.
[219] A. Chakraborty, M. Sivakumar, S. Gopalakrishnan, Int. J. Solids Struct. 43 (2) (2006) 279–294, https://doi.org/10.1016/j.ijsolstr.2005.03.044 http://www.sciencedirect.com/science/article/pii/S0020768305001575.
[220] C.-P. Wu, H.-Y. Li, J. Vib. Control 22 (1) (2016) 89–107, https://doi.org/10.1177/1077546314528367.
[221] F.F. Abraham, J.Q. Broughton, N. Bernstein, E. Kaxiras, EPL (Europhys. Lett.) 44 (6) (1998) 783 http://stacks.iop.org/0295-5075/44/i=6/a=783.
[222] G.J. Wagner, W.K. Liu, J. Comput. Phys. 190 (1) (2003) 249–274, https://doi.org/10.1016/S0021-9991(03)00273-0 http://www.sciencedirect.com/science/article/pii/S0021999103002730.
[223] M.H. Ulz, J. Mech. Phys. Solids 74 (2015) 1–18, https://doi.org/10.1016/j.jmps.2014.10.002 http://www.sciencedirect.com/science/article/pii/S0022509614002002.
[224] T. Withrow, C. Oberdorfer, W. Windl, E.A. Marquis, Microsc. Microanal. 23 (S1) (2017) 646–647, https://doi.org/10.1017/S1431927617003890.
[225] H.S. Park, W.K. Liu, Comput. Methods Appl. Mech. Eng. 193 (17) (2004) 1733–1772, https://doi.org/10.1016/j.cma.2003.12.054 multiple Scale Methods for Nanoscale Mechanics and Materials http://www.sciencedirect.com/science/article/pii/S0045782504000301.
[226] Q. Lu, B. Bhattacharya, Eng. Fract. Mech. 72 (13) (2005) 2037–2071, https://doi.org/10.1016/j.engfracmech.2005.01.009 http://www.sciencedirect.com/science/article/pii/S0013794405000603.
[227] A. Pantano, D.M. Parks, M.C. Boyce, M. Buongiorno Nardelli, J. Appl. Phys. 96 (11) (2004) 6756–6760, https://doi.org/10.1063/1.1809252.
[228] X. Xu, K. Liao, Mater. Phys. Mech. 4 (2001) 148–151 , 10.1.1.424.6233 http://citeseerx.ist.psu.edu/viewdoc/download?doi=10.1.1.424.6233&rep=rep1&type=pdf.
[229] M. Arroyo, T. Belytschko, Meccanica 40 (4) (2005) 455–469, https://doi.org/10.1007/s11012-005-2133-y.
[230] X. Chen, G. Cao, Nanotechnology 17 (4) (2006) 1004 http://stacks.iop.org/0957-4484/17/i=4/a=027.
[231] X. Wang, X. Wang, Compos. Part B: Eng. 35 (2) (2004) 79–86, https://doi.org/10.1016/S1359-8368(03)00084-2 nanocomposites http://www.sciencedirect.com/science/article/pii/S1359836803000842.
[232] X. Wang, Y. Zhang, X. Xia, C. Huang, Int. J. Solids Struct. 41 (22) (2004) 6429–6439, https://doi.org/10.1016/j.ijsolstr.2004.04.038 http://www.sciencedirect.com/science/article/pii/S0020768304002136.
[233] Y. Chandra, F. Scarpa, S. Adhikari, J. Zhang, E.I. Saavedra Flores, H. Peng, Compos. Part B 102 (1–8) (2016), https://doi.org/10.1016/j.compositesb.2016.06.070.
[234] Y. Chandra, E.I. Ltdc:Saavedra Flores, F. Scarpa, S. Adhikari, Physica E 83 (2016) 434–441, https://doi.org/10.1016/j.physe.2016.01.021.
[235] Y. Chandra, R. Chowdhury, S. Adhikari, F. Scarpa, Physica E: Low-dimens. Syst. Nanostruct. 44 (1) (2011) 12–16, https://doi.org/10.1016/j.physe.2011.06.020 http://www.sciencedirect.com/science/article/pii/S1386947711002232.
[236] Y. Chandra, R. Chowdhury, F. Scarpa, S. Adhikaricor, Thin Solid Films 519 (18) (2011) 6026–6032, https://doi.org/10.1016/j.tsf.2011.04.012 http://www.sciencedirect.com/science/article/pii/S0040609011008248.
[237] A. Haque, A. Ramasetty, Compos. Struct. 71 (1) (2005) 68–77, https://doi.org/10.1016/j.compstruct.2004.09.029 http://www.sciencedirect.com/science/article/pii/S0263822304003356.
[238] A.G. Arani, S. Maghamikia, M. Mohammadimehr, A. Arefmanesh, J. Mech. Sci. Technol. 25 (3) (2011) 809–820, https://doi.org/10.1007/s12206-011-0127-3.
[239] J. Lee, D. Yoon, H. Cheong, Nano Lett. 12 (2012) 1–24, https://doi.org/10.1021/nl301073.
[240] W.B. Choi, Y.W. Jin, H.Y. Kim, S.J. Lee, M.J. Yun, J.H. Kang, Y.S. Choi, N.S. Park, N.S. Lee, J.M. Kim, Appl. Phys. Lett. 78 (11) (2001) 1547–1549, https://doi.org/10.1063/1.1349870.
[241] F. Ito, Y. Tomihari, Y. Okada, K. Konuma, A. Okamoto, IEEE Electron Device Lett. 22 (9) (2001) 426–428, https://doi.org/10.1109/55.944328.
[242] J.Z. Liu, Q. Zheng, Q. Jiang, Phys. Rev. Lett. 86 (2001) 4843–4846, https://doi.org/10.1103/PhysRevLett.86.4843.
[243] L. Shi, J.H. Seol, A.L. Moore, I. Jo, Z. Yao, J. Heat Transf. 133 (2001) 22403, https://doi.org/10.1115/1.4002608 http://heattransfer.asmedigitalcollection.asme.org/article.aspx?articleid=1449046.
[244] M. Arroyo, T. Belytschko, J. Mech. Phys. Solids 50 (9) (2002) 1941–1977, https://doi.org/10.1016/S0022-5096(02)00002-9 http://www.sciencedirect.com/science/article/pii/S0022509602000029.
[245] G.M. Odegard, T.S. Gates, L.M. Nicholson, K.E. Wise, Compos. Sci. Technol. 62 (14) (2002) 1869–1880, https://doi.org/10.1016/S0266-3538(02)00113-6 http://www.sciencedirect.com/science/article/pii/S0266353802001136.
[246] D. Qian, G.J. Warner, W.K. Liu, M.F. Yu, R.S. Ruoff, Appl. Mech. Rev. 55 (6) (2002) 495–533, https://doi.org/10.1115/1.1490129 http://appliedmechanicsreviews.asmedigitalcollection.asme.org/article.aspx?articleid=1397363.
[247] A. Fennimore, T. Yuzvinsky, H. Wei-Qiang, M.S. Fuhrer, J. Cumings, A. Zettl, Nature 424 (2003), https://doi.org/10.1038/nature01823.
[248] J.P. Clifford, D.L. John, L.C. Castro, D.L. Pulfrey, IEEE Trans. Nanotechnol. 3 (2) (2004) 281–286, https://doi.org/10.1109/TNANO.2004.828539.
[249] W. Lu, D. Wang, L. Chen, Nano Lett. 7 (9) (2007) 2729–2733, https://doi.org/10.1021/nl071208m pMID: 17705550.
[250] P. Makaram, S. Selvarasah, X. Xiong, C.-L. Chen, A. Busnaina, N. Khanduja, M.R. Dokmeci, Nanotechnology 18 (39) (2007) 395204 http://stacks.iop.org/0957-4484/18/i=39/a=395204.
[251] D.L. Niemann, B.P. Ribaya, N. Gunther, M. Rahman, J. Leung, C.V. Nguyen, Nanotechnology 18 (48) (2007) 485702 http://stacks.iop.org/0957-4484/18/i=48/a=485702.
[252] P. Butti, U. Shorubalko, I. nd Sennhauser, K. Ensslin, Appl. Phys. 114 (2013) 33710, https://doi.org/10.1063/1.4815956.
[253] J.-M. Bonard, C. Klinke, K.A. Dean, B.F. Coll, Phys. Rev. B 67 (2003) 115406, https://doi.org/10.1103/PhysRevB.67.115406.
[254] O. Glukhova, A. Zhbanov, I. Torgashov, N. Sinitsyn, G. Torgashov, Appl. Surf. Sci. 215 (1) (2003) 149–159, https://doi.org/10.1016/S0169-4332(03)00279-4 iVESC, http://www.sciencedirect.com/science/article/pii/S0169433203002794.
[255] S.H. Jo, Y. Tu, Z.P. Huang, D.L. Carnahan, D.Z. Wang, Z.F. Ren, Appl. Phys. Lett. 82 (20) (2003) 3520–3522, https://doi.org/10.1063/1.1576310.
[256] Y. Konishi, S. Hokushin, H. Tanaka, L. Pan, S. Akita, Y. Nakayama, Jpn. J. Appl. Phys. 44 (4R) (2005) 1648 http://stacks.iop.org/1347-4065/44/i=4R/a=1648.
[257] N. Srivastava, R.V. Joshi, K. Banerjee, IEEE International Electron Devices Meeting, 2005. IEDM Technical Digest, (2005), pp. 249–252, https://doi.org/10.1109/IEDM.2005.1609320.
[258] K. Kordás, G. Tóth, P. Moilanen, M. Kumpumäki, J. Vähäkangas, A. Uusimäki, R. Vajtai, P.M. Ajayan, Appl. Phys. Lett. 90 (12) (2007) 123105, https://doi.org/10.1063/1.2714281.
[259] J.L. Garcia-Pomar, A. Cortijo, M. Nieto-Vesperinas, Phys. Rev. Lett. 1000 (2008) 236801 doi:10.1103/PhysRevLett.100.236801. URL https://link.aps.org/doi/10.1103/PhysRevLett.100.236801.
[260] A. Malesevic, R. Kemps, A. Vanhulsel, M.P. Chowdhury, A. Volodin, C. Van Haesendonck, J. Appl. Phys. 104 (8) (2008) 84301 arXiv:https://doi.org/10.1063/1.2999636, doi:10.1063/1.2999636. URL https://doi.org/10.1063/1.2999636.
[261] K. Alam, Semicond. Sci. Technol. 24 (8) (2009) 15007 http://stacks.iop.org/0268-1242/24/i=1/a=015007.
[262] N. Srivastava, H. Li, F. Kreupl, K. Banerjee, IEEE Trans. Nanotechnol. 8 (4) (2009) 542–559, https://doi.org/10.1109/TNANO.2009.2013945.
[263] M. Foxe, G. Lopez, I. Childres, R. Jalilian, A. Patil, C. Roecker, J. Boguski, I. Jovanovic, Y. Chen, IEEE Trans. Nanotechnol. 11 (2012) 581–587, https://doi.org/10.1109/TNANO.2012.2186312.
[264] S.M. Cooper, B.A. Cruden, M. Meyyappan, R. Raju, S. Roy, Nano Lett. 4 (2) (2004) 377–381, https://doi.org/10.1021/nl0350682.
[265] A.A. Gusev, O. Guseva, Adv. Mater. 19 (18) (2007) 2672–2676, https://doi.org/10.1002/adma.200602018.
[266] L. Wang, R. Zhou, H. Xin, Microwave, IEEE Trans. Microw. Theory Tech. 56 (2) (2008) 499–506, https://doi.org/10.1109/TMTT.2007.914627.
[267] A. Tselev, N. Lavrik, I. Vlassiouk, D. Briggs, M. Rutgers, R. Proksch, S. Kalinin, Nanotechnology 23 (2012) 1–11, https://doi.org/10.1088/0957-4484/23/38/385706.
[268] I. Heller, J. Kong, H.A. Heering, K.A. Williams, S.G. Lemay, C. Dekker, Nano Lett. 5 (1) (2005) 137–142 pMID: 15792427. arXiv:https://doi.org/10.1021/nl048200m, doi:10.1021/nl048200m.URL https://doi.org/10.1021/nl048200m.
[269] S.R. Lustig, A. Jagota, C. Khripin, M. Zheng, J. Phys. Chem. B 109 (7) (2005) 2559–2566 pMID: 16851257. arXiv:https://doi.org/10.1021/jp0452913, doi:10.1021/jp0452913.URL https://doi.org/10.1021/jp0452913.
[270] S. Garaj, W. Hubbard, A. Reina, J. Kong, D. Branton, J.A. Golovchenko, Nature 467 (2010) 190193 doi:http//dx.doi.org/10.1038/nature09379. URL https://www.nature.com/articles/nature09379.
[271] M. Huang, T.A. Pascal, H. Kim, W.A. Goddard, J.R. Greer, Nano Lett. 11 (3) (2011) 1241–1246, https://doi.org/10.1021/nl104227t pMID: 21309539.
[272] O. Loh, X. Wei, C. Ke, J. Sullivan, H.D. Espinosa, Small 7 (2011) 79–86, https://doi.org/10.1002/smll.201001166.
[273] S. Jin, S.J. Dunham, X. Xie, J. Kim, C. Lu, A. Islam, F. Du, J. Kim, J. Felts, Y. Li, F. Xiong, M. Wahab, M. Menon, E. Cho, K. Grosse, D.J. Lee, H. Chung, E. Pop, M. Alam, W. King, Y. Huang, J. Rogers, Nat. NanoTechnol. 8 (2013) 347–355, https://doi.org/10.1038/NNANO.201356.

[274] C. Chen, Y. Lu, E.S. Kong, Y. Zhang, S.-T. Lee, Small 4 (9) (2008) 1313–1318, https://doi.org/10.1002/smll.200701309.
[275] S. Pisana, P.M. Braganca, E.E. Marinero, B.A. Gurney, Nano Lett. 10 (1) (2010) 341–346, https://doi.org/10.1021/nl903690y pMID: 20030395.
[276] J. Lu, H. Zhang, W. Shi, Z. Wang, Y. Zheng, T. Zhang, N. Wang, Z. Tang, P. Sheng, Nano Lett. 11 (7) (2011) 2973–2977, https://doi.org/10.1021/nl201538m pMID: 21696168.
[277] N. Papasimakis, S. Thongrattanasiri, N. Zheludev, F. Abajo, Light: Sci. Appl. 2 (2013) 1–4, https://doi.org/10.1038/lsa.201334.
[278] Z. Qi, A. Kitty, H. Parkz, V. Pereira, D. Campbellyy, A. Netozz, Nanoscale 90 (2014) 1–35, https://doi.org/10.1016/j.carbon.2014.07.040.
[279] W. Bao, K. Myhro, Z. Zhao, Z. Chen, W. Jang, L. Jing, F. Miao, H. Zhang, C. Dames, C. Lau, Nano Lett. 12 (2012) 5470–5474, https://doi.org/10.1021/nl301836.
[280] H. Hosseinzadegan, C. Todd, A. Lal, M. Pandey, M. Levendorf, J. Park, Micro Electro Mech. Syst. (MEMS) (2012) 611–614, https://doi.org/10.1109/MEMSYS.2012.6170262.
[281] M. Zelisko, Y. Hanlumyuang, S. Yang, Y. Liu, C. Lei, J. Li, P. Ajayan, P. Sharma, Nat. Commun. 5 (2014) 1–7, https://doi.org/10.1038/ncomms5284.
[282] X. Hu, Y. Chan, K. Zhang, K. Yung, J. Alloys Compd. 580 (2013) 162–171, https://doi.org/10.1016/j.jallcom.2013.05.124.
[283] D. Qi, Z. Liu, Y. Liu, W. Leow, B. Zhu, H. Yang, J. Yu, W. Wang, H. Wang, S. Yin, X. Chen, Adv. Mater. 27 (2015) 5559–5566, https://doi.org/10.1002/adma.201502549.
[284] M. Freitag, Y. Martin, J.A. Misewich, R. Martel, P. Avouris, Nano Lett. 3 (8) (2003) 1067–1071, https://doi.org/10.1021/nl034313e.
[285] M. Huang, H. Yan, C. Chen, D. Song, T.F. Heinz, J. Hone, Proc. Natl. Acad. Sci. 106 (18) (2009) 7304–7308, https://doi.org/10.1073/pnas.0811754106 http://www.pnas.org/content/106/18/7304.
[286] M.J. Leamy, A. DiCarlo, Comput. Methods Appl. Mech. Eng. 198 (17) (2009) 1572–1584, https://doi.org/10.1016/j.cma.2009.01.004 http://www.sciencedirect.com/science/article/pii/S004578250900036X.
[287] T. Echtermeyer, L. Britnell, P. Jasnos, A. Lombardo, R. Gorbachev, A. Grigorenko, A. Geim, A. Ferrari, K. Novoselov, Nat. Commun. 2 (458) (2011) 2620–2632, https://doi.org/10.1038/ncomms1464 https://www.nature.com/articles/ncomms1464.
[288] S. Koester, H. Li, M. Li, Optics Express 20 (2012) 20330–20341, https://doi.org/10.1364/OE.20.020330.
[289] p Li, T. Taubner, ACS Nano 6 (2012) 10107–10114, https://doi.org/10.1021/nn303845a.
[290] M. Nesterov, J. Abad, A. Nikitin, F. Garcia-Vidal, L. Martin-Moreno, Laser Photonics Rev. 7 (2013) L7–L11, https://doi.org/10.1002/lpor.201200079.
[291] R. Degl'Innocenti, D. Jessop, Y. Shah, J. Sibik, J. Zeitler, P. Kidambi, S. Hofmann, H. Beere, D. Ritchiea, Opt. Eng. 53 (5) (2014) 1–5, https://doi.org/10.1117/1.OE.53.5.057108.
[292] G. Giannopoulos, P. Kakavas, N. Anifantis, Comput. Mater. Sci. 41 (4) (2008) 561–569, https://doi.org/10.1016/j.commatsci.2007.05.016 http://www.sciencedirect.com/science/article/pii/S0927025607001565.
[293] S. Georgantzinos, N. Anifantis, Comput. Mater. Sci. 47 (1) (2009) 168–177, https://doi.org/10.1016/j.commatsci.2009.07.006 http://www.sciencedirect.com/science/article/pii/S0927025609002869.
[294] S. Georgantzinos, D. Katsareas, N. Anifantis, Physica E: Low-Dimens. Syst. Nanostruct. 43 (10) (2011) 1833–1839, https://doi.org/10.1016/j.physe.2011.06.037 http://www.sciencedirect.com/science/article/pii/S1386947711002542.
[295] S. Georgantzinosae, G. Giannopoulosb, N. Anifantisa, J. Appl. Phys. 120 (2016) 14305, https://doi.org/10.1063/1.4957289.
[296] R. Ansari, R. Rajabiehfard, B. Arash, J. Therm. Stress. 34 (8) (2011) 817–834, https://doi.org/10.1080/01495739.2011.586268.
[297] R. Ansari, R. Rajabiehfard, B. Arash, Comput. Mater. Sci. 49 (4) (2010) 831–838, https://doi.org/10.1016/j.commatsci.2010.06.032 http://www.sciencedirect.com/science/article/pii/S0927025610003794.
[298] A. Anjomshoa, A. Shahidi, B. Hassani, E. Jomehzadeh, Appl. Math. Model. 38 (2014) 5934–5955, https://doi.org/10.1016/j.apm.2014.03.036.
[299] C. Demir, O. Civalek, Int. J. Eng. Appl. Sci. 8 (2016) 109–117, https://doi.org/10.24107/ijeas.252149.
[300] B. Deepak, R. Ganguli, S. Gopalakrishnan, Int. J. Mech. Sci. 64 (2012) 110–126, https://doi.org/10.1016/j.ijmecsci.2012.07.009.
[301] M. Mitra, S. Gopalakrishnan, Smart Mater. Struct. 15 (2016) 104–122, https://doi.org/10.1088/0964-1726/15/1/039.
[302] M. Xu, A. Tabarraei, J. Paci, J. Oswald, T. Belytschko, Int. J. Fract. 173 (2012) 163–173, https://doi.org/10.1007/s10704-011-9675-x.
[303] M. Hajian, M. Moradi, Eng. Anal. Bound. Elem. 98 (2019) 54–63, https://doi.org/10.1016/j.enganabound.2018.10.005 http://www.sciencedirect.com/science/article/pii/S0955799718302315.
[304] B. Liu, Y. Huang, H. Jiang, S. Qu, K. Hwang, Comput. Methods Appl. Mech. Eng. 193 (17) (2004) 1849–1864, https://doi.org/10.1016/j.cma.2003.12.037 multiple Scale Methods for Nanoscale Mechanics and Materials http://www.sciencedirect.com/science/article/pii/S0045782504000350.
[305] F. Scarpa, S. Adhikari, J. Phys. D: Appl. Phys. 41 (8) (2008) 85306 http://stacks.iop.org/0022-3727/41/i=8/a=085306.
[306] B. Liu, H. Jiang, Y. Huang, S. Qu, M.-F. Yu, K.C. Hwang, Phys. Rev. B 72 (2005) 35435, https://doi.org/10.1103/PhysRevB.72.035435.
[307] V.B. Shenoy, C.D. Reddy, Y.-W. Zhang, ACS Nano 4 (8) (2010) 4840–4844, https://doi.org/10.1021/nn100842k pMID: 20731459.
[308] I. Luxmoore, C. Adlem, M. McCarthy, Appl. Phys. Lett. 103 (2013) 1–5, https://doi.org/10.1063/1.4821939.
[309] Z. Cao, L. Tao, D. Akinwande, R. Huang, K. Liechti, J. Appl. Mech. 82 (2015), https://doi.org/10.1115/1.4030591 081008-1-081008-9..
[310] B. Jang, C.-H. Kim, S.T. Choi, K.-S. Kim, K.-S. Kim, H.-J. Lee, S. Cho, J.-H. Ahn, J.-H. Kim, 2D Materials 4 (2) (2017) 24002 http://stacks.iop.org/2053-1583/4/i=2/a=024002.
[311] C. Li, T.-W. Chou, Int. J. Solids Struct. 40 (10) (2003) 2487–2499, https://doi.org/10.1016/S0020-7683(03)00056-8 http://www.sciencedirect.com/science/article/pii/S0020768303000568.
[312] C. Li, T.-W. Chou, Compos. Sci. Technol. 63 (11) (2003) 1517–1524, https://doi.org/10.1016/S0266-3538(03)00072-1 modeling and Characterization of Nanostructured Materials http://www.sciencedirect.com/science/article/pii/S0266353803000721.
[313] C. Li, T. Chou, J. Nanosci. Nanotechnol. 3 (5) (2003) 423–430, https://doi.org/10.1166/jnn.2003.233.
[314] K.-T. Lau, M. Chipara, H.-Y. Ling, D. Hui, Compos. Part B: Eng. 35 (2) (2004) 95–101, https://doi.org/10.1016/j.compositesb.2003.08.008 nanocomposites, http://www.sciencedirect.com/science/article/pii/S1359836803001070.
[315] C. Li, R.S. Ruoff, T.-W. Chou, Compos. Sci. Technol. 65 (15) (2005) 2407–2415, https://doi.org/10.1016/j.compscitech.2005.06.019 20th Anniversary Special Issue http://www.sciencedirect.com/science/article/pii/S0266353805002265.
[316] C.D. Reddy, S. Rajendran, K.M. Liew, Int. J. Nanosci. 4 (4) (2005) 631–636, https://doi.org/10.1142/S0219581X05003528.
[317] X. Sun, W. Zhao, Mater. Sci. Eng.: A 390 (1) (2005) 366–371, https://doi.org/10.1016/j.msea.2004.08.020 http://www.sciencedirect.com/science/article/pii/S0921509304010561.
[318] Y. Chandra, F. Scarpa, R. Chowdhury, S. Adhikari, J. Sienz, Sci. Direct 46 (2013) 147–153, https://doi.org/10.1016/j.compositesa.2012.11.006.
[319] Y. Chandra, R. Chowdhury, F. Scarpac, S. Adhikarib, J. Sienza, C. Arnoldd, T. Murmu, D. Boulda, Mater. Sci. Eng. B 177 (2012) 303–310, https://doi.org/10.1016/j.mseb.2011.12.024.
[320] K. Tserpes, P. Papanikos, Compos. Part B: Eng. 36 (5) (2005) 468–477, https://doi.org/10.1016/j.compositesb.2004.10.003 http://www.sciencedirect.com/science/article/pii/S1359836805000193.
[321] R. Chowdhury, C.Y. Wang, S. Adhikari, J. Phys. D: Appl. Phys. 43 (8) (2010) 85405 http://stacks.iop.org/0022-3727/43/i=8/a=085405.
[322] S. Adhikari, R. Chowdhury, J. Appl. Phys. 107 (12) (2010) 124322, https://doi.org/10.1063/1.3435316.
[323] F. Scarpa, S. Adhikari, A.S. Phani, Nanotechnology 20 (6) (2009) 65709 http://stacks.iop.org/0957-4484/20/i=6/a=065709.
[324] T. Kaneko, J. Phys. D: Appl. Phys. 8 (16) (1975) 1927 http://stacks.iop.org/0022-3727/8/i=16/a=003.
[325] D. Marquardt, J. Soc. Ind. Appl. Math. 11 (2) (1963) 431–441, https://doi.org/10.1137/0111030.
[326] J. Przemienicki, Theory of Matrix Structural Analysis, Book:McGraw-Hill, New York, 1968.
[327] X. Chen, Y. Liu, Comput. Mater. Sci. 29 (1) (2004) 1–11, https://doi.org/10.1016/S0927-0256(03)00090-9 http://www.sciencedirect.com/science/article/pii/S0927025603000909.
[328] S. Namilae, N. Chandra, J. Eng. Mater. Technol. 127 (2) (2005) 222–232, https://doi.org/10.1115/1.1857940 https://materialstechnology.asmedigitalcollection.asme.org/article.aspx?articleid=1427426.
[329] X. Wang, X. Wang, J. Xiao, Compos. Struct. 69 (3) (2005) 315–321, https://doi.org/10.1016/j.compstruct.2004.07.009 http://www.sciencedirect.com/science/article/pii/S0263822304002387.
[330] J. Xiao, B. Gama, J. Gillespie, Int. J. Solids Struct. 42 (11) (2005) 3075–3092, https://doi.org/10.1016/j.ijsolstr.2004.10.031 http://www.sciencedirect.com/science/article/pii/S0020768304006213.
[331] Y. Liu, X. Chen, Mech. Mater. 35 (1) (2003) 69–81, https://doi.org/10.1016/S0167-6636(02)00200-4 http://www.sciencedirect.com/science/article/pii/S0167663602002004.
[332] H. Wan, F. Delale, L. Shen, Mech. Res. Commun. 32 (5) (2005) 481–489, https://doi.org/10.1016/j.mechrescom.2004.10.011 http://www.sciencedirect.com/science/article/pii/S0093641304001041.
[333] J.Z. Liu, Q. Zheng, Q. Jiang, Phys. Rev. B 67 (2003) 75414, https://doi.org/10.1103/PhysRevB.67.075414.
[334] A. Pantano, M.C. Boyce, D.M. Parks, Phys. Rev. Lett. 91 (2003) 145504, https://doi.org/10.1103/PhysRevLett.91.145504.
[335] S. Zhang, S.L. Mielke, R. Khare, D. Troya, R.S. Ruoff, G.C. Schatz, T. Belytschko, Phys. Rev. B 71 (2005) 115403, https://doi.org/10.1103/PhysRevB.71.115403.
[336] G. Cao, X. Chen, Phys. Rev. B 73 (2006) 155435, https://doi.org/10.1103/PhysRevB.73.155435.
[337] G. Cao, X. Chen, J.W. Kysar, J. Mech. Phys. Solids 54 (6) (2006) 1206–1236, https://doi.org/10.1016/j.jmps.2005.12.003 http://www.sciencedirect.com/science/article/pii/S0022509605002395.
[338] A. Hemmasizadeh, M. Mahzoon, E. Hadi, R. Khandan, Thin Solid Films 516 (21) (2008) 7636–7640, https://doi.org/10.1016/j.tsf.2008.05.040 http://www.sciencedirect.com/science/article/pii/S0040609008006135.
[339] A. Pantano, G. Modica, F. Cappello, Mater. Sci. Eng.: A 486 (1) (2008) 222–227, https://doi.org/10.1016/j.msea.2007.08.078 http://www.sciencedirect.com/science/article/pii/S0921509307016309.
[340] J. Yvonnet, A. Mitrushchenkov, G. Chambaud, Q.-C. He, Comput. Methods Appl. Mech. Eng. 200 (5) (2011) 614–625, https://doi.org/10.1016/j.cma.2010.09.007 http://www.sciencedirect.com/science/article/pii/S0045782510002665.
[341] K. Tserpes, P. Papanikos, G. Labeas, S. Pantelakis, Theor. Appl. Fract. Mech. 49 (1) (2008) 51–60, https://doi.org/10.1016/j.tafmec.2007.10.004 http://www.sciencedirect.com/science/article/pii/S0167844207000961.
[342] L. Nasdala, G. Ernst, Comput. Mater. Sci. 33 (4) (2005) 443–458, https://doi.org/

10.1016/j.commatsci.2004.09.047 http://www.sciencedirect.com/science/article/pii/S0927025604002605.
[343] l Nasdala, a Kempe, r Rolfes, Compos. Sci. Technol. 72 (2012) 989–1000, https://doi.org/10.1016/j.compscitech.2012.03.008.
[344] A. Ghavamian, M. Rahmandoust, A. Ochsner, Compos.: Part B 44 (2013) 52–59, https://doi.org/10.1016/j.compositesb.2012.07.040.
[345] R. Rafiee, A. Eskandariyun, Phys. E: Low-dimens. Syst. Nanostruct. 90 (2017) 42–48, https://doi.org/10.1016/j.physe.2017.03.006 http://www.sciencedirect.com/science/article/pii/S138694771631459X.
[346] W.D. Cornell, P. Cieplak, C.I. Bayly, I.R. Gould, K.M. Merz, D.M. Ferguson, D.C. Spellmeyer, T. Fox, J.W. Caldwell, P.A. Kollman, J. Am. Chem. Soc. 117 (19) (1995) 5179–5197, https://doi.org/10.1021/ja00124a002.
[347] S.S. Gupta, R.C. Batra, J. Comput. Theor. Nanosci. 7 (10) (2010) 2151–2164, https://doi.org/10.1166/jctn.2010.1598 https://www.ingentaconnect.com/content/asp/jctn/2010/00000007/00000010/art00049.
[348] X. Wei, J. Kysar, Int. J. Solids Struct. 49 (2012) 3201–3209, https://doi.org/10.1016/j.ijsolstr.2012.06.019.
[349] O.A. Shenderova, V.V. Zhirnov, D.W. Brenner, Crit. Rev. Solid State Mater. Sci. 27 (3–4) (2002) 227–356, https://doi.org/10.1080/10408430208500497.
[350] C.J. Shearer, A.D. Slattery, A.J. Stapleton, J.G. Shapter, C.T. Gibson, Nanotechnology 27 (12) (2016) 125704, https://doi.org/10.1088/0957-4484/27/12/125704.
[351] C. Lee, X. Wei, J. Kysar, J. Hone, Science 321 (2008) 385–388.
[352] B.I. Yakobson, C.J. Brabec, J. Bernholc, Phys. Rev. Lett. 76 (1996) 2511–2514, https://doi.org/10.1103/PhysRevLett.76.2511.
[353] E. Hernández, C. Goze, P. Bernier, A. Rubio, Phys. Rev. Lett. 80 (1998) 4502–4505, https://doi.org/10.1103/PhysRevLett.80.4502.
[354] A. Pantano, M.C. Boyce, D.M. Parks, J. Eng. Mater. Technol. 126 (3) (2004) 279–284 http://materialstechnology.asmedigitalcollection.asme.org/article.aspx?articleid=1427218.
[355] A. Pantano, D.M. Parks, M.C. Boyce, J. Mech. Phys. Solids 52 (4) (2004) 789–821, https://doi.org/10.1016/j.jmps.2003.08.004 http://www.sciencedirect.com/science/article/pii/S0022509603001340.
[356] J.P. Lu, Phys. Rev. Lett. 79 (1997) 1297–1300, https://doi.org/10.1103/PhysRevLett.79.1297.
[357] Z. Song, Z. Xu, X. Huang, J. Kim, Q. Zheng, J. Appl. Mech. 80 (2013) 040911-1-040911-4. http://appliedmechanics.asmedigitalcollection.asme.org/.
[358] Z. Zhang, W. Duan, C. Wang, J. Appl. Phys. 113 (2013), https://doi.org/10.1063/1.4772621 014902-1-014902-7.
[359] C. Baykasoglu, A. Mugan, Physica E 45 (2012) 151–161, https://doi.org/10.1016/j.physe.2012.07.021.
[360] C. Baykasoglu, A. Mugan, Comput. Mater. Sci. 55 (2012) 228–236, https://doi.org/10.1016/j.commatsci.2011.12.007.
[361] A.J. Gil, S. Adhikari, F. Scarpa, J. Bonet, J. Phys.: Condens. Matter 22 (14) (2010) 145302 http://stacks.iop.org/0953-8984/22/i=14/a=145302.
[362] B. Arash, Q. Wang, K. Liew, Comput. Methods Appl. Mech. Eng. 223–224 (2012) 1–9, https://doi.org/10.1016/j.cma.2012.02.002.
[363] S. Niaki, J. Mianroodi, M. Sadeghi, R. Naghdabadi, Compos. Struct. 94 (2012) 2365–2372, https://doi.org/10.1016/j.compstruct.2012.02.027.
[364] M. Hartmann, M. Todt, F. Rammerstorfer, F. Fischer, O. Paris, EuroPhys. Lett. 103 (2013) 68004, https://doi.org/10.1209/0295-5075/103/68004.
[365] S. Jiang, S. Shi, X. Wang, J. Phys. D: Appl. Phys. 47 (2013) 45104, https://doi.org/10.1088/0022-3727/47/4/045104.
[366] X. Zhu, W. Yan, N. Mortensen, S. Xiao, Optics Express 21 (2013) 3486–3491, https://doi.org/10.1364/OE.21.003486.
[367] S. Iijima, C. Brabec, A. Maiti, J. Bernholc, J. Chem. Phys. 104 (5) (1996) 2089–2092.
[368] K.M. Liew, C.H. Wong, X.Q. He, M.J. Tan, S.A. Meguid, Phys. Rev. B 69 (2004) 115429, https://doi.org/10.1103/PhysRevB.69.115429.
[369] K. Mylvaganam, L. Zhang, Carbon 42 (10) (2004) 2025–2032.
[370] E.I. Saavedra Flores, S. Adhikari, M. Friswell, F. Scarpa, 11th International Conference on the Mechanical Behavior of Materials (ICM11), vol. 10, (2011), pp. 2256–2261, https://doi.org/10.1016/j.proeng.2011.04.373 http://www.sciencedirect.com/science/article/pii/S1877705811005613.
[371] E.I. Saavedra Flores, S. Adhikari, M. Friswell, F. Scarpa, Comput. Mater. Sci. 50 (3) (2011) 1083–1087, https://doi.org/10.1016/j.commatsci.2010.11.005 http://www.sciencedirect.com/science/article/pii/S0927025610006269.
[372] C. Baykasoglu, A. Mugan, Eng. Fract. Mech. 96 (2012) 241–250, https://doi.org/10.1016/j.engfracmech.2012.08.010.
[373] R. Khare, S.L. Mielke, G.C. Schatz, T. Belytschko, Comput. Methods Appl. Mech. Eng. 197 (41) (2008) 3190–3202, https://doi.org/10.1016/j.cma.2007.11.029 recent Advances in Computational Study of Nanostructures http://www.sciencedirect.com/science/article/pii/S004578250700446X.
[374] M.M. Shokrieh, R. Rafiee, Mech. Compos. Mater. 46 (2) (2010) 155–172, https://doi.org/10.1007/s11029-010-9135-0.
[375] L.A. Girifalco, M. Hodak, R.S. Lee, Phys. Rev. B 62 (2000) 13104–13110, https://doi.org/10.1103/PhysRevB.62.13104.
[376] M.M. Shokrieh, R. Rafiee, Compos. Struct. 92 (3) (2010) 647–652, https://doi.org/10.1016/j.compstruct.2009.09.033 http://www.sciencedirect.com/science/article/pii/S0263822309003729.
[377] L. Battezzati, C. Pisani, F. Ricca, J. Chem. Soc. Faraday Trans. 2 (71) (1975) 1629–1639, https://doi.org/10.1039/F29757101629.
[378] K.P. Saffar, N. JamilPour, A.R. Najafi, G. Rouhi, A.R. Arshi, A. Fereidoon, Int. J. Mech. Aerosp. Ind. Mechatron. Manuf. Eng. 2 (11) (2008) 1209–1212 http://waset.org/Publications?p=23.
[379] U.A. Joshi, P. Joshi, S.P. Harsha, S.C. Sharma, Int. J. Eng. Sci. Technol. 2 (5) (2010) 1098–1107.
[380] U.A. Joshi, S.C. Sharma, S. Harsha, Phys. E: Low-dimens. Syst. Nanostruct. 43 (8) (2011) 1453–1460, https://doi.org/10.1016/j.physe.2011.04.005 http://www.sciencedirect.com/science/article/pii/S1386947711001184.
[381] A. Dikshit, J. Samuel, R.E. DeVor, S.G. Kapoor, J. Manuf. Sci. Eng. 130 (3) (2008) 31114, https://doi.org/10.1115/1.2927431 http://manufacturingscience.asmedigitalcollection.asme.org/article.aspx?articleid=1452065.
[382] F. Scarpa, S. Adhikari, J. Non-Cryst. Solids 354 (35) (2008) 4151–4156, https://doi.org/10.1016/j.jnoncrysol.2008.06.065 functional and Nanostructured Materials http://www.sciencedirect.com/science/article/pii/S0022309308003840.
[383] S. Dey, T. Mukhopadhyay, S. Adhikari, Compos. Struct. 171 (7) (2017) 227–250.
[384] R. Rafiee, V. Firouzbakht, Mech. Mater. 78 (2014) 74–84, https://doi.org/10.1016/j.mechmat.2014.07.021 http://www.sciencedirect.com/science/article/pii/S0167663614001483.
[385] R. Rafiee, A. Eskandariyun, Compos. Part B: Eng. 173 (2019) 106842, https://doi.org/10.1016/j.compositesb.2019.05.053 http://www.sciencedirect.com/science/article/pii/S1359836819303002.
[386] R. Rafiee, R. Pourazizi, Mater. Res. 17 (2014) 758–766, https://doi.org/10.1590/S1516-14392014005000071.
[387] S. Jeong, F. Zhu, H. Lim, Y. Kim, G. Yun, Compos. Struct. 207 (2018) 858–870, https://doi.org/10.1016/j.compstruct.2018.09.025.
[388] M. Shokrieh, R. Rafiee, Iran. Polym. J. 21 (2012) 397–402, https://doi.org/10.1007/s13726-012-0043-0.
[389] R. Rafiee, Compos. Struct. 97 (2013) 304–309, https://doi.org/10.1016/j.compstruct.2012.10.028.
[390] R. Rafiee, R. Pourazizi, Comput. Mater. Sci. 96 (2015) 573–578, https://doi.org/10.1016/j.commatsci.2014.03.056.
[391] J.D. Eshelby, R.E. Peierls, Proc. R. Soc. Lond. Ser. A. Math. Phys. Sci. 241 (1226) (1957) 376–396.
[392] Y. Benveniste, Mech. Mater. 6 (2) (1987) 147–157, https://doi.org/10.1016/0167-6636(87)90005-6 http://www.sciencedirect.com/science/article/pii/0167663687900056.
[393] D.A. Brune, J. Bicerano, Polymer 43 (2) (2002) 369–387, https://doi.org/10.1016/S0032-3861(01)00543-2 http://www.sciencedirect.com/science/article/pii/S0032386101005432.
[394] N. Sheng, M. Boyce, D. Parks, G. Rutledge, J. Abes, R. Cohen, Polymer 45 (2) (2004) 487–506, https://doi.org/10.1016/j.polymer.2003.10.100 conformational Protein Conformations http://www.sciencedirect.com/science/article/pii/S0032386103010425.
[395] J. Wang, R. Pyrz, Compos. Sci. Technol. 64 (7) (2004) 925–934, https://doi.org/10.1016/S0266-3538(03)00024-1 http://www.sciencedirect.com/science/article/pii/S0266353803000241.
[396] Ł. Figiel, C. Buckley, Comput. Mater. Sci. 44 (4) (2009) 1332–1343, https://doi.org/10.1016/j.commatsci.2008.09.005 http://www.sciencedirect.com/science/article/pii/S0927025608004084.
[397] J.-J. Luo, I.M. Daniel, Compos. Sci. Technol. 63 (11) (2003) 1607–1616, https://doi.org/10.1016/S0266-3538(03)00060-5 modeling and Characterization of Nanostructured Materials http://www.sciencedirect.com/science/article/pii/S0266353803000605.
[398] P. Lu, Y. Leong, P. Pallathadka, C. He, Int. J. Eng. Sci. 73 (2013) 33–55, https://doi.org/10.1016/j.ijengsci.2013.08.003 http://www.sciencedirect.com/science/article/pii/S0020722513001225.
[399] A.A. Gusev, J. Mech. Phys. Solids 45 (9) (1997) 1449–1459, https://doi.org/10.1016/S0022-5096(97)00016-1 http://www.sciencedirect.com/science/article/pii/S0022509697000161.
[400] K. Matous, M.G. Geers, V.G. Kouznetsova, A. Gillman, J. Comput. Phys. 330 (2017) 192–220, https://doi.org/10.1016/j.jcp.2016.10.070 http://www.sciencedirect.com/science/article/pii/S0021999116305782.
[401] Ł. Figiel, AIP Conf. Proc. 1353 (1) (2011) 1226–1231, https://doi.org/10.1063/1.3589684.
[402] G. Cricri, E. Garofalo, F. Naddeo, L. Incarnato, J. Polym. Sci. Part B: Polym. Phys. 50 (3) (2012) 207–220, https://doi.org/10.1002/polb.23001.
[403] J. Ptaszny, G. Dziatkiewicz, P. Fedelinski, Int. J. Multisc. Comput. Eng. 12 (2014) 33–43, https://doi.org/10.1615/IntJMultCompEng.2014007103 http://www.dl.begellhouse.com/journals/61fd1b191cf7e96f,319e71c10c72804e,41f862d41678b436.html.
[404] D. Weidt, Ł. Figiel, Comput. Mater. Sci. 82 (2014) 298–309, https://doi.org/10.1016/j.commatsci.2013.10.001 http://www.sciencedirect.com/science/article/pii/S0927025613006009.
[405] D. Weidt, Ł. Figiel, Compos. Sci. Technol. 115 (2015) 52–59, https://doi.org/10.1016/j.compscitech.2015.04.018 http://www.sciencedirect.com/science/article/pii/S0266353815001761.
[406] Ł. Figiel, Compos. Commun. 8 (2018) 101–105, https://doi.org/10.1016/j.coco.2017.12.004 http://www.sciencedirect.com/science/article/pii/S2452213917300980.
[407] R.M. Boumbimba, K. Wang, N. Bahlouli, S. Ahzi, Y. Rémond, F. Addiego, Mech. Mater. 52 (2012) 58–68, https://doi.org/10.1016/j.mechmat.2012.04.006 http://www.sciencedirect.com/science/article/pii/S0167663612000786.
[408] K. Hbaieb, Q. Wang, Y. Chia, B. Cotterell, Polymer 48 (3) (2007) 901–909, https://doi.org/10.1016/j.polymer.2006.11.062 http://www.sciencedirect.com/science/article/pii/S0032386106013097.
[409] S. Song, Y. Chen, Z. Su, C. Quan, V.B. Tan, Compos. Sci. Technol. 85 (2013) 50–57, https://doi.org/10.1016/j.compscitech.2013.05.019 http://www.sciencedirect.com/science/article/pii/S0266353813002376.
[410] C. Pisano, P. Priolo, Ł. Figiel, Comput. Mater. Sci. 55 (2012) 10–16, https://doi.

org/10.1016/j.commatsci.2011.12.015 http://www.sciencedirect.com/science/article/pii/S0927025611006768.
[411] G.L. Dai Jr., Comput. Mater. Sci. 95 (2014) 684–692, https://doi.org/10.1016/j.commatsci.2014.08.011.
[412] P.E. Spencer, R. Spares, J. Sweeney, P.D. Coates, Mech. Time-Depend. Mater. 12 (4) (2008) 313–327, https://doi.org/10.1007/s11043-008-9064-7.
[413] Ł. Figiel, F.P.E. Dunne, C.P. Buckley, Model. Simul. Mater. Sci. Eng. 18 (1) (2009) 15001, https://doi.org/10.1088/0965-0393/18/1/015001.
[414] C. Pisano, Ł. Figiel, Compos. Sci. Technol. 75 (2013) 35–41, https://doi.org/10.1016/j.compscitech.2012.12.002 http://www.sciencedirect.com/science/article/pii/S0266353812004095.
[415] Ł. Figiel, Comput. Mater. Sci. 84 (2014) 244–254, https://doi.org/10.1016/j.commatsci.2013.12.012 http://www.sciencedirect.com/science/article/pii/S0927025613007611.
[416] E.I. Saavedra Flores, K. Saavedra, J. Hinojosa, Y. Chandra, R. Das, Int. J. Solids Struct. 81 (2016) 219–232, https://doi.org/10.1016/j.ijsolstr.2015.11.027 http://www.sciencedirect.com/science/article/pii/S0020768315004898.
[417] M. Zahedi, R. Malekimoghadam, R. Rafiee, U. Icardi, Eng. Fract. Mech. 209 (2019) 245–259, https://doi.org/10.1016/j.engfracmech.2019.01.031 http://www.sciencedirect.com/science/article/pii/S0013794418311330.
[418] D. Weidt, Ł. Figiel, Predictions of Energy Absorption of Aligned Carbon Nanotube/Epoxy Composites, Springer Berlin Heidelberg, Berlin, Heidelberg, 2013, pp. 207–224, https://doi.org/10.1007/978-3-642-40322-4_9.
[419] O.L. Manevitch, G.C. Rutledge, J. Phys. Chem. B 108 (4) (2004) 1428–1435, https://doi.org/10.1021/jp0302818.
[420] R. Rafiee, R. Shahzadi, Compos. Part B: Eng. 152 (2018) 31–42, https://doi.org/10.1016/j.compositesb.2018.06.033 http://www.sciencedirect.com/science/article/pii/S135983681831031X.
[421] R. Rafiee, R. Shahzadi, Polym. Compos. 40 (2) (2019) 431–445, https://doi.org/10.1002/pc.24725.
[422] G. Odegard, T. Gates, K. Wise, C. Park, E. Siochi, Compos. Sci. Technol. 63 (11) (2003) 1671–1687, https://doi.org/10.1016/S0266-3538(03)00063-0 modeling and Characterization of Nanostructured Materials http://www.sciencedirect.com/science/article/pii/S0266353803000630.
[423] R. Rafiee, M. Mahdavi, Comput. Mater. Sci. 112 (2016) 356–363, https://doi.org/10.1016/j.commatsci.2015.10.041 http://www.sciencedirect.com/science/article/pii/S0927025615006989.
[424] J. Kulothungan, M. Muruganathan, H. Mizuta, Micromachines 7 (2016) 1–8, https://doi.org/10.3390/mi7080143.
[425] A. Patnaik, K. Senthilnathan, R. Jha, IEEE Photonics Technol. Lett. 27 (2015) 2437–2440, https://doi.org/10.1109/LPT.2015.2467189.
[426] C.-Y. Li, T.-W. Chou, Nanotechnology 15 (11) (2004) 1493 http://stacks.iop.org/0957-4484/15/i=11/a=021.
[427] C. Li, T.-W. Chou, Appl. Phys. Lett. 84 (25) (2004) 5246–5248, https://doi.org/10.1063/1.1764933.
[428] D.H. Wu, W.T. Chien, C.S. Chen, H.H. Chen, Sens. Actuators A: Phys. 126 (1) (2006) 117–121, https://doi.org/10.1016/j.sna.2005.10.005 http://www.sciencedirect.com/science/article/pii/S0924424705005728.
[429] C. Li, T.-W. Chou, Appl. Phys. Lett. 84 (1) (2004) 121–123, https://doi.org/10.1063/1.1638623.
[430] A.N. Watkins, J. Ingram, J.D. Jordan, R.A. Wincheski, J.M. Smits, P.A. Williams, NSTI Conf-Nanotech 3 (2004) 149 http://www.sciencedirect.com/science/article/pii/S0020768304002136.
[431] C.K.M. Fung, M.Q.H. Zhang, R.H.M. Chan, W.J. Li, 18th IEEE International Conference on Micro Electro Mechanical Systems, 2005. MEMS 2005, (2005), pp. 251–254, https://doi.org/10.1109/MEMSYS.2005.1453914.
[432] T. Sakhaee-Pour, M.T. Ahmadian, A. Vafai, ASME Proceedings Micro and Nano Systems – IMECE2007, (2007), pp. 99–104 http://proceedings.asmedigitalcollection.asme.org/proceeding.aspx?articleid=1590557.
[433] A. Sakhaee-Pour, M. Ahmadian, A. Vafai, Solid State Commun. 147 (7) (2008) 336–340, https://doi.org/10.1016/j.ssc.2008.04.016 http://www.sciencedirect.com/science/article/pii/S0038109808002081.
[434] R. Chowdhury, S. Adhikari, J. Mitchell, Phys. E: Low-dimens. Syst. Nanostruct. 42 (2) (2009) 104–109, https://doi.org/10.1016/j.physe.2009.09.007 http://www.sciencedirect.com/science/article/pii/S1386947709003427.
[435] H. Lee, J. Hsu, S. Lin, W. Chang, Appl. Phys. 114 (2013) 123506, https://doi.org/10.1063/1.4823735.
[436] K.J. Loh, T.-C. Hou, J.P. Lynch, N.A. Kotov, J. Nondestruct. Eval. 28 (1) (2009) 9–25, https://doi.org/10.1007/s10921-009-0043-y.
[437] S. Georgantzinos, N. Anifantis, Phys. E: Low-dimens. Syst. Nanostruct. 42 (5) (2010) 1795–1801, https://doi.org/10.1016/j.physe.2010.02.002 http://www.sciencedirect.com/science/article/pii/S138694771000086X.
[438] A.Y. Joshi, S. Harsha, S.C. Sharma, Phys. E: Low-dimens. Syst. Nanostruct. 42 (8) (2010) 2115–2123, https://doi.org/10.1016/j.physe.2010.03.033 http://www.sciencedirect.com/science/article/pii/S1386947710001943.
[439] A.Y. Joshi, S.C. Sharma, S. Harsha, J. Nanotechnol. Eng. Med 1 (3) (2010) 31007, https://doi.org/10.1115/1.4002072 http://nanoengineeringmedical.asmedigitalcollection.asme.org/article.aspx?articleid=1452311.
[440] A.Y. Joshi, A. Bhatnagar, S. Harsha, S.C. Sharma, J. Nanotechnol. Eng. Med 1 (3) (2010) 31004, https://doi.org/10.1115/1.4001897 http://nanoengineeringmedical.asmedigitalcollection.asme.org/article.aspx?articleid=1452296.
[441] A.Y. Joshi, S.C. Sharma, S. Harsha, Sensors and Actuators A: Physical 168 (2) (2011) 275–280, https://doi.org/10.1016/j.sna.2011.04.031 http://www.sciencedirect.com/science/article/pii/S0924424711002780.
[442] J. Dash, R. Jha, IEEE PHOTONICS TECHNOLOGY LETTERS 26 (2014) 1092–1095, https://doi.org/10.1109/LPT.2014.2315233.
[443] S. Jiang, H. Gong, X. Guo, X. Wang, Solid State Communications 193 (2014) 30–33, https://doi.org/10.1016/j.ssc.2014.05.020.
[444] C. Li, J. Xiao, T. Guo, S. Fan, W. Jin, Microsyst Technol 21 (2014) 1–10, https://doi.org/10.1007/s00542-014-2333-2.
[445] H. Tian, Y. Shu, Y. Cui, W. Mi, Y. Yang, D. Xie, T. Ren, Nanoscale 6 (2014) 699–705, https://doi.org/10.1039/C3NR04521H.
[446] A. Tsiamaki, S. Georgantzinos, N. Anifantis, Sensors and Actuators A: Physical 217 (2014) 29–38, https://doi.org/10.1016/j.sna.2014.06.015.
[447] J. Wang, B. Singh, J. Park, S. Rathi, I. Lee, S. Maeng, H. Joh, C. Lee, G. Kim, Sensors and Actuators B: Chemical 194 (2014) 296–302, https://doi.org/10.1016/j.snb.2013.12.009.
[448] P. Maharana, R. Jha, P. Padhy, Sensors and Actuators B: Chemical 207 (2015) 117–122, https://doi.org/10.1016/j.snb.2014.10.006.
[449] X. Zhang, S. Hu, M. Wang, J. Yu, Q. Khan, J. Shang, L. Ba, Nanotechnology 26 (2015) 1–11, https://doi.org/10.1088/0957-4484/26/11/115501.
[450] J. Kenry, J. Yeo, M. Yu, K. Shang, C. Loh, Lim, Nano micro small 12 (2016) 1315–1321, https://doi.org/10.1002/smll.201502911.
[451] J. Shi, T. Natsuki, X. Lei, Q. Ni, Appl. Phys. Lett. 104 (2014) 223101, https://doi.org/10.1063/1.4880729.
[452] E. Marenić, A. Ibrahimbegovic, J. Sorić, P. Guidault, Materials 6 (2013) 3764–3782, https://doi.org/10.3390/ma6093764.
[453] Y. Won, Y. Gao, M. Panzer, S. Dogbe, L. Pan, T. Kenny, K. Goodson, CARBON 50 (2012) 347–355, https://doi.org/10.1016/j.carbon.2011.08.009.
[454] A.F. Avila, G.S.R. Lacerda, Mat. Res. 11 (3) (2008) 325–333, https://doi.org/10.1590/S1516-14392008000300016 http://www.scielo.br/scielo.php?pid=S1516-14392008000300016&script=sci_arttext.
[455] J. Ge, H. Jiang, Z.Y. Sun, G.J. Yu, B. Su, T. Sun, Innovative Materials: Engineering and Applications II, vol. 730 of Key Engineering Materials, Trans Tech Publications, 2017, pp. 548–553 doi:10.4028/www.scientific.net/KEM.730.548.
[456] P. Zhou, X. Yang, L. He, Z. Hao, W. Luo, B. Xiong, X. Xu, C. Niu, M. Yan, L. Mai, Applied Physics Letters 106 (2015) 111908, https://doi.org/10.1063/1.4915514.
[457] A. Gangele, A. Pandey, Int. J. Mech. Sci. 142–143 (2018) 491–501, https://doi.org/10.1016/j.ijmecsci.2018.05.012.
[458] M. Schiebold, J. Mehner, 2018 Symposium on Design, Test, Integration and Packaging of MEMS and MOEMS (DTIP), (2018), pp. 1–6 doi:https://doi.org/10.1109/DTIP.2018.8394197.
[459] M. Meo, M. Rossi, Compos. Sci. Technol. 66 (11) (2006) 1597–1605, https://doi.org/10.1016/j.compscitech.2005.11.015 http://www.sciencedirect.com/science/article/pii/S0266353805004367.
[460] S. Kirtania, D. Chakraborty, Journal of Reinforced Plastics and Composites 26 (15) (2007) 1557–1570, https://doi.org/10.1177/0731684407079517.
[461] A. Sakhaee-Pour, Solid State Communications 149 (1) (2009) 91–95, https://doi.org/10.1016/j.ssc.2008.09.050 http://www.sciencedirect.com/science/article/pii/S0038109808005796.
[462] S. Georgantzinos, G. Giannopoulos, N. Anifantis, Materials and Design 31 (10) (2010) 4646–4654, https://doi.org/10.1016/j.matdes.2010.05.036 http://www.sciencedirect.com/science/article/pii/S0261306910003298.
[463] J. Xiao, J. Staniszewski, J. Gillespie, Materials Science and Engineering: A 527 (3) (2010) 715–723, https://doi.org/10.1016/j.msea.2009.10.052 http://www.sciencedirect.com/science/article/pii/S0921509309011812.
[464] S. Arghavan, A. Singh, J. Nanotechnol. Eng. Med 2 (3) (2011) 31005, https://doi.org/10.1115/1.4004323 https://nanoengineeringmedical.asmedigitalcollection.asme.org/article.aspx?articleid=1452750.
[465] S. Georgantzinos, G. Giannopoulos, D. Katsareas, P. Kakavas, N. Anifantis, Comput. Mater. Sci. 50 (7) (2011) 2057–2062, https://doi.org/10.1016/j.commatsci.2011.02.008 http://www.sciencedirect.com/science/article/pii/S0927025611000851.
[466] G. Giannopoulos, I. Liosatos, A. Moukanidis, Phys. E: Low-dimens. Syst. Nanostruct. 44 (1) (2011) 124–134, https://doi.org/10.1016/j.physe.2011.08.001 http://www.sciencedirect.com/science/article/pii/S1386947711002876.
[467] M.A. Zhuravkov, Y.E. Nagornyi, V.I. Repchenkov, Nanotechnol. Russia 6 (9) (2011) 597, https://doi.org/10.1134/S1995078011050168.
[468] K. Alzebdeh, Int. J. Mech. Mater. Des. 8 (2012) 269–278, https://doi.org/10.1007/s10999-012-9193-7.
[469] S. Georgantzinos, D. Katsareas, N. Anifantis, Int. J. Mech. Sci. 55 (2012) 85–94, https://doi.org/10.1016/j.ijmecsci.2011.12.006.
[470] X. Lu, Z. Hu, Compos.: Part B 43 (2012) 1902–1913, https://doi.org/10.1016/j.compositesb.2012.02.002.
[471] E. Mohammadpour, M. Awang, Appl. Phys. A Mater. Sci. Process. 106 (2012) 581–588, https://doi.org/10.1007/s00339-011-6625-4.
[472] A. Tapia, R. Peon-Escalante, C. Villanueva, F. Aviles, Comput. Mater. Sci. 55 (2012) 255–262, https://doi.org/10.1016/j.commatsci.2011.12.013.
[473] K. Tserpes, Acta Mech. 223 (2012) 669–678, https://doi.org/10.1007/s00707-011-0594-8.
[474] A. Golkarian, M. Jabbarzadeh, Sci. Direct 74 (2013) 138–142, https://doi.org/10.1016/j.commatsci.2013.03.026.
[475] S. Kordkheili, H. Sani, Comput. Mater. Sci. 69 (2013) 335–343, https://doi.org/10.1016/j.commatsci.2012.11.027.
[476] S. Wang, J. Guo, L. Zhou, Phys. E: Low-dimens. Syst. Nanostruct. 48 (2013) 29–35, https://doi.org/10.1016/j.physe.2012.11.002.
[477] S.-P. Wang, J.-G. Guo, Y. Jiang, Mater. Des. 10 (1) (2013) 250–256, https://doi.org/10.1166/jctn.2013.2687 https://www.ingentaconnect.com/content/asp/jctn/2013/00000010/00000001/art00039.
[478] K. Alzebdeh, Solid State Commun. 177 (2014) 25–28, https://doi.org/10.1016/j.ssc.2013.09.017.

[479] J. Fu, F. Bernard1, S. Kamali-Bernard1, Appl. Mech. Mater. 711 (2014) 137–142, https://doi.org/10.4028/www.scientific.net/AMM.711.137.
[480] P. Lengvarský, J. Bocko, Am. J. Mech. Eng. 3 (2015) 225–229, https://doi.org/10.12691/ajme-3-6-14.
[481] G. López Polín, M. Jaafar, F. Guinea, R. Roldán, C. Gómez-Navarro, J. Gómez-Herrero, Carbon 124 (2015) 42–48, https://doi.org/10.1016/j.carbon.2017.08.023.
[482] A. Genoese, A. Genoese, N. Rizzi, G. Salerno, Compos. Part B: Eng. 115 (2016) 316–329, https://doi.org/10.1016/j.compositesb.2016.09.064.
[483] A. Malakouti, A. Montazeri, Superlattices Microstruct. 94 (2016) 1–12, https://doi.org/10.1016/j.spmi.2016.03.049.
[484] Z. Song, Z. Xu, Extreme Mech. Lett. 6 (2016) 82–87, https://doi.org/10.1016/j.eml.2015.12.010.
[485] A.R. Alian, S.A. Meguid, Int. J. Mech. Mater. Des. (2017), https://doi.org/10.1007/s10999-017-9389-y.
[486] S. Korobeynikov, V. Alyokhin, A. Babichev, Int. J. Eng. Sci. 133 (2018) 109–131, https://doi.org/10.1016/j.ijengsci.2018.09.001.
[487] A. Kalamkarov, A. Georgiades, S. Rokkam, V. Veedu, M. Ghasemi-Nejhad, Int. J. Solids Struct. 43 (22) (2006) 6832–6854, https://doi.org/10.1016/j.ijsolstr.2006.02.009 http://www.sciencedirect.com/science/article/pii/S0020768306000412.
[488] T.C. Theodosiou, D.A. Saravanos, Proceedings of CANEUS2006, (2006), pp. 55–64, https://doi.org/10.1115/CANEUS2006-11062 http://proceedings.asmedigitalcollection.asme.org/proceeding.aspx?articleid=1594605.
[489] V.P. Veedu, D. Askari, M.N. Ghasemi-Nejhad, J. Nanosci. Nanotechnol. 6 (7) (2006) 2159–2166, https://doi.org/10.1166/jnn.2006.348 https://www.ingentaconnect.com/content/asp/jnn/2006/00000006/00000007/art00043.
[490] B. Jalalahmadi, R. Naghdabadi, J. Phys.: Conf. Ser. 61 (1) (2007) 497 http://stacks.iop.org/1742-6596/61/i=1/a=101.
[491] T. Liu, X. Wang, Phys. Lett. A 365 (1) (2007) 144–148, https://doi.org/10.1016/j.physleta.2006.12.059 http://www.sciencedirect.com/science/article/pii/S0375960106019979.
[492] M. Wang, X. Qiu, X. Zhang, Nanotechnology 18 (7) (2007) 75711 http://stacks.iop.org/0957-4484/18/i=7/a=075711.
[493] C.W. Fan, J.H. Huang, C.B. Hwu, Y.Y. Liu, Advances in Fracture and Materials Behavior, Vol. 33 of Advanced Materials Research, Trans Tech Publications, 2008, pp. 937–942, https://doi.org/10.4028/www.scientific.net/AMR.33-37.937.
[494] P. Papanikos, D. Nikolopoulos, K. Tserpes, Comput. Mater. Sci. 43 (2) (2008) 345–352, https://doi.org/10.1016/j.commatsci.2007.12.010 http://www.sciencedirect.com/science/article/pii/S0927025607003333.
[495] Z.Q. Zhang, B. Liu, Y.L. Chen, H. Jiang, K.C. Hwang, Y. Huang, Nanotechnology 19 (39) (2008) 395702 http://stacks.iop.org/0957-4484/19/i=39/a=395702.
[496] M. Brcic, M. Canadija, J. Brnic, D. Lanc, S. Krscanski, G. Vukelic, Est. J. Eng. 15 (2) (2009) 77–86.
[497] H.-C. Cheng, Y.-L. Liu, Y.-C. Hsu, W.-H. Chen, Int. J. Solids Struct. 46 (7) (2009) 1695–1704, https://doi.org/10.1016/j.ijsolstr.2008.12.013 http://www.sciencedirect.com/science/article/pii/S0020768308005131.
[498] C.W. Fan, Y.Y. Liu, C. Hwu, Appl. Phys. A 95 (3) (2009) 819–831, https://doi.org/10.1007/s00339-009-5080-y.
[499] M. Rahmandoust, A. Öchsner, J. Nano Res. 6 (2009) 185–196, https://doi.org/10.4028/www.scientific.net/JNanoR.6.185.
[500] M. Rossi, M. Meo, Compos. Sci. Technol. 69 (9) (2009) 1394–1398, https://doi.org/10.1016/j.compscitech.2008.09.010 special Issue on the 12th European Conference on Composite Materials (ECCM12), organized by the European Society for Composite Materials (ESCM), http://www.sciencedirect.com/science/article/pii/S0266353808003370.
[501] F. Scarpa, S. Adhikari, C.Y. Wang, J. Phys. D: Appl. Phys. 42 (14) (2009) 142002 URL http://stacks.iop.org/0022-3727/42/i=14/a=142002.
[502] A. Muc, Mater. Des. 31 (4) (2010) 1671–1675, https://doi.org/10.1016/j.matdes.2009.03.046 design of Nanomaterials and Nanostructures,URL http://www.sciencedirect.com/science/article/pii/S026130690900418X.
[503] M.N. Nahas, M. Abd-rabou, Finite Element Modeling of Carbon Nanotubes 10 (2010).
[504] M.M. Shokrieh, R. Rafiee, Mater. Des. 31 (2) (2010) 790–795, https://doi.org/10.1016/j.matdes.2009.07.058 URL http://www.sciencedirect.com/science/article/pii/S026130690900421X.
[505] J.M. Wernik, S.A. Meguid, Acta Mech. 212 (1) (2010) 167–179, https://doi.org/10.1007/s00707-009-0246-4.
[506] A.F. Avila, A.C. Eduardo, A.S. Neto, Comput. Struct. 89 (11) (2011) 878–892, https://doi.org/10.1016/j.compstruc.2011.02.017 computational Fluid and Solid Mechanics 2011 URL http://www.sciencedirect.com/science/article/pii/S0045794911000605.
[507] E. Mohammadpour, M. Abdullah, M. Awang, J. Appl. Sci. 11 (2011) 1653–1657, https://doi.org/10.3923/jas.2011.1653.1657.
[508] E. Mohammadpour, M. Awang, Appl. Phys. A 104 (2) (2011) 609–614, https://doi.org/10.1007/s00339-011-6385-1.
[509] E. Mahmoudinezhad, R. Ansari, A. Basti, M. Hemmatnezhad, Comput. Mater. Sci. 62 (2012) 6–11, https://doi.org/10.1016/j.commatsci.2012.05.004.
[510] R. Rafiee, M. Heidarhaei, Compos. Struct. 94 (2012) 2460–2464, https://doi.org/10.1016/j.compstruct.2012.03.010.
[511] M. Rahmandoust, A. Öchsner, J. Nanosci. Nanotechnol. 12 (2012) 8129–8136, https://doi.org/10.1166/jnn.2012.4521.
[512] J. RANGEL, W. BROSTOW, V. CASTANO, Polimery 58 (2013) 276–281 http://yadda.icm.edu.pl/baztech/element/bwmeta1.element.baztech-article-BAT4-0014-0048.
[513] G. Domínguez-Rodríguez, A. Tapia, F. Avilés, Comput. Mater. Sci. 82 (2014) 257–263, https://doi.org/10.1016/j.commatsci.2013.10.003.
[514] M. Zuberi, V. Esat, ASME 2014 12th Biennial Conference on Engineering Systems Design and Analysis, (2014), pp. 1–7, https://doi.org/10.1115/ESDA2014-20156.
[515] M. Brcic, M. Canadija, J. Brnic, IOP Conference Series: Materials Science and Engineering, (2018), pp. 1–5, https://doi.org/10.1088/1757-899X/378/1/012006.
[516] F. Karimzadeh, S. Ziaei-Rad, S. Adibi, Metall. Mater. Trans. B 38 (4) (2007) 695–705, https://doi.org/10.1007/s11663-007-9065-y.
[517] D. Luo, W.-X. Wang, Y. Takao, Compos. Sci. Technol. 67 (14) (2007) 2947–2958, https://doi.org/10.1016/j.compscitech.2007.05.005 polymer Nanocomposites - Modeling, Mechanical and Functional Properties. URL http://www.sciencedirect.com/science/article/pii/S0266353807001935.
[518] M.M. Shokrieh, R. Rafiee, Mech. Res. Commun. 37 (2) (2010) 235–240, https://doi.org/10.1016/j.mechrescom.2009.12.002 URL http://www.sciencedirect.com/science/article/pii/S0093641309001700.
[519] U. Joshi, S. Sharma, S. Harsha, Compos.: Part B 43 (2012) 2063–2071, https://doi.org/10.1016/j.compositesb.2012.01.063.
[520] M. Nahas, M. Alzahrani, Comput. Theor. Nanosci. 9 (2012) 1–4, https://doi.org/10.1166/jctn.2012.2082.
[521] R. Rafiee, A. Fereidoon, M. Heidarhaei, Comput. Mater. Sci. 56 (2012) 25–28, https://doi.org/10.1016/j.commatsci.2011.12.025.
[522] B. Mortazavi, J. Bardon, S. Ahzi, Comput. Mater. Sci. 69 (2013) 100–106, https://doi.org/10.1016/j.commatsci.2012.11.035.
[523] B. Mortazavi, M. Baniassadi, J. Bardon, S. Ahzi, Compos. Part B Eng. 45 (2013) 1117–1125, https://doi.org/10.1016/j.compositesb.2012.05.015.
[524] J. Huang, D. Rodrigue, Mater. Des. 55 (2014) 653–663, https://doi.org/10.1016/j.matdes.2013.10.039.
[525] P. Joshi, S. Upadhyay, Comput. Mater. Sci. 81 (2014) 332–338, https://doi.org/10.1016/j.ssc.2014.05.020.
[526] K. Spanos, S. Georgantzinos, N. Anifantis, Compos. Part B: Eng. 63 (2014) 85–93, https://doi.org/10.1016/j.compositesb.2014.03.020.
[527] T. Chen, L. Pan, M. Lin, B. Wang, L. Liu, Y. Li, J. Qiu, K. Zhu, Polym. Test. 47 (2015) 4–11, https://doi.org/10.1016/j.polymertesting.2015.08.001.
[528] K. Spanos, S. Georgantzinos, N. Anifantis, Sci. Direct 132 (2015) 536–544, https://doi.org/10.1016/j.compstruct.2015.05.078.
[529] D. Banerjee, T. Nguyen, T. Chuang, Comput. Mater. Sci. 114 (2016) 209–218, https://doi.org/10.1016/j.commatsci.2015.12.026.
[530] A. Gupta, S. Harsha, Compos. Part B 95 (2016) 172–178, https://doi.org/10.1016/j.compositesb.2016.04.005.
[531] K. Zarasvand, H. Golestanian, Mater. Des. 109 (2016) 314–323, https://doi.org/10.1016/j.matdes.2016.07.071.
[532] Z. Shokrieh, M. Seifi, M. Shokrieh, Mech. Mater. 115 (2017) 16–21, https://doi.org/10.1016/j.mechmat.2017.09.006 URL http://www.sciencedirect.com/science/article/pii/S0167663617303691.
[533] K. Bhowmik, P. Kumar, N. Khutia, A. Chowdhury, Mater. Today Proc. 5 (2018) 20528–20534, https://doi.org/10.1016/j.matpr.2018.06.430.
[534] E. García-Macías, C.F. Guzmán, E.I. Saavedra Flores, R. Castro-Triguero, Compos. Part B 159 (2018) 114–131, https://doi.org/10.1016/j.compositesb.2018.09.057.
[535] M. Karimi, R. Ghajar, A. Montazeri, Compos. Struct. 201 (2018) 528–539, https://doi.org/10.1016/j.compstruct.2018.05.140.
[536] M. Parizi, H. Shahverdi, M. Mondali, Polym. Compos. (2018), https://doi.org/10.1002/pc.24871.
[537] S. Rahimian-Koloor, H. Moshrefzadeh-Sani, S. Hashemianzadeh, M. Shokrieh, Curr. Appl. Phys. 18 (2018) 559–566, https://doi.org/10.1016/j.cap.2018.02.007.
[538] D. Askari, M.N. Ghasemi-Nejhad, J. Comput. Theor. Nanosci. 8 (4) (2011) 783–794, https://doi.org/10.1166/jctn.2011.1753 URL https://www.ingentaconnect.com/content/asp/jctn/2011/00000008/00000004/art00037.
[539] P. Zhao, G. Shi, Comput. Mater. Contin. 5 (1) (2011) 49–58.
[540] B. Zhang, H. Xiao, G. Yang, X. Liu, Eng. Fract. Mech. 141 (2015) 111–119, https://doi.org/10.1016/j.engfracmech.2015.05.021.
[541] S. Guryel, B. Hajgato, Y. Dauphin, J. Blairon, H. Miltner, F. Proft, P. Geerlingsa, G. Lier, Phys. Chem. Chem. Phys. 15 (2013) 659–665, https://doi.org/10.1039/C2CP43033A.
[542] J. Zhao, L. Wang, J. Jiang, Z. Wang, W. Guo, T. Rabczuk, J. Appl. Phys. 113 (2013) 1–40, https://doi.org/10.1063/1.4791579.
[543] S. Zhang, R. Khare, Q. Lu, T. Belytschko, Int. J. Numer. Methods Eng. 70 (8) (2007) 913–933, https://doi.org/10.1002/nme.1895.
[544] B. Hajgato, S. Guryel, Y. Dauphin, J. Blairon, H. Miltner, G. Lier, F. Proft, P. Geerlings, Phys. Chem. 116 (2012) 22608–22618, https://doi.org/10.1021/jp307469.
[545] C. Cao, M. Daly, C. Singh, Y. Sun, T. Filleter, Carbon 81 (2015) 497–504, https://doi.org/10.1016/j.carbon.2014.09.082.
[546] J. Fu, F. Bernard, S. Kamali-Bernard, J. Nano Res. 33 (2015) 92–105, https://doi.org/10.4028/www.scientific.net/JNanoR.33.92.
[547] S. Gajbhiye, S. Singh, J. Phys. D: Appl. Phys. 48 (2015), https://doi.org/10.1088/0022-3727/48/14/145305 145305.1 - 145305-17.
[548] K. Tserpes, P. Papanikos, S. Tsirkas, Compos. Part B: Eng. 37 (7) (2006) 662–669, https://doi.org/10.1016/j.compositesb.2006.02.024 URL http://www.sciencedirect.com/science/article/pii/S1359836806000448.
[549] M. Meo, M. Rossi, Mater. Sci. Eng.: A 454–455 (2007) 170–177, https://doi.org/10.1016/j.msea.2006.11.158 URL http://www.sciencedirect.com/science/article/pii/S0921509306025378.
[550] K. Tserpes, P. Papanikos, Compos. Struct. 79 (4) (2007) 581–589, https://doi.org/10.1016/j.compstruct.2006.02.020 URL http://www.sciencedirect.com/science/article/pii/S0263822306000663.
[551] J. Xiao, J. Staniszewski, J. Gillespie, Compos. Struct. 88 (4) (2009) 602–609,

https://doi.org/10.1016/j.compstruct.2008.06.008 URL http://www.sciencedirect.com/science/article/pii/S0263822308001979.
[552] S. Ghaderi, E. Hajiesmaili, Mater. Sci. Eng. A 582 (2013) 225–234, https://doi.org/10.1016/j.msea.2013.05.060.
[553] A.L. Pontefisso Jr., Composites 96 (2016) 338–349, https://doi.org/10.1016/j.compositesb.2016.04.006.
[554] A. Shajari, R. Ghajar, M. Shokrieh, Comput. Mater. Sci. 142 (2018) 395–409, https://doi.org/10.1016/j.commatsci.2017.10.006.
[555] F. Scarpa, S. Adhikari, R. Chowdhury, Phys. Lett. A 374 (19) (2010) 2053–2057, https://doi.org/10.1016/j.physleta.2010.02.063 URL http://www.sciencedirect.com/science/article/pii/S0375960110002240.
[556] M. Zaeri, S. Ziaei-Rad, A. Vahedi, F. Karimzadeh, Carbon 48 (13) (2010) 3916–3930, https://doi.org/10.1016/j.carbon.2010.06.059 URL http://www.sciencedirect.com/science/article/pii/S0008622310004653.
[557] x Liu, T. Metcalf, J. Robinson, J. Houston, F. Scarpa, Nano Lett. 12 (2012) 1013–1017, https://doi.org/10.1021/nl204196v.
[558] C.W. To, Finite Elem. Anal. Des. 42 (5) (2006) 404–413, https://doi.org/10.1016/j.finel.2005.08.004 URL http://www.sciencedirect.com/science/article/pii/S0168874X05001046.
[559] A. Sakhaee-Pour, Comput. Mater. Sci. 45 (2) (2009) 266–270, https://doi.org/10.1016/j.commatsci.2008.09.024 URL http://www.sciencedirect.com/science/article/pii/S0927025608004394.
[560] A. Shakouri, T.Y. Ng, R.M. Lin, Nanotechnology 22 (29) (2011) 295711 URL http://stacks.iop.org/0957-4484/22/i=29/a=295711.
[561] A. Parashar, P. Mertiny, Comput. Theor. Nanosci. 10 (2013) 292–296, https://doi.org/10.1166/jctn.2013.2694.
[562] M. Fadaee, Appl. Math. Model. 40 (2016) 1863–1872, https://doi.org/10.1016/j.apm.2015.09.029.
[563] C. Li, T.-W. Chou, Mech. Mater. 36 (11) (2004) 1047–1055, https://doi.org/10.1016/j.mechmat.2003.08.009 URL http://www.sciencedirect.com/science/article/pii/S0167663603001455.
[564] N. Hu, K. Nunoya, D. Pan, T. Okabe, H. Fukunaga, Int. J. Solids Struct. 44 (20) (2007) 6535–6550, https://doi.org/10.1016/j.ijsolstr.2007.02.043 URL http://www.sciencedirect.com/science/article/pii/S0020768307001114.
[565] M. Rahmandoust, A. Öchsner, J. Nano Res. 16 (2012) 153–160, https://doi.org/10.4028/www.scientific.net/JNanoR.16.153.
[566] A.Y.T. Leung, X. Guo, X.Q. He, H. Jiang, Y. Huang, J. Appl. Phys. 99 (12) (2006) 124308, https://doi.org/10.1063/1.2206607.
[567] S. Pradhan, U. Mandal, Phys. E: Low-dimens. Syst. Nanostruct. 53 (2013) 223–232, https://doi.org/10.1016/j.physe.2013.04.029.
[568] M. Mirzaei, Y. Kiani, Compos. Struct. 180 (2017) 606–616, https://doi.org/10.1016/j.compstruct.2017.08.057 URL http://www.sciencedirect.com/science/article/pii/S0263822317323061.
[569] A. Soleimani, M. Naei, M. Mashhadi, Microsyst. Technol. 23 (2016) 2859–2871, https://doi.org/10.1007/s00542-016-3098-6.
[570] C.M. Wang, Y.Q. Ma, Y.Y. Zhang, K.K. Ang, J. Appl. Phys. 99 (11) (2006) 114317, https://doi.org/10.1063/1.2202108.
[571] A. Sears, R.C. Batra, Phys. Rev. B 73 (2006) 85410, https://doi.org/10.1103/PhysRevB.73.085410.
[572] X. Guo, H.J. Leung, X.Q. He, Y. Huang, J. Appl. Mech. 74 (2) (2007) 347–351, https://doi.org/10.1115/1.2198548 arXiv: http://appliedmechanics.asmedigitalcollection.asme.org/article.aspx?articleid=1416581.
[573] A.G. Arani, R. Rahmani, A. Arefmanesh, Phys. E: Low-dimens. Syst. Nanostruct. 40 (7) (2008) 2390–2395, https://doi.org/10.1016/j.physe.2007.11.011 URL http://www.sciencedirect.com/science/article/pii/S1386947707007825.
[574] X. Guo, A. Leung, X. He, H. Jiang, Y. Huang, Compos. Part B: Eng. 39 (1) (2008) 202–208, https://doi.org/10.1016/j.compositesb.2007.02.025 marine Composites and Sandwich Structures. URL http://www.sciencedirect.com/science/article/pii/S1359836807000583.
[575] X. Yao, Q. Han, H. Xin, Comput. Mater. Sci. 43 (4) (2008) 579–590, https://doi.org/10.1016/j.commatsci.2007.12.019 URL http://www.sciencedirect.com/science/article/pii/S0927025608000074.
[576] R. Ansari, S. Rouhi, Phys. E: Low-dimens. Syst. Nanostruct. 43 (1) (2010) 58–69, https://doi.org/10.1016/j.physe.2010.06.023 URL http://www.sciencedirect.com/science/article/pii/S1386947710003589.
[577] Z. Kang, M. Li, Q. Tang, Comput. Mater. Sci. 50 (1) (2010) 253–259, https://doi.org/10.1016/j.commatsci.2010.08.011 URL http://www.sciencedirect.com/science/article/pii/S0927025610004763.
[578] E.I. Saavedra Flores, S. Adhikari, M. Friswell, F. Scarpa, Phys. E: Low-dimens. Syst. Nanostruct. 44 (2) (2011) 525–529, https://doi.org/10.1016/j.physe.2011.10.006 URL http://www.sciencedirect.com/science/article/pii/S1386947711003687.
[579] R. Ansari, S. Rouhib, M. Aryayi, M. Mirnezhada, Sci. Iran. 19 (2012) 1984–1990, https://doi.org/10.1016/j.scient.2012.10.004.
[580] A. Ghavamian, A. Ochsner, Physica E 46 (2012) 241–249, https://doi.org/10.1016/j.physe.2012.08.002.
[581] J. Bocko, P. Lengvarský, J. Mech. Sci. Technol. 31 (4) (2017) 1825–1833, https://doi.org/10.1007/s12206-017-0330-y.
[582] S.K. Georgantzinos, G.I. Giannopoulos, Diam. Relat. Mater. 80 (2017) 27–37, https://doi.org/10.1016/j.diamond.2017.10.005 URL http://www.sciencedirect.com/science/article/pii/S0925963517304442.
[583] A. Parashar, P. Mertiny, Nano Express 7 (2012) 1–6, https://doi.org/10.1186/1556-276X-7-515.
[584] D. Garcia-Sanchez, A.M. van der Zande, A.S. Paulo, B. Lassagne, P.L. McEuen, A. Bachtold, Nano Lett. 8 (5) (2008) 1399–1403, https://doi.org/10.1021/nl080201h pMID: 18402478.
[585] C. Wang, L. Lan, Y. Liu, H. Tan, X. He, Int. J. Solids Struct. 50 (2013) 1812–1823, https://doi.org/10.1016/j.ijsolstr.2013.02.002.
[586] A. Swain, T. Roy, B. Nanda, Int. J. Theor. Appl. Res. Mech. Eng. (IJTARME) 2 (2013) 130–133.
[587] C. Dinckal, Iran. J. Sci. Technol. Trans. Mech. Eng. 40 (2016) 43–55, https://doi.org/10.1007/s40997-016-0010-z.
[588] M. Vinyas, Compos. Part B 158 (2018) 286–301, https://doi.org/10.1016/j.compositesb.2018.09.086.
[589] M. Yas, M. Heshmati, Appl. Math. Model. 36 (2012) 1371–1394, https://doi.org/10.1016/j.apm.2011.08.037.
[590] P. Zhu, Z. Lei, K. Liew, Compos. Struct. 94 (2012) 1450–1460, https://doi.org/10.1016/j.compstruct.2011.11.010.
[591] P. Malekzadeh, A. Zarei, Thin-Walled Struct. 82 (2014) 221–232, https://doi.org/10.1016/j.tws.2014.04.016.
[592] K. Mehar, S. Panda, A. Dehengia, V. Kar, J. Sandw. Struct. Mater. 18 (2015) 151–173, https://doi.org/10.1177/1099636215613324.
[593] E. García-Macías, R. Castro-Triguero, E.I. Saavedra Flores, M.I. Friswell, R. Gallego, Compos. Struct. 140 (2016) 473–490, https://doi.org/10.1016/j.compstruct.2015.12.044.
[594] M. Song, S. Kitipornchai, J. Yang, Compos. Struct. 159 (2017) 579–588, https://doi.org/10.1016/j.compstruct.2016.09.070 URL http://www.sciencedirect.com/science/article/pii/S0263822316314672.
[595] A. Sakhaee-Pour, M.T. Ahmadian, R. Naghdabadi, Nanotechnology 19 (8) (2008) 85702 URL http://stacks.iop.org/0957-4484/19/i=8/a=085702.
[596] K. Hashemnia, M. Farid, R. Vatankhah, Comput. Mater. Sci. 47 (1) (2009) 79–85, https://doi.org/10.1016/j.commatsci.2009.06.016 URL http://www.sciencedirect.com/science/article/pii/S0927025609002705.
[597] M. Sadeghi, R. Naghdabadi, Nanotechnology 21 (10) (2010) 105705 URL http://stacks.iop.org/0957-4484/21/i=10/a=105705.
[598] Wave Propagation and Structural Dynamics in Graphene Nanoribbons, 2010, vol. 7646.
[599] F. Scarpa, R. Chowdhury, K. Kam, S. Adhikari, M. Ruzzene, Nanoscale Res. Lett. 6 (1) (2011) 430, https://doi.org/10.1186/1556-276X-6-430.
[600] S. Arghavan, A. Singh, J. Phys. D: Appl. Phys. 45 (2012) 1–8, https://doi.org/10.1088/0022-3727/45/45/455305.
[601] S. Rouhi, R. Ansari, Physica E 44 (2012) 764–772, https://doi.org/10.1016/j.physe.2011.11.020.
[602] E. Mahmoudinezhad, R. Ansari, Phys. E: Low-dimens. Syst. Nanostruct. 47 (2013) 12–16, https://doi.org/10.1016/j.physe.2012.09.029.
[603] W. Xu, L. Wang, J. Jiang, World Sci. 13 (3) (2016) 1650011, https://doi.org/10.1142/S0219876216500110.
[604] A. Tsiamaki, D. Katsareas, N. Anifantis, J. Appl. Phys. 123 (2018) 204307, https://doi.org/10.1063/1.5023908.
[605] C. Li, T.-W. Chou, Appl. Phys. Lett. 84 (1) (2004) 121–123, https://doi.org/10.1063/1.1638623.
[606] R.F. Gibson, E.O. Ayorinde, Y.-F. Wen, Compos. Sci. Technol. 67 (1) (2007) 1–28, https://doi.org/10.1016/j.compscitech.2006.03.031 URL http://www.sciencedirect.com/science/article/pii/S026635380600131X.
[607] M. Mir, A. Hosseini, G. Majzoobi, Comput. Mater. Sci. 43 (3) (2008) 540–548, https://doi.org/10.1016/j.commatsci.2007.12.024 URL http://www.sciencedirect.com/science/article/pii/S0927025608000050.
[608] S.K. Georgantzinos, G.I. Giannopoulos, N.K. Anifantis, Comput. Mech. 43 (6) (2009) 731–741, https://doi.org/10.1007/s00466-008-0341-8.
[609] A. Sakhaee-Pour, M. Ahmadian, A. Vafai, Thin-Walled Struct. 47 (6) (2009) 646–652, https://doi.org/10.1016/j.tws.2008.11.002 URL http://www.sciencedirect.com/science/article/pii/S0263823108002413.
[610] E. Ghavanloo, F. Daneshmand, M. Rafiei, Phys. E: Low-dimens. Syst. Nanostruct. 42 (9) (2010) 2218–2224, https://doi.org/10.1016/j.physe.2010.04.024 URL http://www.sciencedirect.com/science/article/pii/S1386947710002249.
[611] E. Ghavanloo, M. Rafiei, F. Daneshmand, Phys. Lett. A 375 (19) (2011) 1994–1999, https://doi.org/10.1016/j.physleta.2011.03.025 URL http://www.sciencedirect.com/science/article/pii/S0375960111003409.
[612] A.Y. Joshi, S.C. Sharma, S. Harsha, Phys. E: Low-dimens. Syst. Nanostruct. 43 (5) (2011) 1040–1045, https://doi.org/10.1016/j.physe.2010.12.011 URL http://www.sciencedirect.com/science/article/pii/S1386947710007186.
[613] S. Arghavan, A. Singh, J. Sound Vib. 330 (13) (2011) 3102–3122, https://doi.org/10.1016/j.jsv.2011.01.032 URL http://www.sciencedirect.com/science/article/pii/S0022460X11000800.
[614] T. Chang, Appl. Math. Model. 36 (2012) 1964–1973, https://doi.org/10.1016/j.apm.2011.08.020.
[615] R. Ansari, M. Hemmatnezhad, Nonlinear Dyn. 67 (2012) 373–383, https://doi.org/10.1007/s11071-011-9985-6.
[616] R. FirouzAbadi, A. Hosseinian, Comput. Mater. Sci. 53 (2012) 12–17, https://doi.org/10.1016/j.commatsci.2011.09.010.
[617] R. Ansari, S. Rouhi, M. Aryayi, Appl. Math. Mech. 34 (10) (2013) 1187–1200, https://doi.org/10.1007/s10483-013-1738-9.
[618] A. Patel, A. Joshi, Comput. Mater. Sci. 79 (2013) 230–238, https://doi.org/10.1016/j.commatsci.2013.06.022.
[619] S. Chu, S. Wu, W. Chang, Comput. Theor. Nanosci. 10 (2013) 119–122, https://doi.org/10.1166/jctn.2013.2666.
[620] R. Ansari, A. Momen, S. Rouhi, S. Ajori1, Shock Vib. (2014) 1–8, https://doi.org/10.1155/2014/410783.
[621] R. Moghadam, S. Hosseini, M. Salehi, Physica E 62 (2014) 80–89, https://doi.org/10.1016/j.physe.2014.04.008.
[622] G.I. Giannopoulos, S.K. Georgantzinos, Acta Mech. 228 (6) (2017) 2377–2390, https://doi.org/10.1007/s00707-017-1812-9.
[623] J. Palacios, R. Ganesan, Int. Conf. Theor. Appl. Nanosci. Nanotechnol. (106)

(2018) 1–4, https://doi.org/10.11159/tann18.106.
[624] A. Fereidoon, R. Rafiee, R. Moghadam, Mech. Compos. Mater. 49 (3) (2013) 325–332.
[625] N. Fantuzzi, F. Tornabene, M. Bacciocchi, R. Dimitri, Compos. Part B: Eng. 115 (2017) 384–408, https://doi.org/10.1016/j.compositesb.2016.09.021 composite lattices and multiscale innovative materials and structures. URL http://www.sciencedirect.com/science/article/pii/S1359836816319011.
[626] A. Parashar, P. Mertiny, Lett. Fract. Micromech. 176 (2012) 119–126, https://doi.org/10.1007/s10704-012-9718-y.
[627] A. Parashar, P. Mertiny, Solid State Commun. 173 (2013) 56–60, https://doi.org/10.1016/j.ssc.2013.08.028.
[628] J.-L. Tsai, S.-H. Tzeng, Y.-J. Tzou, Int. J. Solids Struct. 47 (3) (2010) 503–509, https://doi.org/10.1016/j.ijsolstr.2009.10.017 URL http://www.sciencedirect.com/science/article/pii/S0020768309004107.
[629] T. Theodosiou, D. Saravanos, Comput. Mater. Sci. 82 (2014) 56–65, https://doi.org/10.1016/j.commatsci.2013.09.032.
[630] X. Liu, Q. Li, P. Egberts, R. Carpick, Adv. Mater. 1 (2) (2014) 1–9, https://doi.org/10.1002/admi.201300053.
[631] Y. Jia, Z. Chen, W. Yan, Compos. Part B 81 (2015) 64–71, https://doi.org/10.1016/j.compositesb.2015.07.003.
[632] A. Parashar, P. Mertiny, Nano Express 7 (2012) 1–8, https://doi.org/10.1186/1556-276X-7-595.
[633] B.M. Powar, R.K. Shirsat, Int. J. Eng. Sci. 7 (2017) 15137–15144 URL http://ijesc.org/upload/72d0cd9944e9b76b9caa350a3b240430.Finite.
[634] A. Parashar, P. Mertiny, Int. J. Fract. 179 (2013) 221–228, https://doi.org/10.1007/s10704-012-9779-y.
[635] A.A. Balandin, S. Ghosh, W. Bao, I. Calizo, D. Teweldebrhan, F. Miao, C.N. Lau, Nano Lett. 8 (3) (2008) 902–907, https://doi.org/10.1021/nl0731872 pMID: 18284217.
[636] S. Berber, Y.-K. Kwon, D. Tománek, Phys. Rev. Lett. 84 (2000) 4613–4616, https://doi.org/10.1103/PhysRevLett.84.4613.
[637] W. Jang, Z. Chen, W. Bao, C.N. Lau, C. Dames, Nano Lett. 10 (10) (2010) 3909–3913, https://doi.org/10.1021/nl101613u pMID: 20836537.
[638] B. Mortazavi, M. Pötschke, G. Cuniberti, Nanoscale 6 (2014) 3344–3352, https://doi.org/10.1016/j.matdes.2014.01.007.
[639] B. Mortazavi, T. Rabczuk, Carbon 85 (2015) 1–7, https://doi.org/10.1016/j.carbon.2014.12.046.
[640] B. Mortazavi, O. Benzerara, H. Meyer, J. Bardon, S. Ahzi, Carbon 60 (2013) 356–365, https://doi.org/10.1016/j.carbon.2013.04.048.
[641] M.J. Assael, C.F. Chen, I. Metaxa, W.A. Wakeham, Int. J. Thermophys. 25 (2004) 971–985, https://doi.org/10.1023/B:IJOT.0000038494.22494.04.

glossary-section

glossary-section

E: Young's modulus. 38, 40
AFEM: Atomic-scale finite element method. 17, 44, 52, 59
AFM: Atomic force microscopy. 41, 43
BEM: Boundary element method. 17
BLGS: Bilayer graphene sheet. 58, 68
C-C: Carbon-carbon. 10, 17–23, 26, 55, 61
CNC: Carbon nano coil. 10
CNCN: Carbon nano cone. 10
CNT: Carbon nano tube. 10–13, 15, 16, 22, 24, 39, 40, 48, 50–52, 55, 56, 60, 69, 161, 163
CTE: Coefficient of thermal expansion. 69
CVD: Chemical vapour deposition. 11, 12, 18
CVFEM: Control volume finite element method. 17, 69
DEM: Distinct element method. 15
DFT: Density functional theory. 15, 52
DGTD: Discontinuous Galerkin time-domain. 15
DLGS: Double layer graphene sheet. 42, 51, 60
DOF: Degrees of freedom. 17, 20
DQM: Differential quadrature method. 15
DSC: Discrete singular convolution. 15
DWCNT: Double wall carbon nano tube. 49, 55, 58, 60
EG: E
FE: Finite element. 16, 20, 29, 41, 42, 47, 48, 50, 51, 56, 58, 60–62, 65, 66, 68, 70, 71, 162
FE-Analytical: A method that combines finite element method with analytical calculations. 68, 69
FE-EX: A method that combines FEM with experiments. 46, 52, 53, 69
FE-MD: A method that combines finite element method with molecular dynamics simulations. 69
FEM: Finite element method. 9, 10, 14–17, 38, 40, 51, 52, 55, 56, 58, 60, 61, 64, 68–70
GANSGraphene associated nano structures. 9: –13, 15, 16, 70, 72, 162
GNI: Graphene nano islands. 10
GNR: Graphene nano platelets. 10, 14, 42, 51, 61, 62, 68
GNR: Graphene nano ribbon. 10, 11
GO: Graphene oxide. 10, 12, 13, 40, 42, 50, 51
GRP: Graphene reinforced plastic. 28, 162
HDPE: High density polyethylene. 13
ILS: Interlaminar strength. 12
ILSS: Interlaminar shear strength. 66
MBFB: Representing the matrix by beam elements and nanoreinforcement by beam elements. 64, 67
MD: Molecular dynamics. 14–16, 40, 41, 51, 52, 68, 69
MDFEM: Molecular dynamics finite element method. 52
MLGS: Multi-layer graphene sheet. 15, 42, 50, 51, 55, 56, 58, 60, 68
MM: Molecular mechanics. 14, 15, 41, 43, 61, 64
MPFP: Representing matrix and nanoreinforcements by 2D plate elements. 45, 49
MSHFME: Representing the matrix by shell elements and nanoreinforcement by beam elements. 67
MSHFME: Representing the matrix by shell elements and nanoreinforcement by membrane elements. 67
MSHFSH: Representing the matrix by shell elements and nanoreinforcement by shell elements. 64
MSOFBE: Representing matrix by 3D solid elements and nanoreinforcements by beam elements. 45, 49
MSOFP: Representing the matrix by 3D elements and nanoreinforcement by plane elements. 49
MSOFSH: Representing matrix by 3D solid elements and nanoreinforcements by shell elements. 45, 46
MSOFSO: Representing matrix and nanoreinforcements by 3D solid elements. 45, 46, 49, 53, 69, 70
MSOFSP: Representing matrix by 3D solid elements and representing nanoreinforcements by beam elements in a space frame configuration. 45, 46, 49
MWCNT: Multi-wall carbon nano tube. 11, 38, 41, 48, 51, 55, 56, 58, 60, 62, 65, 68
OE: Representing the entire nanocomposite with one tetrahedron element. 45, 53
OOFEM: Object oriented finite element method. 17, 69
PA6: Polyamide 6. 13
PEEK: Poly-etherether-ketone. 13, 65, 70
PEO: Polyethylene oxide matrix. 14
PET: Polyethylene terephthalate. 12, 32
PGS: Pillared graphene structure. 11, 43
PMMA: Polymethyl methacrylate. 12, 38, 58
PVA: Polyvinyl alcohol. 12, 13
PVC: Polyvinyl chloride. 12
PVDF: Polyvinylidene diuoride. 13
QM: Quantum mechanics. 64
rGO: Reduced graphene Oxide. 10, 13, 14, 42
RVE: Representative element method. 9, 17, 27, 32, 36, 42, 48, 50, 51, 64–66, 73
SBFEM: Scaled boundary finite element method. 17, 52
SERR: Strain energy release rate. 61, 62, 64, 71
SF: Space frame. 40, 41, 43, 47, 48, 50, 51, 55, 58, 60, 61, 64, 66, 69
SFEM: Spectral finite element method. 17
SGFEM: Strain gradient finite element analysis. 62
SIFStress intensity f: actor. 61, 64, 71
SLGS: Single layer graphene sheet. 15, 40–42, 48, 50, 51, 55, 56, 60–62, 64, 68, 69, 163
SpFEM: Spring based finite element method. 41, 43, 48
SWCNT: Single wall carbon nano tube. 11, 15, 17, 35, 38, 39, 41, 48, 49, 51, 55, 58, 60–62, 64–66, 68, 69, 163
TB: Tight binding. 15
TLGS: Triple layer graphene sheet. 50, 51, 56, 60
TWCNT: Triple wall carbon nano tube. 58
XFEM: Extended finite element method. 17, 57, 61, 64

Y. Chandra is a researcher at the College of Engineering in Swansea University, Wales, UK. His research focuses on finite element method, nano materials, multiscale modelling of graphene and associated nano structures. He has published several papers on computational modelling of graphene and its composites.

S. Adhikari is the chair of Aerospace Engineering in the College of Engineering of Swansea University. His PhD was from Cambridge University in Engineering. He is a Fellow of the Royal Aeronautical Society. His research interest is in structural dynamics, probabilistic methods and computational mechanics. He has published over 300 journal papers and 5 books in these areas.

E.I. Saavedra Flores is currently director of the Civil Engineering Department at the University of Santiago, Chile. His PhD was carried out in the Zienkiewicz Centre for Computational Engineering, at Swansea University, Wales, UK, in the field of computational mechanics of solids and structures. He has published extensively in peer-reviewed journals. His main research interests are multi-scale finite element methods in non-linear solid mechanics, constitutive modelling of wood materials and cross-laminated timber structures.

Ł. Figiel is an Associate Professor at the University of Warwick - he is a core staff in the International Institute for Nanocomposites Manufacturing (IINM) in WMG Department of the University of Warwick, and in the Warwick Centre for Predictive Modelling (WCPM). His main research interests are in multiscale modelling of functional nanostructured materials.